Rhodium-Zeolite Hydroformylation of Propylene
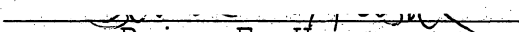
by

Edward James Rode

Dissertation submitted to the Faculty of the

Virginia Polytechnic Institute and State University

in partial fulfillment of the requirements for the degree of

DOCTOR OF PHILOSOPHY

in

Chemical Engineering

APPROVED:

_____
Mark E. Davis

_____   _____
Brian E. Hahson   John G. Dillard

_____   _____
Garth L. Wilkes   Felix Sebba

March, 1985
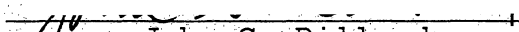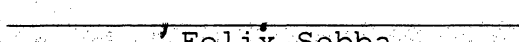Blacksburg, Virginia

RHODIUM-ZEOLITE HYDROFORMYLATION OF PROPYLENE

by

Edward James Rode

Committee Chairman: Mark E. Davis

Chemical Engineering

(ABSTRACT)

The purpose of this research was to characterize the rhodium exchanged NaX and NaY zeolites as propylene hydroformylation catalysts. Catalytic activity was measured in a differential bed reactor. Flow _in situ_ infrared spectroscopy was used to probe the coordination chemistry of the zeolite modified rhodium carbonyls.

The catalytic activity of rhodium zeolites at atmospheric pressure and between 100-150°C was measured. The rate of n-butyraldehyde production was approximately 5×10^{-3} moles/g-Rh hr at 150°C. Regioselectivity was dependent upon pretreatment. Precarbonylation with carbon monoxide, drying with air, and heating with N_2 prior to hydroformylation conditions produced a straight to branched isomer ratio (n/i) of 1.9-2.3. Partial reduction with 10% H_2 in N_2 at

127°C lowered n/i to 1.3. Hydrogenation to propane was 3-10 times faster than the hydroformylation rate at 150°C.

Catalytic activity was sensitive to cation exchange conditions. Rhodium form, pH, temperature, and salt concentration altered catalyst behavior. Only $RhCl_3 \cdot 3H_2O$ preparations on NaY zeolite produced consistent results. In general, temperatures above 80°C, a pH above 4, and a salt concentration of 0.1N NaCl were required in order to produce an active hydroformylation catalyst. Ammine complexes did not activate under any circumstances.

It was found that the degree of hydration controlled the formation of rhodium carbonyls. On NaY, the hydrated rhodium zeolite reacted with CO at 120°C to form $Rh_6(CO)_{16}$. By drying the zeolite in air at 190°C, two rhodium dicarbonyls, $Rh(CO)_2(O_z)_2$-NaY and $Rh(CO)_2(O_z)(H_2O)$-NaY, were formed. The rhodium carbonyls were reacted with n-hexyl diphenylphosphine to determine rhodium locations. $Rh(CO)_2(O_z)_2$-NaY was located at the surface while the other two species were located within the zeolite cages. One dicarbonyl species, $Rh(CO)_2(O_z)_2$-NaX, was observed on NaX. It was determined by reactions with phosphines that this species resides in the zeolite cages.

Reaction intermediates identified by FTIR under hydroformylation conditions suggested that the heterogeneous cata-

lyst proceeds through a mechanism similar to that occurring in solution. Heterogeneous reaction orders also agreed with those reported for homogeneous hydroformylations.

Addition of dimethylphenylphosphine (DMP) to the rhodium zeolites significantly increased regioselectivity. Rates were slightly less than those from the unmodified rhodium carbonyls. However, the phosphine modified rhodium zeolites deactivated within 16 hours. Continuous exposure to DMP decreased the rate of deactivation.

ACKNOWLEDGEMENTS

TABLE OF CONTENTS

LIST OF TABLES

LIST OF FIGURES

Chapter I

INTRODUCTION

Over the last several decades, catalyst development has included the application of organometallic compounds as homogeneous catalysts because of their ability to achieve high selectivity. Many large scale processes now use organometallic complexes as catalysts. Examples include ethylene oxidation to acetaldehyde and hydroformylation of olefins to aldehydes and alcohols. On a smaller scale, the synthesis of expensive compounds such as asymmetric amino acids has been achieved. However, the practical utilization of these complex catalytic systems has been difficult because of several inherent characteristics. These traits include:

1. the separation of catalyst from product and reactants;

2. the corrosive nature of many catalyst solutions;

3. the limited engineering flexibility due to mild conditions;

4. the instability of organometallic catalytic systems.

Heterogeneous catalysts typically do not yield reaction selectivities comparable to homogeneous systems, but they do offer (a) the ease of separation of the products from the catalyst, (b) the elimination of solvents (alleviates corro-

sion problems), and (c) the ability to operate at higher temperatures (allows better energy utilization).

An outgrowth of the realization of these problems has been the subsequent development of a composite catalyst which possesses the characteristics of both heterogeneous and homogeneous systems. Specifically, studies were initiated to incorporate the selective homogeneous catalysts onto supports. These catalysts have been called "heterogenized homogeneous complexes." The main goal of creating these heterogenized homogeneous catalysts was to overcome the separation problem of homogeneous catalysis while retaining high selectivity. These catalysts also enabled more detailed study of the catalytic active site. By knowing the location of the heterogenized homogeneous catalysts, experiments were conducted which attempted to alter the support surrounding the complex in order to enhance selectivity. Obviously, these are ideal circumstances which drive the interest to research such systems.

Methods for immobilizing transition metal complexes have been studied extensively since Grubbs and Knoll demonstrated that Rh(I) anchored on phosphine modified polystyrene acts as an olefin hydrogenation catalyst (1). To date, supports such as organic polymers, carbon, inorganic oxides, and aluminosilicates have also been investigated (2).

Heterogenization is generally achieved in one of three ways:

1. a support may serve as a ligand for a metal complex thus immobilizing the metal via a chemical bond;

2. a complex may be physically adsorbed on the surface or within the pores of a support without the formation of chemical bonds to the surface; or

3. a complex may be dissolved in an nonvolatile solvent which is adsorbed in the pores of a support, i.e., supported liquid phase (SLP).

Each of these methods has its advantages and limitations. For heterogeneous operations in the liquid phase, method (1) is preferred since the dry (2) or SLP (3) catalysts may easily be destroyed by immersion in solvents or liquid reactants. On the other hand, all three of these preparations can be used for gas-solid reaction systems. Therefore, if a catalyst preparation technique is to be developed which allows for liquid phase conversions, methods (2) and (3) are unacceptable.

Heterogenization of metal complexes via method (1) can be achieved by different techniques. Typically, the specifics of the immobilization procedures depend upon the physico-chemical properties of the supports. For the case of a polymer, functionalization of the polymer with appropriate li-

gands allows formation of metal to functional group bonds. This technique has received the most attention, and several reviews have appeared (2-4). One case of interest is the attachment of $-CH_2PPh_2$ to Amberlite XAD-2, according to the following scheme:

$$\xrightarrow[SnCl_4]{CH_3OCH_2Cl} \;\; CH_2Cl \;\; \xrightarrow{KPPh_2} \;\; CH_2PPh_2 \;\; \xrightarrow[RhCl(C_8H_{12})_2]{} \;\; CH_2\!-\!P\!-\!Rh \quad\quad (1)$$
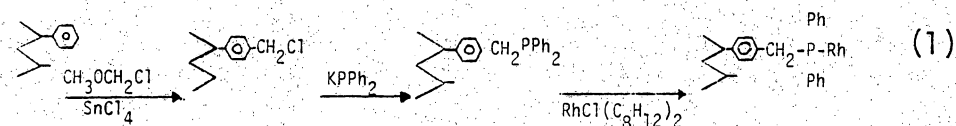
The last step involves addition of Rh via $RhCl(C_8H_{12})_2$ (5). Also, the surface hydroxyl groups of metal oxides and aluminosilicates can serve as the site of attachment for metal complexes (6-8). Ichikawa (6-8) generated hydroformylation catalysts by depositing rhodium carbonyls from solutions on TiO_2, ThO_2, CeO_2, La_2O_3, ZnO, MgO, Al_2O_3, SiO_2, CaO and activated carbon. Surface hydroxyl groups also can be functionalized in a manner similar to Eq. 1 (9) prior to the attachment of the metal complex.

Zeolites can offer ion exchange as another method of metal incorporation. For example, Mantovani et al. (10) exchanged $Rh(NH_3)_6Cl_3$ into NaY zeolite in order to form a hydroformylation catalyst. The catalytic species was formed in situ under the CO/H_2 reaction atmosphere.

Advantages and disadvantages to these different
techniques exists. However, the properties are mostly at-
tributable to the support characteristics. Polymers possess
flexibility that is both an asset and a weakness to catalyt-
ic systems. Organic matrices can be functionalized to carry
up to 10 milliequivalents/g matrix (3). Such a density of
sites allows for enhanced site-site cooperation in multi-
functional catalysts. Selection of a proper solvent may al-
low matrix swelling also to enhance such interaction. How-
ever, the swelling is often difficult to control since
temperature and pressure effect the polymer. Swelling can
be detrimental in that it can cause active sites to lie deep
within the polymer beads and increase the resistance to dif-
fusion. Also, polymer flexibility can allow chelating
through polymer-active site interactions. Inorganic sup-
ports have approximately tenfold fewer sites available for
functional group attachment and their framework are more
rigid. Hence the diffusional problem may not be as severe
as with polymer materials, and there is less potential for
deactivation via chelating. Inorganic oxides feature great-
er thermal stability than polymer supports. Therefore, the
upper limit is normally set by the thermal stability of the
supported metal complex.

The purpose of this thesis is to initiate a study of a novel immobilization technique. The method is centered around the ability to physically entrap a transition metal complex within a zeolite. Ideally, the transition metal exchanged into the zeolite will be reacted in situ with phosphorus containing compounds and carbon monoxide to form an intrazeolitic complex capable of catalyzing the hydroformylation of propylene. The catalyst will not be able to diffuse out of the zeolite due to its tertiary size. Because numerous rhodium phosphine complexes are hydroformylation catalysts, a wide selection of phosphorus compounds will allow fine tuning of the size of the intrazeolitic catalysts.

Chapter II

BACKGROUND

2.1   HYDROFORMYLATION

Hydroformylation is chosen as the test reaction for this study due to its industrial importance. The production of butyraldehyde from propylene, carbon monoxide and hydrogen has been quoted as being the most important industrial synthesis which utilizes a metal carbonyl catalyst (11). The reaction stoichometry for the hydroformylation of propylene is given below:

$$CH_2=CHCH_3 + CO + H_2 --> CH_3CH_2CH_2CH=O + (CH_3)_2CH(CHO) \qquad (2)$$
$$\qquad\qquad\qquad\qquad\qquad (n) \qquad\qquad\qquad\qquad (i)$$
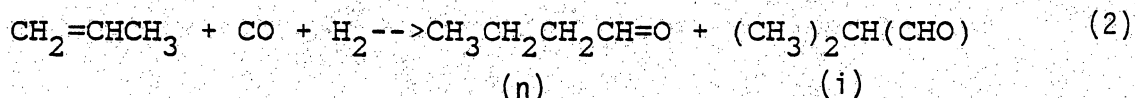
N-butyraldehyde is the desired product since it can be hydrogenated to n-butanol (used industrially as a solvent), or further reacted through aldol condensation and subsequent hydrogenation to form ethylhexanol. Ethylhexanol can be reacted to form dioctyl phthalate which is used as a plasticizer for polyvinyl chloride resins.

Due to processing considerations, it is most frequently desired to stop this series of reactions at butyraldehyde production. This allows maximum flexibility for product utilization. Therefore, the unfavorable side reactions are the hydrogenation of propylene, aldol condensation of butyraldehyde, and butyraldehyde hydrogenation.

Propylene hydroformylation proceeds only in the presence of a catalyst. While a number of transition metals catalyze this reaction, the two which show the greatest activity and selectivity toward desired products are cobalt and rhodium. Catalyst systems which are used most frequently are:

1. hydrido cobalt carbonyls;

2. hydrido cobalt carbonyl complexes containing tertiary phosphine ligands; and

3. tertiary phosphine hydrido rhodium carbonyl species.

Hydridorhodium carbonyls also activate this reaction and are 10^2-10^3 more active than the analogous cobalt carbonyls, but do not show good selectivity (n/i=1 for Rh, n/i=4 for Co) (12). Hydridocobalttricarbonyl catalyzes the hydrogenation of aldehydes to alcohols, whereas the rhodium carbonyl exhibits little aldehyde hydrogenation activity. Because of the higher activity and increased selectivity, modified rhodium catalysts have been studied most extensively and are replacing cobalt in most new commercial processes. In fact, modified rhodium catalysts are used by 7 butyraldehyde production facilities worldwide. These produce 1.1 metric tons per year of butyraldehyde, or roughly 25% of the total production. Three plants are also under construction (13).

Figure 1 shows the hydroformylation catalytic cycle with rhodium carbonyl catalysts. Rhodium can be introduced into

the reaction environment in a number of forms, e.g., as $Rh_4(CO)_{12}$, as rhodium salts of carboxylic acids, as $RhCl_3$ or as $RhCl_3 \cdot 3H_2O$. However, all these rhodium compounds transform in situ to the catalytically active species, $RhH(CO)_3$ (14). This reaction mechanism is completely analogous to cobalt carbonyl catalysis. The proposed steps of the cycle are:

1. coordination of an olefin (16 to 18 electrons)

2. hydride migration to form rhodium alkyl (18 to 16 electrons)

3. addition of carbon monoxide (16 -18 electrons)

4. alkyl migration to carbonyl to form acyl (18-16 electrons)

5. hydrogenolysis of acyl to yield aldehyde.

The last step of the mechanism is currently a topic of debate in the literature (15). Two proposed mechanisms are 1) oxidative addition of hydrogen to give an 18 electron complex, or 2) binuclear elimination, e.g., elimination by $(CO)_4CoH$ to produce aldehyde and $Co_2(CO)_7$.

Osborn et al (16) discovered that $RhCl(PPh_3)_3$ in benzene was capable of catalyzing the hydroformylation of 1-pentene or 1-hexene at essentially ambient conditions. Tertiary phosphine complexes of the form $RhCl(CO)L_2$, where $L=PBu_3$ (Bu=butyl), PPh_3 (Ph=phenyl), or $RhH(CO)(PPh_3)_3$, were used

$$MR(CO)_a(L)_b$$

RCH=CH$_2$

$$MH(CO)_a(L)_b$$

CO

(-RCHO)

$$M(COR)(CO)_a(L)_b$$
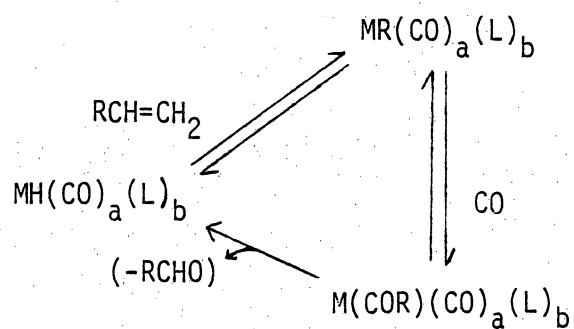
Figure 1: Hydroformylation Mechanism for Rh Carbonyls

(where M=metal, L=ligand)

as catalytic precursors. These all reacted to form the active species, $RhH(CO)_2L_2$. Not only does this system operate under mild conditions, but in the presence of excess phosphine, it also enhances the selectivity to $n/i = 10-14$, while significantly lowering the rate of hydrogenation of propylene to propane. However, a compromise exists between the selectivity and the rate of hydroformylation. At $100^{\circ}C$ and 35 atm, the rate is decreased 5 times as the PPh_3/Rh ratio is varied from 5:1 to 50:1 (17).

2.2   INDUSTRIAL HYDROFORMYLATION PROCESSES

Table 1 summarizes the behavior of cobalt and rhodium hydroformylation catalysts. On going from left to right there is a marked decrease in the energy requirement in terms of both milder operation conditions and greater product selectivity. In view of rapidly increasing energy costs and raw material prices, as well as more stringent environmental standards, it is likely that future practices will favor high efficiency processes which operate under mild reaction conditions with few by-products. From Table 1 one can see that the modified rhodium complex is most likely to be used in development of future hydroformylation process.

Industrial hydroformylation processes are often coined "oxo" processes. One aspect of oxo processes which is of

TABLE 1

Operating Data for Cobalt and Rhodium Hydroformylation (18)

	Unmodified Co	Modified Co	Modified Rh
Temperature (C)	140-180	160-200	80-120
Pressure (atm.)	250-350	50-100	15-20
%metal/olefin	0.1-1.0	0.5-1.0	$10(-2)-10(-3)$
n/i ratio	3-4:1	6-8:1	10-14:1

particular importance in continuous commercial operation is the separation of the catalyst from the products, since the hydroformylation reaction proceeds homogeneously. From Table 1 one might expect that oxo processes would be catalyzed by rhodium complexes. Since the relative prices of rhodium to cobalt metal are approximately 3500:1, severe economic penalties accompany catalyst loss of rhodium through incomplete separation of products. An amount of rhodium equivalent to 1 part per billion of aldehyde product would be an unacceptable separation (19). Therefore, most oxo processes employ a cobalt catalyst due to its availability and low cost.

In spite of the aforementioned difficulties, homogeneous processes based on rhodium are prospering with lower plant capital costs and energy requirements apparently outweighing the high catalyst investment. Monsanto has developed an oxo process for the hydroformylation of propylene, with $Rh(CO)(PPh_3)_2Cl$ as the catalyst, which avoids the need of catalyst regeneration. A "gas-sparged" reactor which contains the catalyst dissolved in a high boiling solvent sparges gaseous propylene, hydrogen, and carbon monoxide through the liquid phase catalyst (20, 21). The butyraldehyde product is continuously removed in the vapor effluent (22). Union Carbide Corp., Davy Powergas Ltd., and Johnson-

Matthey Co. Ltd. won the 1977 Kirkpatrick Chemical Engineering Achievement Award for developing and commercially implementing a rhodium based hydroformylation process (23). They used a gas-sparged reactor operating at 80-120°C, 200-400 psi, in the presence of triphenylphosphine. Rhodium losses to product are reported as "minimal", but the plant includes equipment for periodic makeup and removal of catalyst.

With present technology, one could employ a gas sparged reactor or SLP (only at lab or pilot scale) catalysts to perform propylene hydroformylation. These two catalysts systems are limited to reaction temperatures around 90°C-120°C due to the evaporation of triphenylphosphine and solvent at higher temperatures (22). Also, if using SLP, the conversion of propylene must be kept low in order to prevent capillary condensation of butyraldehyde into the pores (24). Various other solvents and ligands have been tested (25), but the triphenylphosphine is vastly superior in terms of activity and selectivity.

The development of a heterogeneous catalyst for this reaction is very much needed. A useful heterogeneous based system would:

1. not elute rhodium from the catalyst;

2. operate at temperatures above 90°C;

3. be applicable to other hydroformylation reactions,
     e.g., ethylene (gas phase), 1-hexene (liquid phase).

2.3   HETEROGENEOUS HYDROFORMYLATION CATALYSTS

As mentioned in the introduction, the three basic types
of immobilization are SLP, functionalization of the support,
and physisorption of a complex onto the surface. All three
methods have been used to form rhodium hydroformylation ca-
talysts.

The role of transition metal complexes on inorganic sup-
ports is the closest in nature to the proposed immobiliza-
tion technique. Hence only these will be reviewed exten-
sively. A brief discussion of functionalized polymers and
SLP follows. For more information concerning polymer sup-
ported catalysts and SLP, reviews have recently appeared
(2, 4, 26, 27).

Functionalizing polymers or silica hydroxyl groups with
phosphines to create heterogeneous hydroformylation cata-
lysts has met with mixed success. Typically, reactions are
carried out below 150°C and at pressures up to 400 psi in
the liquid phase. The following comments can be made about
rhodium complexes attached to functionalized supports:

1. increased selectivity similar to homogeneous analogs
     were frequently obtained;

2. mechanistically, the heterogeneous and homogeneous
catalysts behaved similarly, i.e., similar H_2 and CO
partial pressure dependencies;

3. rhodium elution was a major problem;

4. some polymers were not stable in high aldehyde con-
centrations (eliminates high conversions per reactor
pass);

5. diffusion resistances slowed the rate except at high
temperatures.

In general, it is felt that this method shows promise. Work
is continuing on these systems.

In recent years, supported liquid phase catalysts have
been studied more intensely. Most of the above comments
concerning functionalized polymers can be applied to SLP
systems. High selectivities have been obtained with only
one order of magnitude decrease in rate in comparison to the
analogous homogeneous system. However, the difficulty lies
in creating a stable catalyst. High n/i can be obtained
with high phosphine loadings, but the maximum test life has
been 500 hours, compared to the 18 month commercial catalyst
stability (28).

The remainder of the heterogeneous hydroformylation cata-
lysts studied have dealt with the deposition of rhodium com-
plexes onto supports or with the exchange of rhodium into

zeolites. The reaction selectivity for these supported rhodium catalysts in the absence of phosphine was between n/i=1-2.5. Also the rates are typically much slower than SLP, but comparable to that of the functionalized polymers.

Hjortkjaer et al. (29) deposited $HRh(CO)(PPh_3)_3$ from benzene onto silica, alumina, and NaX zeolite . The reaction selectivity was found to be higher for the alumina catalysts (n/i≈2). Catalytic runs lasted only 5 hours and the system deactivated up to 50% of the initial rate. Selectivity was not observed to be a funtion of time.

Rony and Roth (30) used alumina to support $RhCl(CO)(PPh_3)_2$. The reaction selectivity was around 2.

Rhodium clusters adsorbed on basic oxides such as ZnO, MgO, TiO_2 and CaO were shown to be active for ethene and propene hydroformylation (7). These complexes adsorbed on ZnO showed the following relative activities at 158°C and atmospheric pressure: $Rh_4(CO)_{12} > Rh_6(CO)_{12} > Rh_7(CO)_{16}NEt_4 > Rh_{13}(CO)_{23}H_{2-3}2NBu_4$.

$Rh(CO)_2Cp$, (Cp=cyclopentadienyl), $Rh_2(CO)_3Cp_2$ and $RhCl_3$ impregnated on ZnO showed only negligible activity. The same clusters adsorbed onto acidic oxides such as alumina, silica-alumina, and V_2O_5 had only small activity compared to the basic supports. Pretreatment consisted of evacuation at 160°C for 1 hour at 10^{-4} torr, or activation under hydrofor-

mylation conditions. Rates for propylene hydroformylation were around $6-18 \times 10^{-3}$ moles/g-Rh hr at 158°C. Evacuation produced the more active catalyst. Activation energies were reportedly between 14-16.5 kcal/mole, depending upon the starting rhodium carbonyl.

Temperature programmed desorption (TPD) studies showed that on the basic oxides, $Rh_6(CO)_{16}$ cluster decomposition did not occur at 160°C. On acidic oxides, clusters decomposed at 155-160°C, which is lower than the decomposition temperature of the pure clusters. This suggested that the basic supports stabilized the cluster and strengthened the metal carbonyl bonding.

Rhodium zeolite hydroformylation catalysts have been reported (31, 32). These investigations used $RhCl_3 \cdot 3H_2O$ exchanged onto NaY, and reported rates for ethylene and propylene hydroformylation at atmospheric pressure. However, these two studies were not in complete agreement with each other.

The results of Arai and Tominaga (31) included rates and activation energies. The catalyst was loaded to 3.7 wt.% Rh, and the reactor was charged with -10/+20 mesh particles. The contact time was 10g-Rh/hr. The selectivity to hydroformylation was poor, with hydrogenation to hydroformylation of 37.6 at 150°C. Regioselectivity (n/i) was 1.2. The

rates at 150°C were 7.0×10^{-2}, 1.0×10^{-3}, 9.0×10^{-4} moles/g-Rh hr for hydrogenation, n-butyraldehyde and iso-butyraldehyde production, respectively. It was found that the relative rates for different substrates were ethylene> propylene> butene. Activation energies calculated over 130-170°C were 8.7, 7.3 and 24.2 kcal/mole for n-butyraldehyde, iso-butyraldehyde and propane production, respectively. The catalyst was pretreated by air drying prior to reaction conditions. The infrared spectra of the catalyst revealed the $Rh(CO)_2$ - NaY species.

Takahashi and Kobayashi (32) attempted to elucidate the location of the active site by comparing the activities of ethylene and propylene on RhNaY catalysts which were pretreated differently and varied in Rh content. Table 2 presents their results. They classified the catalysts into two groups. "Type A" were catalysts which had lower propionaldehyde activation energies (E_{PA}) and selectivities (S). "Type B" were grouped together due to their higher (E_{PA}) and S values. Furthermore, a Type A catalyst produced a straight line when the ratio of ethylene hydroformylation rate (r_{PA}) was plotted against propylene hydroformylation rate (r_{BA}). Also, E_{PA} and S for hydroformylation on $RhCl_3/SiO_2$, a support with larger pores than NaY, were approximately equal to Type A values. The authors concluded

TABLE 2

Propylene Hydroformylation Over Rh-NaY Zeolites (32)

Run	Catalyst	Rh content $(10^{-6}$ mol/g cat)	Pretreatment with He-H$_2$ $(0.1 \times 10^5$ Pa, 400 K, 5 h)	10^{-6} mol min g cat			$S_{n\text{-}BA}$[b]	r_P[c] $(10^{-6}$ mol min g cat)
				$r_{n\text{-}BA}$[a]	$r_{iso\text{-}BA}$[a]	r_{BA}[a]		
1	1	50	No	0.10	0.11	0.21	0.48	0.38
2[c]			Yes	0.15	0.24	0.39	0.38	1.06
3	4	150	No	0.15	0.15	0.30	0.50	0.55
4			Yes	0.24	0.21	0.45	0.53	1.38
5	6	280	No	0.36	0.40	0.76	0.47	1.60
6[d]			No	0.35	0.41	0.76	0.46	1.60
7			Yes	0.16	0.12	0.28	0.57	1.26
8[d]			Yes	0.14	0.10	0.24	0.58	1.43
9	7	350	No	0.38	0.48	0.86	0.44	1.80
10			Yes	0.08	0.06	0.14	0.57	1.18
11	RhCl$_3$/SiO$_2$	170	Yes	0.53	0.96	1.49	0.36	1.29

Note. Reaction conditions were He–C$_3$H$_6$ (30%)–CO (10%)–H$_2$ (30%) at 400 K.

[a] Steady-state rates for the formation of *n*-butyraldehyde, iso-butyraldehyde, both butyraldehydes, and propane, respectively.

[b] The *n*-isomer selectivity is defined by $r_{n\text{-}BA}/(r_{n\text{-}BA} + r_{iso\text{-}BA})$.

[c] The pretreatment was performed for 48h.

[d] The ethylene hydroformylation was followed by the propylene hydroformylation.

that the Type A active sites resided on the external surface
or in the entrance of the pore.

On the other hand, Type B active sites were suggested to
be in the pores and inaccessible by propylene. This conclu-
sion was supported by:

1. a higher reduction in r_{BA} to r_{PA} after pretreatment
   suggested some inaccessible propylene active sites;

2. higher S for Type B suggested steric influence of the
   support;

3. a lack of change of E_A^N and E_A^I as a function of pre-
   treatment compared to the 40-56 kJ/mole range ob-
   served for E_{PA};

4. a faster rate of propionaldehyde desorption compared
   to butyraldehyde desorption suggested that the pores
   of the zeolite were not used in catalysis, for propy-
   lene hydroformylation.

Takahashi and Kobayashi found that the rhodium zeolite
catalysts were stable for up to one month without deactiva-
tion or selectivity shifts. Startup time normally took
60-80 hours. However, by preadsorbing aldehyde onto the su-
port, the start up time was reduced to less than 20 hours.
Hence, the slow rise in activity is due to the adsorption of
the product on the zeolite.

Centola et al. (33) performed propylene hydroformylation studies on cobalt exchanged NaX loaded from 1-12 wt.%. Reaction conditions were 160-220°C and 140-200 atm. Selectivities were dependent upon temperature and pressure, but were less than 1.88. Conversions were less than 1% after 6 hours contact. An intense maximum in aldehyde production rate occurred at 2 hours process time. The authors attributed this to cobalt loss. However, after steady state was reached, no cobalt appeared to elute.

2.4 METHANOL CARBONYLATION

Methanol carbonylation has been the primary reaction studied with rhodium exchanged zeolites (34 - 42). These investigations reported different types of zeolites and different ion exchange procedures, and their results were not in complete agreement with one another. However, these studies include information which may aid in th investigation of the reaction system used in this report, thus a brief discussion follows. Nefedov et al. (41, 42), Yamanis et al. (38) and Scurrell et al. (34) used NaX while Yashima et al. (35), Takahashi et al. (40), and Gelin et al. (36) used NaY.

Compilation of the results in these investigations can be summarized as follows: (43)

1. steady state was achieved in approximately 2 hours;

2. the rate was first order in methyl iodide partial pressure;

3. activation energies ranged from 13.4 to 16.7 kcal/mole, although these may be low due to mass transfer considerations (38);

4. RhNaX catalysts deactivated above 242°C;

5. RhNaY deactivated at 200°;

6. deactivation showed a non-zero order dependence for RhNaY;

7. deactivation of RhNaX followed zero order behavior.

Points 4-7 indicate that differences arise from the zeolite type. However the direct comparison is difficult due to the work being performed in separate laboratories. Studies involving the investigation of differences between NaX and NaY include Rabo (44) and Davis et. al. (43). (A discussion appears later describing the structural differences between NaX and NaY).

Higher activity was also observed for RhNaX prepared from $Rh(NH_3)_5Cl$ over that exchanged with $RhCl_3 \cdot 3H_2O$ (37). It was later shown by EXAFS (Extended X-ray Absorption Fine Structure) that the RhNaX prepared from the ammine complex was better dispersed (45). Denley et al. (45) also showed that Rh_2O_3 was the predominant species on the catalyst prepared from $RhCl_3 \cdot 3H_2O$ before and after reactivity measurements.

EXAFS revealed that the predominant form of the $(Rh(NH_3)_5Cl)Cl_2$ exchange was either a highly dispersed oxide o aquo complex immediately following the exchange. After calcination, Rh metal microcrystallites with an average particle size of 9A were observed.

Shannon et al. (46) recently performed a study on the effects of ion exchange upon the location of the rhodium in zeolite NaY. Surface and bulk rhodium content was distinguished by comparing surface rhodium analysis from XPS (x-ray photoelectron spectroscopy) with chemical analysis (CA) values for the bulk. XPS/CA values greater than unity indicated surface rhodium, whereas unity suggested a more uniform metal distribution. $Rh(NH_3)_5Cl^{2+}$, $RhCl_3(aq)$, and $Rh(H_2O)_6^{+3}$ were used as rhodium sources. The zeolites contained roughly 2 wt.% Rh. It was found that all rhodium sources produced a uniform distribution of rhodium. However, rhodium concentration and exchange temperature were critical. The $RhCl_3$ exchange conditions were $90^{\circ}C$ and Rh concentration between 0.002M and 0.006M. At this temperature, the rhodium is exchanged as $Rh(H_2O)_6^{+3}$. Previous studies in which lower temperatures and higher concentrations were used deposited substantial amounts of rhodium onto the zeolite surface. The authors suggested that the heat is required to liberate free Cl^- ions. No additional chlorine was incorporatated into the zeolite.

2.5   ZEOLITES

Faujasites are zeolites with three dimensional pore structures which have found great utility in catalysis (44,47). Zeolites are hydrated crystalline aluminosilicates of the general formula M_x $(AlO_2)_x(SiO_2)_y \cdot zH_2O$ in which M is typically a monovalent or divalent cation. This cation can be exchanged reversibly without destroying the zeolite framework.

The zeolites of interest in this investigation are the synthetic faujasites NaX and NaY. NaX has the empirical formula, $Na_{86}(AlO_2)_{86}(SiO_2)_{106} \cdot 264H_2O$, and that for NaY is $Na_{56}(AlO_2)_{56}(SiO_2)_{136} \cdot 250H_2O$. There exists no topological difference between the two. One significant distinction is that Si/Al=2.5 for NaY, whereas Si/Al=1.2 for NaX. This difference creates dissimilar electrostatic potentials within the structure. Therefore, catalytic activity can be drastically altered.

Figure 2 is a diagram of the faujasite. The alpha cage diameter for NaY and NaX is 12.5A, with pore openings of 8.9A. The beta cage has a diameter of 6.6A, with pore openings only 2.6A wide. In terms of adsorption capacity, the beta cage holds 4 H_2O molecules whereas the alpha cage holds 28 molecules. The pore openings to the alpha cage permit branched chain hydrocarbons and aromatics to pass. Further

details concerning the structural details for zeolites can be found in Breck (48) and Haynes (47).

A feature of zeolites important for catalysis is the ability to exchange the charge balancing cations for transition metals. The Si/Al ratio controls the number of cations and their location. The degree of hydration can affect the cation position also. The cations are located within the α-cage and β-cages, and on the surface. In order to entrap the rhodium complex within the pores, it is necessary to selectively place rhodium within the α-cage.

2.6   INFRARED SPECTROSCOPY

Table 3 shows the infrared band positions for functional groups important to this study. Only general IR information is provided as a reference for the reader. Band positions for specific complexes are referenced in the discussion.
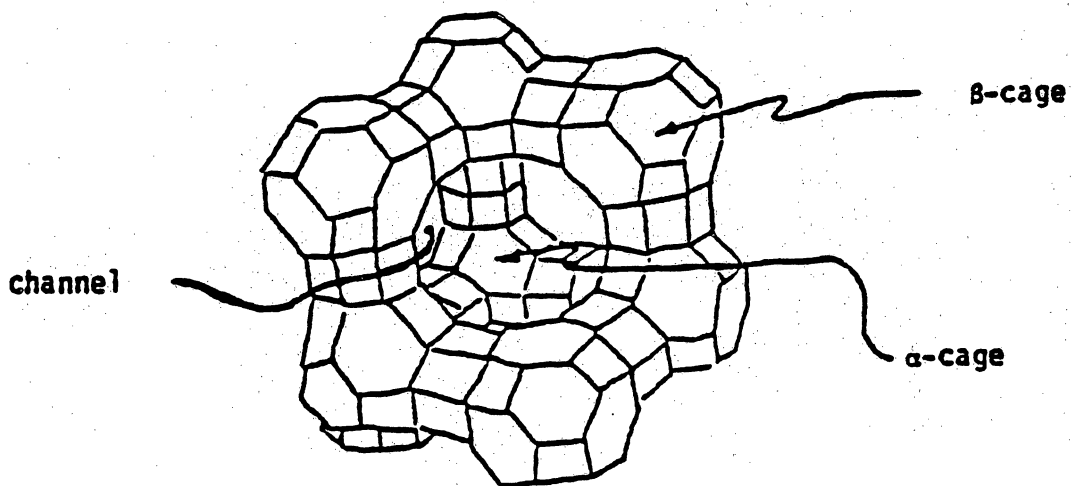
Figure 2:   Schematic Diagram of Zeolite NaX

TABLE 3

IR Frequencies for Various Functional Groups (49)

Metal Complexes	Types of Vibration	Absorption Band
M–H	metal hydride stretch	2100–1900
M–CO	carbonyl stretch	2100–1900
$\underset{\parallel}{\overset{O}{M\text{–}C\text{–}M}}$	bridging carbonyl stretch	1900–1800
$M_3(CO)$	triply bridging carbonyl stretch	1800
$\underset{\parallel}{\overset{}{M\text{–}C\ O\text{–}M'}}$	carbonyl stretch	1650
M–C–R	acyl stretch	1710–1660
M–CH$_2$–	CH$_2$ def	1430–1415
M–11	coordinated olefin	1530–1500

Hydrocarbons		
CH	stretch (aliphatic)	3000–2800
CH	stretch (unsaturated)	3100–3000
–CHO	C–H stretch	2745–2650
CH$_3$	asymmetric deformation	1465–1440
CH$_3$	symmetric deformation	1390–1370
CH	CH bend	1340
CH$_2$	scissor vibration	1480–1440
C=C	olefenic stretch	1680–1620
$\overset{O}{C=C\text{–}C\text{–}}$	carbonyl stretch	1700–1660

Chapter III

OBJECTIVES

It is apparent from the various attempts to heterogenize a homogeneous transition metal complex for the hydroformylation of propylene that the potential for success is good. The use of phosphinated polymers and phosphinated silicas is more advanced than the use of transition metals supported on unmodified inorganic supports. Due to the poor regioselectivity, simple metal supported catalysts are unattractive. Collectively, the studies on supported rhodium carbonyls do exhibit favorable behavior. Most important is the fact that stable catalysts can be formed. Ichikawa's (6-8) studies and the body of methanol carbonylation work provide direction for this investigation in that support and catalyst preparation significantly alter reactivity. However, the use of rhodium zeolites with phosphines has not been explored. Hence, the investigation of the entrapment of rhodium phosphine complexes into zeolite supports is especially appealing.

Prior to forging ahead into the immobilization of rhodium phosphine complexes into zeolites, some basic questions concerning the nature of the binary rhodium carbonyl zeolite catalysts need to be answered. Among these are:

1. What is the position of the metal within the zeolite under reaction conditions?

2. Is the active species for the heterogeneous catalyst the same as for the homogeneous case?

3. How can the performance of the catalyst be optimized if answers are known to (1) and (2)?

These are the fundamental questions to be answered in this dissertation. With these questions in mind, the following research objectives were pursued:

1. to study in a differential reaction system the catalytic activity of the rhodium exchanged zeolite NaX and NaY;

2. to study the effects of catalyst preparation on activity;

3. to determine the effects of pretreatment on catalyst performance;

4. to study by _in situ_ Fourier transform infrared spectroscopy the formation of rhodium carbonyls in order to evaluate the role of the zeolite;

5. to study by _in situ_ FTIR the catalyst under reaction conditions in order to establish the relationships between homogeneous and heterogeneous rhodium carbonyl hydroformylation catalysis;

6. to determine the location (within or on the zeolite)
    of the active catalyst by rhodium carbonyl reaction
    with size discriminating phosphines;

7. to perform preliminary studies on the effect of phos-
    phine addition to catalytic behavior.

Chapter IV

EXPERIMENTAL APPARATUSES AND OPERATING
PROCEDURES

4.1 DIFFERENTIAL REACTOR SYSTEM

Figure 3 is a schematic diagram of the differential bed reactor system used to study the catalytic activity of the catalysts. Material and equipment specifications can be found in Appendix A. A general description of the apparatus and its operation follows.

Hydrogen gas was purified by passing through a platinum catalyst chamber which reacted the trace oxygen with hydrogen to produce water. Water was then removed in a silica gel chamber. Carbon monoxide, propylene, and nitrogen were used without further purification. The flow rate of each gas was measured by a rotameter and controlled by a high accuracy valve. Each gas pressure was measured by the same pressure gauge in order to assure uniformity of gas flow. After the rotameters, the gases were mixed. The gas flow can be diverted to three locations:

1. the gas chromatograph for reactant analysis;

2. to the reactor;

3. to the FTIR flow cell.
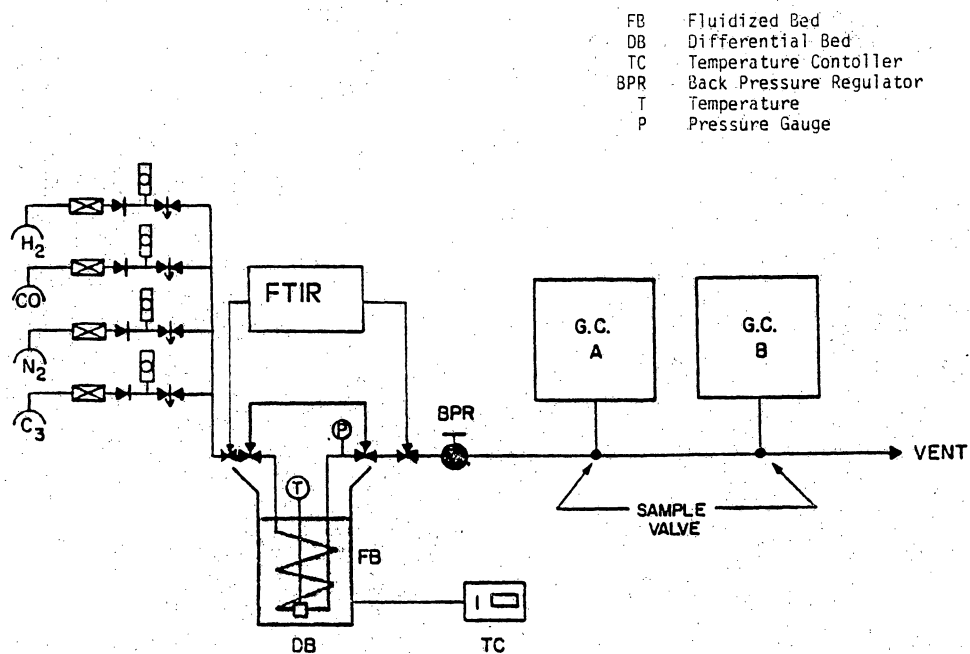
Figure 3: Flow Diagram for Differential Reactor System

For case (2), the gases were sent to the reactor which was immersed in a fluidized bed. A PID controller on the fluidized bed allowed the temperature to be held at set point ±1.0°C. The coil preceeded the reactor in order to preheat the gas. The 1/4" OD, 3" long reactor was held vertically in order to prevent chanelling of the reactant and the product gas. The product stream was then sent to the gas chromatographs for sampling or to vent. The pressure in the reactor was controlled by a back pressure regulator, and could be set up to 3 atmospheres.

Due to the small quantities of products and the difficulty of separating the butyraldehyde, iso-butyraldehyde, propylene and propane on one gas chromatography column, a two column, two sample, two integrator analysis was performed. A 20 µl gas sample was injected onto a Porasil C column which separated propylene from propane. A 500 µl sample was injected onto the Spherosil column which separated the propylene and propane (unresolved) from the two aldehydes. Each detector signal was analyzed by a digital integrator. Details of the mathematical analysis of the two signals are in Appendix E.

The flow system was such that the gases can be used for either reactor analysis or the FTIR flow cell, but not simultaneously.

The catalyst was pressed (10,000 psi) into pellets, which were then screened to -40/ + 70 mesh size. Typically, the reactor was loaded with 0.5-0.8 g catalyst. A thermocouple was imbedded into the catalyst packing in order to accurately measure catalyst temperature.

4.2 IR FLOW CELL DESCRIPTION

A Fourier transform infrared spectrometer (IBM model IR/32) was used to collect IR spectra. The optics bench sample chamber was modified to allow installation of the flow cell. Plexiglas covers replaced the original cover in order to support the cell.

Figure 4 is a schematic diagram of the FTIR flow cell gas flow system. A number of flow patterns can be achieved by proper valve manipulation sequences. The following options are available:

1. gas flow from the rotameter bank in Figure 3 can be fed to the cell at valve V3. Adjusting the back pressure regulator (BPR) allows pressures up to 30 psig under flow conditons;

2. the cell can be closed off by on/off combinations of valves V6 and V3 with valves V4, V5 and V2;

3. the cell can be evacuated;
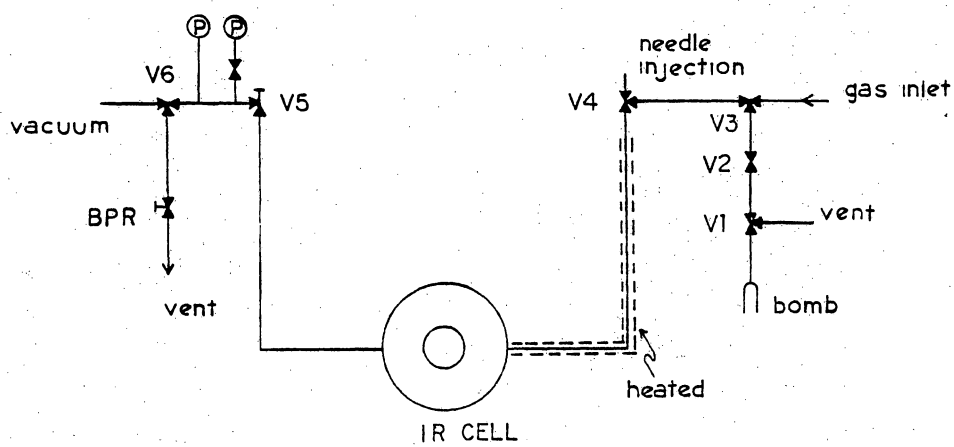
Figure 4: Flow Diagram for IR Flow Cell

4. gases or liquids can be injected via a septum port at V4;

5. bottled gases can be fed into the system unregulated via ports V1 and V2;

6. the tubing section between V4 and the cell is heated so that liquid vaporization will occur.

Appendix C contains a detailed valve position index for each derived flow pattern.

Photographs of the flow cell are shown in Figure 5 . Two Varian stainless steel flanges are used to sandwich a catalyst wafer holder. A copper gasket is used to form a seal on the knife edges of the flanges. The sample holder consist of two circular, aluminum disks 0.030" thick with 1/4" holes in the center. One disk has a 0.010" recess around the center hole where the catalyst is placed. 0.008" deep grooves join the center hole and outer edge in order to allow gas flow. On the back side of each disk are 25 mm x 2 mm IRTRAN-2 windows. Wavenumbers above $700cm^{-1}$ can be observed with these ZnS crystals. On the back side of windows, a 1" x 3/4" x 1/8" Viton o-ring is placed, which fits into the flanges. Hence, the entire cell is sealed at the two o-rings and the copper gaskets. Physical limitations are $200^{o}C$, set by the viton o-rings, and 50 psig, which is set by the optic window thickness. Five round 1/8" OD x 2"
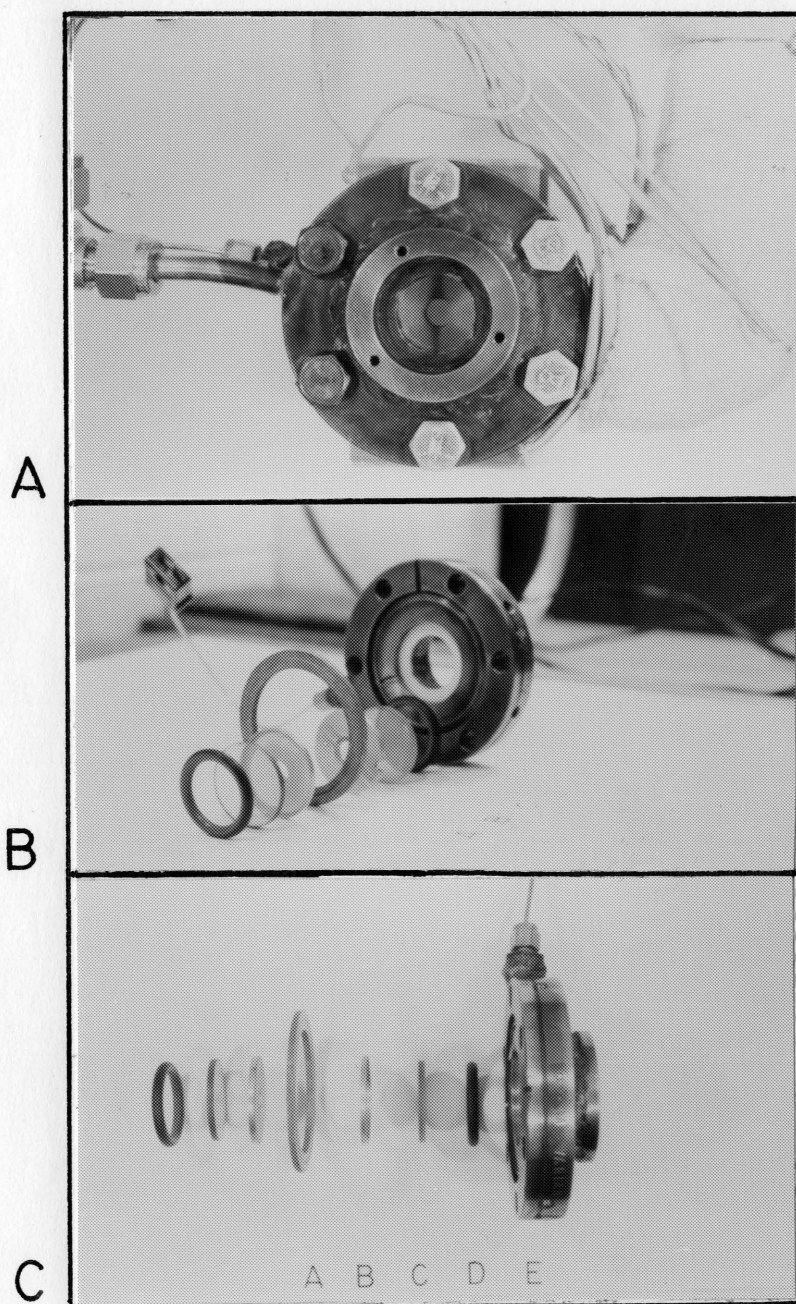
Figure 5:   Pictures of the IR Flow Cell

a) assembled; b) exploded view of cell; c) A) copper gasket, B) aluminum holder, C) IRTRAN-2 window, D) O-ring, E) flange

long, 100 W fire rods are used for heating the cell. Each flange contains 2 fire rods, while the fifth is used to heat the inlet stream (underneath glass wool insulation on right of Figure A). Temperature is controlled by a 10 amp Variac. Settings at 28.5 and 42 result in $120^{\circ}C$ and $190^{\circ}C$, respectively. The relation between temperature ($^{\circ}C$) and the Variac settings is linear. Cell temperature is measured by Type J thermocouple at the aluminum sample holder.

The catalyst is prepared by sieving the powder through a 325 mesh screen. A 3/8" OD wafer is made by pressing the powder to 30,000 psi. The wafer has a density of 5-6 mg/cm^2. Wafer thickness is approximately 0.004 inches. Normally, transmissions of 25% or higher are recorded.

4.3 CATALYST PREPARATION

Rhodium was exchanged into NaX and NaY zeolites, purchased from Strem Chemical, and silica under a variety of conditions. Table 4 shows the various conditions which were used for rhodium incorporation into the supports. Table 4 will serve as the master table for subsequent discussions. Heretofore, reference to a particular catalyst will be by catalyst letter and support. For example, catalyst A in Table 4 will be called AY or AX.

TABLE 4

Methods of Catalyst Preparation

Catalyst	Rh Source	Support	$T(^{o}C)$	pH	NaCl	Time	% Rh
A	$RhCl_3 \cdot 3H_2O$	NaX,NaY	90	6	0.1N	5	1-4
B	$RhCl_3 \cdot 3H_2O$	NaY	90	4	0.1	5	4
C	$RhCl_3 \cdot 3H_2O$	NaY	90	8	0.1	5	4
D	$RhCl_3 \cdot 3H_2O$	NaY	90	6	0.2	5	4
E	$RhCl_3 \cdot 3H_2O$	NaY	90	6	0.0	5	4
F	$RhCl_3 \cdot 3H_2O$	NaX,NaY	90	6	0.1	24	4
G	$RhCl_3 \cdot 3H_2O$	NaY	90	6	0.1	0	4
H	$RhCl_3 \cdot 3H_2O$	NaX,NaY	90	4	0.0	5	1,4
I	$(Rh(NH_3)_5Cl)^{2+}$	NaX,NaY	50	8	--	24	1
J	$(Rh(NH_3)_5Cl)^{2+}$	NaY	50	8	--	5	1
K	$(Rh(NH_3)_5H_2O)^{3+}$	NaX,NaY	50	8	--	24	1
L	$(Rh(NH_3)_5H_2O)^{3+}$	NaY	95	8	--	24	1
M	$(Rh(NH_3)_5H_2O)^{3+}$	SiO_2	80	8	--	24	1
N	$(Rh(NH_3)_5H_2O)^{3+}$	SiO_2	50	8	--	24	1

For each exchange, the procedure was similar. Prior to exchange, zeolites were slurried in distilled water, filtered and dried in air at 120°C. This served to remove any impurities in the commercial product. For catalysts A-H, several grams of zeolite were slurried in 100-150 ml of salt solution (some were without NaCl) and heated to 90°C. The $RhCl_3 \cdot 3H_2O$ was dissolved in 100- 150 ml distilled water. Addition of the rhodium solution was made dropwise over 1.5-2 hours. The zeolite-rhodium slurry was maintained at 90°C for 0, 5, or 24 hours. For the 5 hour exchange, the solution was cooled to room temperature and stirred for another 20-24 hours. The zeolite slurry was filtered and washed with at least two liters of distilled water to remove NaCl. The filter cake was dried to a free flowing powder in an oven with circulating dry air at 120°C for 24 hours.

Cation exchange of $(Rh(NH_3)_5H_2O)^{3+}$ and $(Rh(NH_3)_5Cl)^{2+}$ for Na^+ in NaX and NaY was performed by dissolving the salt in water and adding to a water slurry of the zeolite. The temperature (50 or 95°C) was maintained overnight after which the zeolite was filtered and washed with water. The powder was then dried at room temperature.

Cation exchange of $(Rh(NH_3)_5H_2O)^{3+}$ with silica was performed by dissolving the salt in aqueous NH_4OH which contained slurried silica. The temperature was held constant

at 50 or 80°C overnight after which the solid was filtered, washed and dried at room temperature.

The rhodium content of the solid catalysts was determined by atomic absorption spectroscopy after acid digestion of the solid with acid.

4.4   CATALYST PRETREATMENT

The catalysts were pretreated by many methods, however, four were used repeatedly. The following four pretreatments were duplicated in the IR cell. The main purpose for the use of an IR flow cell was to be able to subject the catalyst in the IR to the same conditions as catalysts placed in the differential reactor system. With this technique, it was possible to study the catalyst surface under a variety of treatments, with the intention to correlate predominant surface species with activity. A description of the most frequently used catalyst treatments follows.

4.4.1   Precarbonylation

The flow system was pressurized to 30 psig with carbon monoxide. Total flow rate was approximately 15-20 ml/min STP. Once the pressure was stable, the temperature was raised to 120°C. In both the flow cell and the reactor, heating from ambient temperature to 120°C could be performed in 30 minutes.

4.4.2   Air Dried

The air purge system for the IBM IR/32 was used as a dry air source (see Appendix C).   The head pressure at the flow system inlet was 5-8 psig.   The catalyst was heated to $190^{\circ}C$ for 5 hours. $190^{\circ}C$ was attainable in roughly 45-60 minutes. The catalyst was then cooled under air flow to $150^{\circ}C$. N_2 flow at 30 ml/min STP for 15 minutes was used to remove O_2. Following N_2 flow, either CO or full reactant flow was then initiated.

4.4.3   Nitrogen Pretreatment

The catalyst was heated to $120^{\circ}C$ under a N_2 flow.   At $120^{\circ}C$, a full reactant stream was started while the system was heating further to $150^{\circ}C$.

4.4.4   Hydrogen/Nitrogen Pretreatment

The catalyst was purged with 10% H_2 in N_2, then heated to $127^{\circ}C$ for 5 hours.   Reactants were then passed over the catalyst.

4.5 HYDROFORMYLATION CONDITIONS

For catalytic activity studies, several sets of hydroformylation conditions were used. However, one was used most frequently. Unless specified otherwise, the reaction conditions were a 3:3:2:1 partial pressure mix of propylene, hydrogen, nitrogen, and carbon monoxide at ambient pressure and 150°C. Total gas flow was 45 ml/min STP.

Chapter V

RESULTS

5.1 RHODIUM CARBONYL FORMATION

The results from in situ flow IR studies are presented here. Assignment of these bands to complexes is withheld until the discussion (Chapter 6). Table 10 in Chapter 6 contains the band positions for complexes formed in this study as well as those reported in the literature.

5.1.1 RhNaY

In Figure 6, a set of IR spectra taken during carbonylation as a function of time and temperature for catalyst AY is shown. Spectrum A, taken at $95^{\circ}C$, shows weak bands at 2069, 2050, 2025 and 1834 cm^{-1} and a sharp band at 2086 cm^{-1}. Upon heating the catalyst to $110^{\circ}C$, the 2070-2020 cm^{-1} region includes more distinct bands while a new band at 1768 cm^{-1} appears. The band at 1768 cm^{-1} continued to grow in intensity with further heating of the sample. Simultaneously, the band at 1834-7 cm^{-1} disappeared. After 10 hours, no spectral changes were observed. The final spectrum featured bands at 2099, 2069, 2020 and 1765 cm^{-1}.

Spectra in Figure 7 were taken at steady state for catalysts AY and IY. The same catalyst as in Figure 6 was sub-
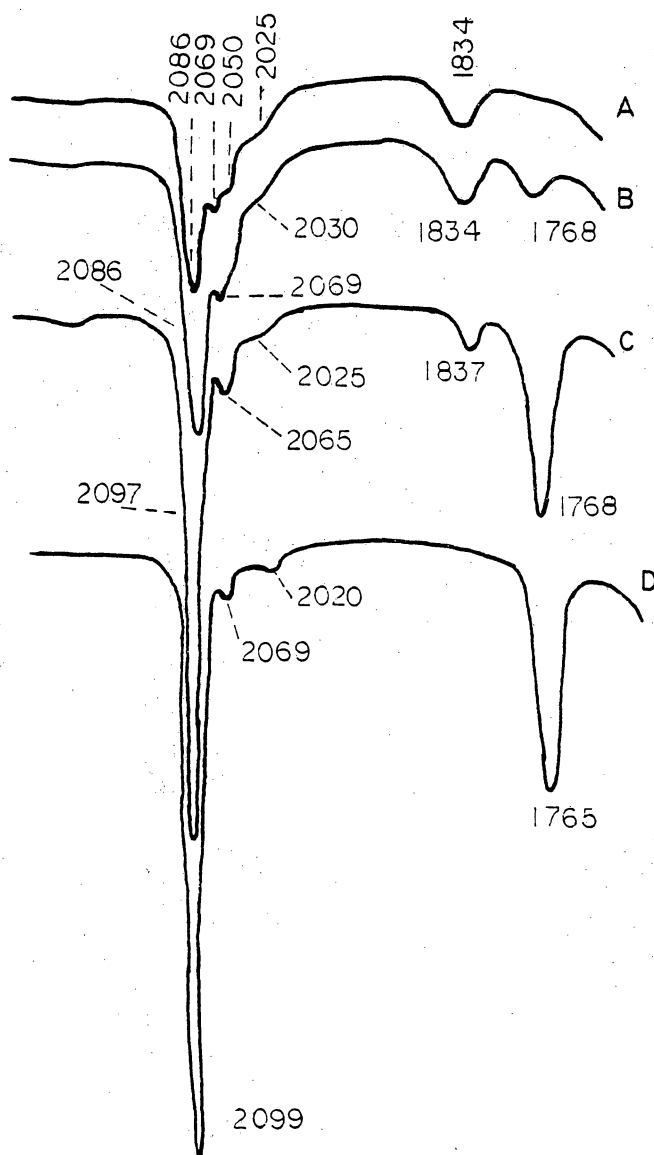
Figure 6: Carbonylation of RhNaY under 30 psig CO

a) T=95°C; b) T=110°C; c) T=120°C; d) T=120°C for 10 hours

jected to carbonylation by the air drying method (spectrum A). For Figure 7b, the catalyst IY was also subjected to the same conditions as A. The catalyst IY precarbonylated spectrum is shown in C. The intermediate spectra for C are approximately the same as shown in Figure 6 .

Figure 8 shows the carbonylation of catalyst HY (recall the catalyst nomenclature: HY is not the acid form of NaY but rather preparation H using NaY listed in Table 4). At 93°C, a sharp band at 2082 cm^{-1} has developed with a shoulder at 2050 cm^{-1}. Weak bands are also present at 1865 and 1832 cm^{-1}. After being at 150°C for 50 minutes, the spectrum contained several new bands. The 2082 band had moved to a higher frequency to 2096 cm^{-1}, and the 2042 cm^{-1} band was resolved. Shoulders appear at 2110 and 2025 cm^{-1} on these two resolved bands. A strong band at 1762 cm^{-1} was also present. The shoulder 1865 cm^{-1} has disappeared while the 1837 cm^{-1} band had intensified. Steady state was reached after 8 hours. The 1837 cm^{-1} band disappeared. Resolved bands were present at 2112, 2099, 2047 and 2022, and 1763 cm^{-1}.
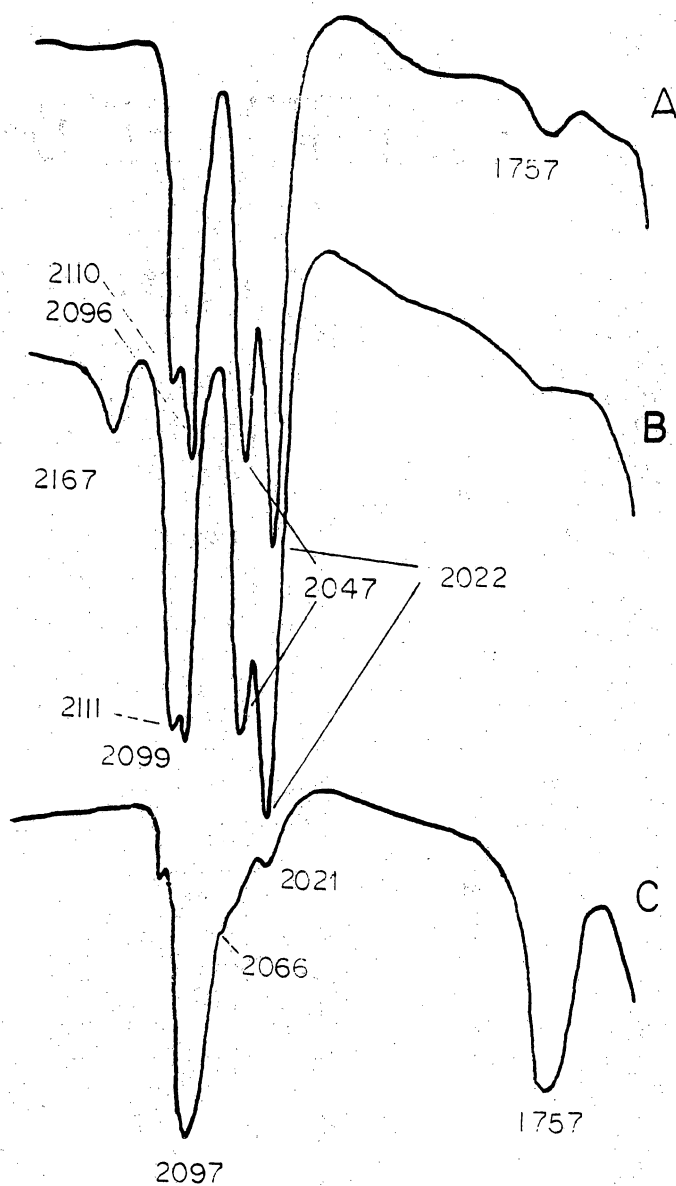
Figure 7: Precarbonylated Catalysts

a) RhNaY from $RhCl_3$ $3H_2O$, dried; b) same as A, but prepared from $(Rh(NH_3)_5Cl)^{2+}$; c) RhNaY from ammine chloride, precarbonylated

5.1.2   RhNaX

Figure 9 shows the spectra taken during the carbonylation of catalyst AX.   Spectrum A is simply the RhNaX zeolite. Bands at 2096 and 2016 cm^{-1} intensify with time.   A slight, broad band developed slowly at approximately 1830 cm^{-1}.

5.2   CATALYTIC ACTIVITY

5.2.1   Active Catalysts

Of the different preparative techniques used to incorporate rhodium into the zeolite, only those exchanges using $RhCl_3 \cdot 3H_2O$ as the rhodium source formed stable hydroformylation catalysts.   Hence, this section presents the results for these active catalysts as a function of preparation pH, NaCl content, zeolite type and catalyst pretreatment.

Following precarbonylation of catalyst AY, a reactant mixture of 3:3:2:1 propylene, hydrogen, nitrogen, and carbon monoxide at a total flow rate of 45 ml/min STP was started. After several hours at 120°C, no hydroformylation activity was observed and the temperature was increased to 135°C. No hydroformylation activity was observed after several hours. The catalyst was then heated to 150°C. After approximately 1 hour, hydroformylation activity was seen. Figure 10 shows the rate behavior for hydrogenation, and iso-butyraldehyde and n-butyraldehyde formation as a function of time at
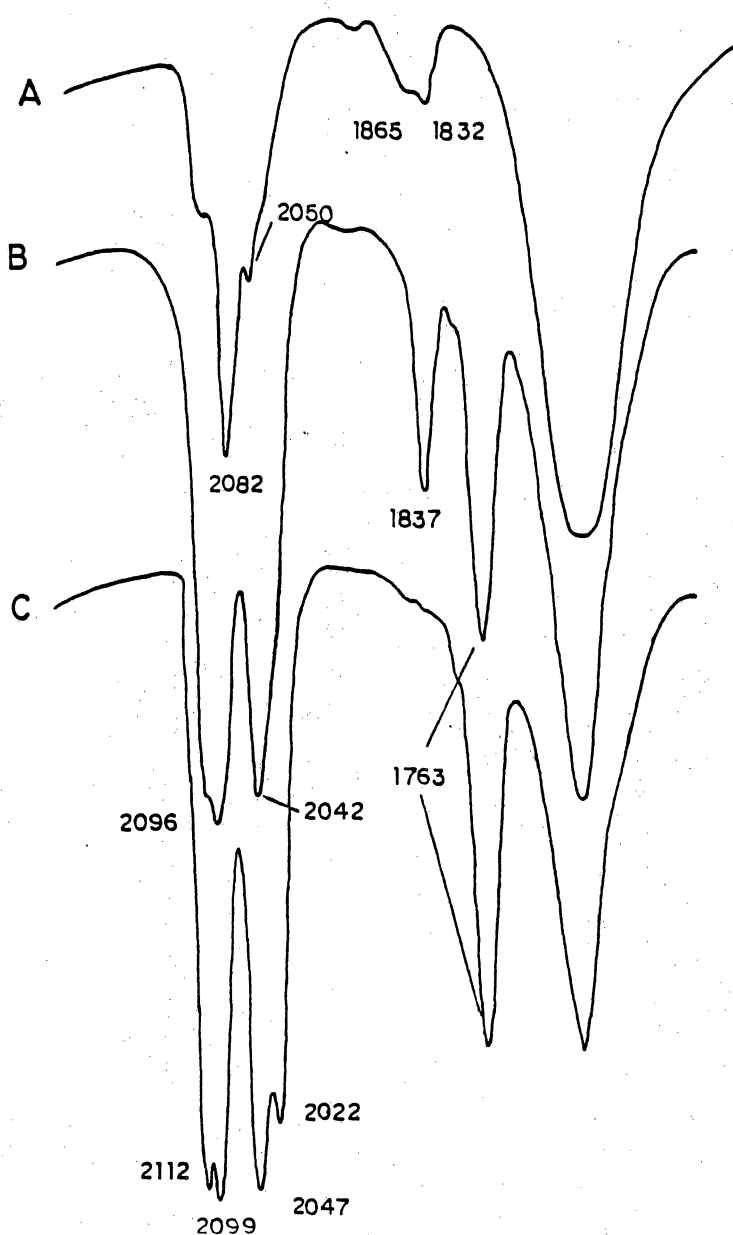
Figure 8:   Catalyst HY Precarbonylated

a) T=93°C; b) 50 minutes at 120°C; c) 8 hours at
120°C, (steady state)
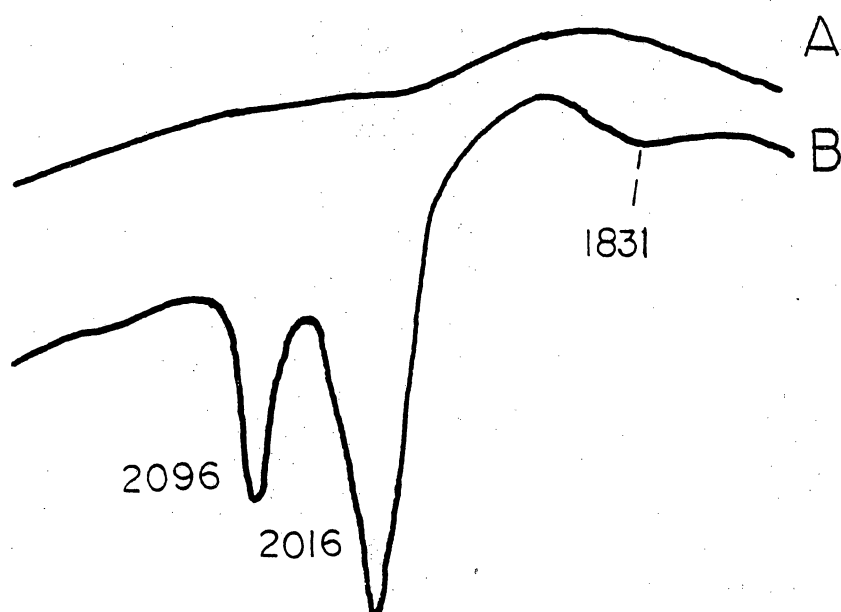
Figure 9:   Carbonylation of Catalyst AX

a) blank zeolite at room temperature; b) after 12
hours under CO

150°C. Hydrogenation activity declined as the butyraldehyde rates increased. The iso-butyraldehyde rate passed through a maximum while the n-butyraldehyde rate slowly increased. Steady state for all three reactions occurs after 18-20 hours. Table 5 summarizes the reactivity data.

Although the catalyst requires 150°C to activate, the catalyst remains active as low as 80°C. Activation energies calculated from rates over this region show no curvature in the Arrhenius plot as seen in Figure 11 . Activation energies for hydrogenation, (E_A^H), iso-butyraldehyde (E_A^I), and n-butyraldehyde (E_A^N) were 21.0, 11.4 and 9.2 kcal/mole, respectively.

It is shown in Figure 12 that the conversion varied linearly with contact time. The conversion was recorded at 45 ml/min STP and at 90 ml/min STP. Conversion was halved when the flow rate was doubled.

Catalyst AY was pretreated with H_2 at 100°C for several hours. A mix of propylene and hydrogen was converted completely to propane. Since rhodium metal is an excellent hydrogenation catalyst, metallic rhodium was believed to be the dominant form of rhodium. Upon exposure to hydroformylation reaction conditions at 150°C, no aldehydes were produced, and the hydrogenation activity decreased appreciably to around 1-2% conversion.
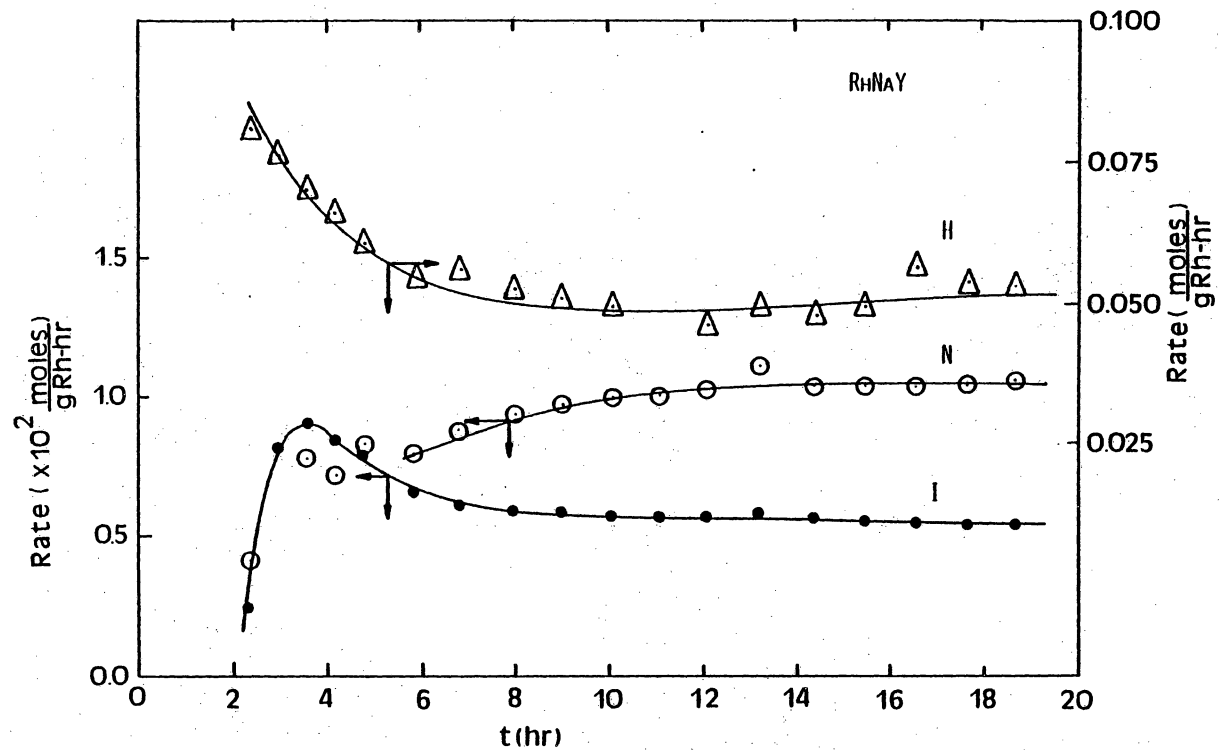
Figure 10: Reaction Rates as a Function of Time for RhNaY

TABLE 5

Reactivity Data For Catalyst AY

Pretreatment	Product	Rate[a]	E_A[b]
Precarbonylated	C_3H_8	5.3×10^{-2}	21.0
	$n-C_4H_8O$	1.0×10^{-2}	9.2
	$i-C_4H_8O$	5.4×10^{-3}	11.4
H_2 at 100°C[c]	C_3H_8	2.3×10^{-2}	18.0[c]
	$n-C_4H_8O$	---	---
	$i-C_4H_8O$	---	---

[a]At 150°C, 1 atmosphere; (moles/g-Rh hr)
[b]At 120-150°C; (Kcal/mole)
[c]For 0.5 hours
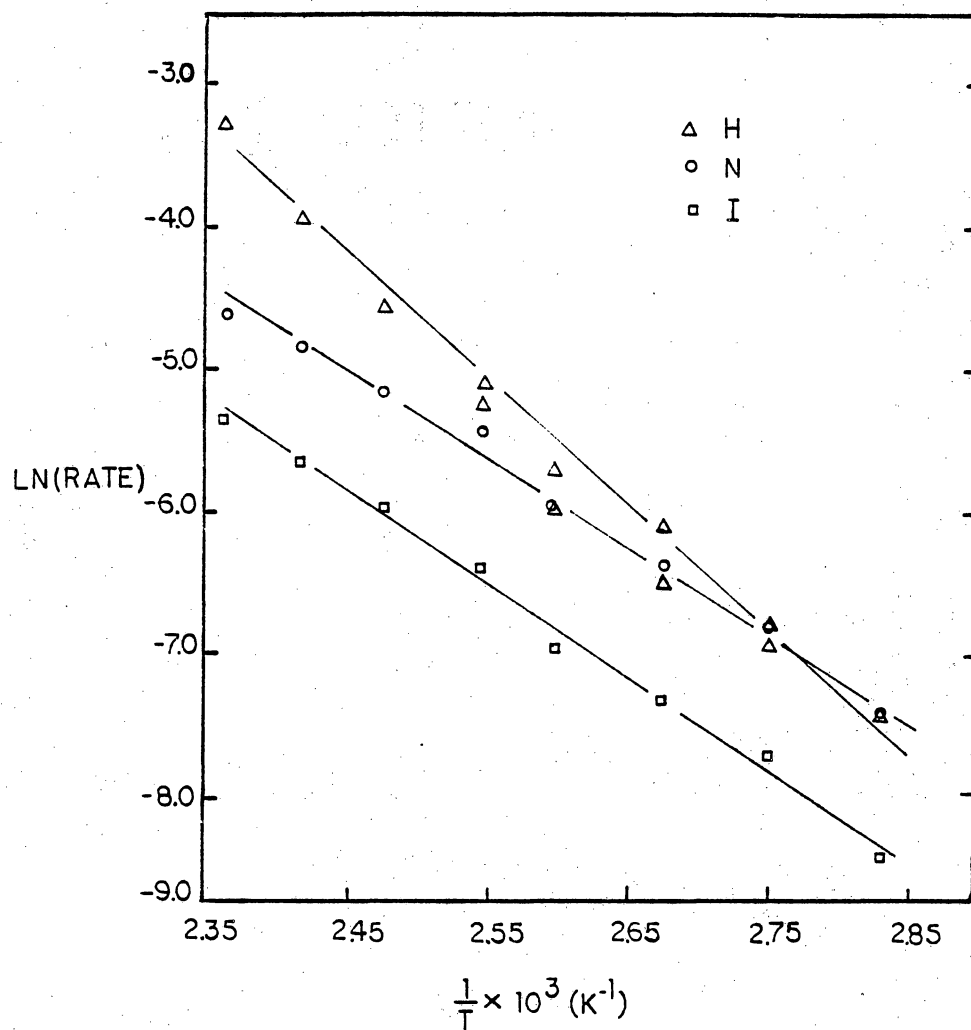
Figure 11: Arrhenius Plot for Catalyst AY
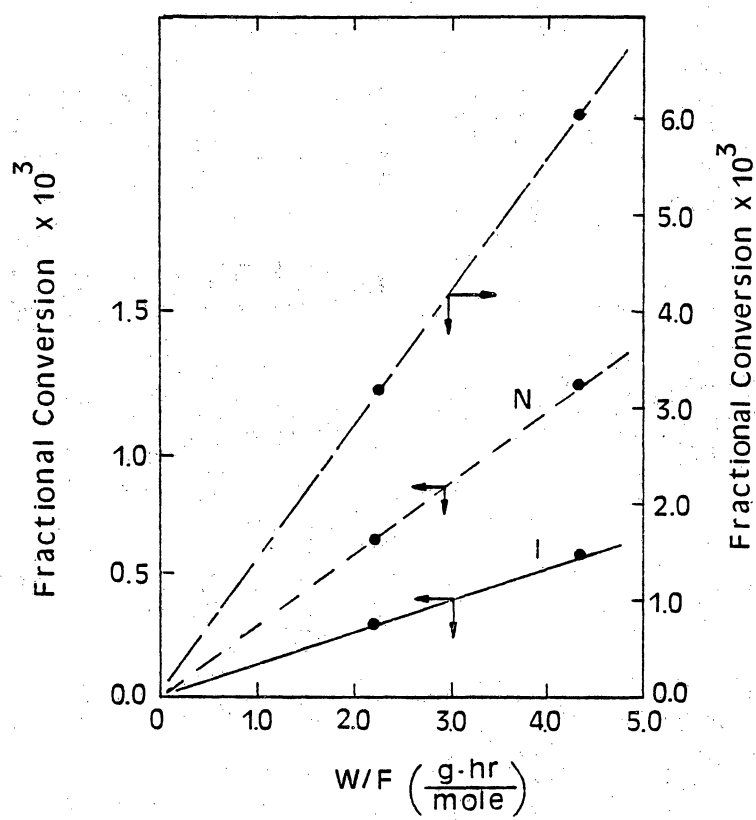
Figure 12:   Conversion versus W/F

TABLE 6

RhNaY (AY) Reactivity for Different Pretreatments

	CO	Dried	N_2	H_2/N_2
r_H x 10^2 (moles/g-Rh hr)	4.5	1.94	2.66	0.62
r_I x 10^3 (moles/g-Rh hr)	4.8	1.11	3.91	0.27
r_N x 10^3 (moles/g-Rh hr)	8.3	2.04	8.67	0.37
E_A^I (kcal/mole)	---	12.1	14.9	---
E_A^N (kcal/mole)	---	10.3	13.7	---
n/i	1.73	1.84	2.21	1.37
Hydrogenation/ Hydroformylation	3.44	6.16	2.11	10.2

Table 6 presents the reactivity data for catalyst AY which had been pretreated by the four methods discussed previously. Rates for the unreduced catalysts do not vary widely. Activation energies are slightly higher than those in Table 5 . Regioselectivity and selectivity were poorest for the H_2/N_2 treated catalyst (1.37 and 10.2, respectively). Of the unreduced catalysts, the nitrogen treated regioselectivity was slightly higher at 2.21.

Table 7 illustrates the effect of pH, NaCl and weight loading on catalytic activity. Adjusting the rhodium zeolite slurry to pH=4 (catalyst BY) prevented hydroformylation activity, while maintaining the pH at 8 (catalyst CY) had no effect on rates or selectivities.

Precarbonylation of catalyst HY, 4 wt.% Rh, failed to produce butyraldehyde. However, approximately 10 unidentified products were observed. Retention times for the majority of these were between propylene and n-butyraldehyde. 1 wt.% loadings of catalyst HY were also tried, but they were inactive.

A NaY slurry at $90^{0}C$ was pH adjusted to 4 with HCl addition and stirred for 5 hours. Exposing this catalyst to reaction conditions yielded roughly the same distribution of products seen for catalyst HY.

TABLE 7

Rhodium Trichloride Exchanges at 95°C

	AY (pH=6)	BY (pH=4)	CY (pH=8)	DY 0.2N NaCl	EY No NaCl
$r_H \times 10^2$	5.3	NA	3.8	---	3.22
$r_I \times 10^3$	5.4	NA	4.7	---	2.28
$r_N \times 10^3$	10.0	NA	9.69	---	5.4
n/i	1.9		2.05	2.0	2.37
$r_H/(r_I + r_N)$	3.4		3.7	---	4.2
E_A^H	21.		17.1	---	25.9
E_A^I	11.4		12.8	---	14.6
E_A^N	9.2		11.6	---	13.6

* Products were 2-methyl-3-hexanone and 4-heptanone
** Required 56 hours to reach steady state
NA denotes "not active"
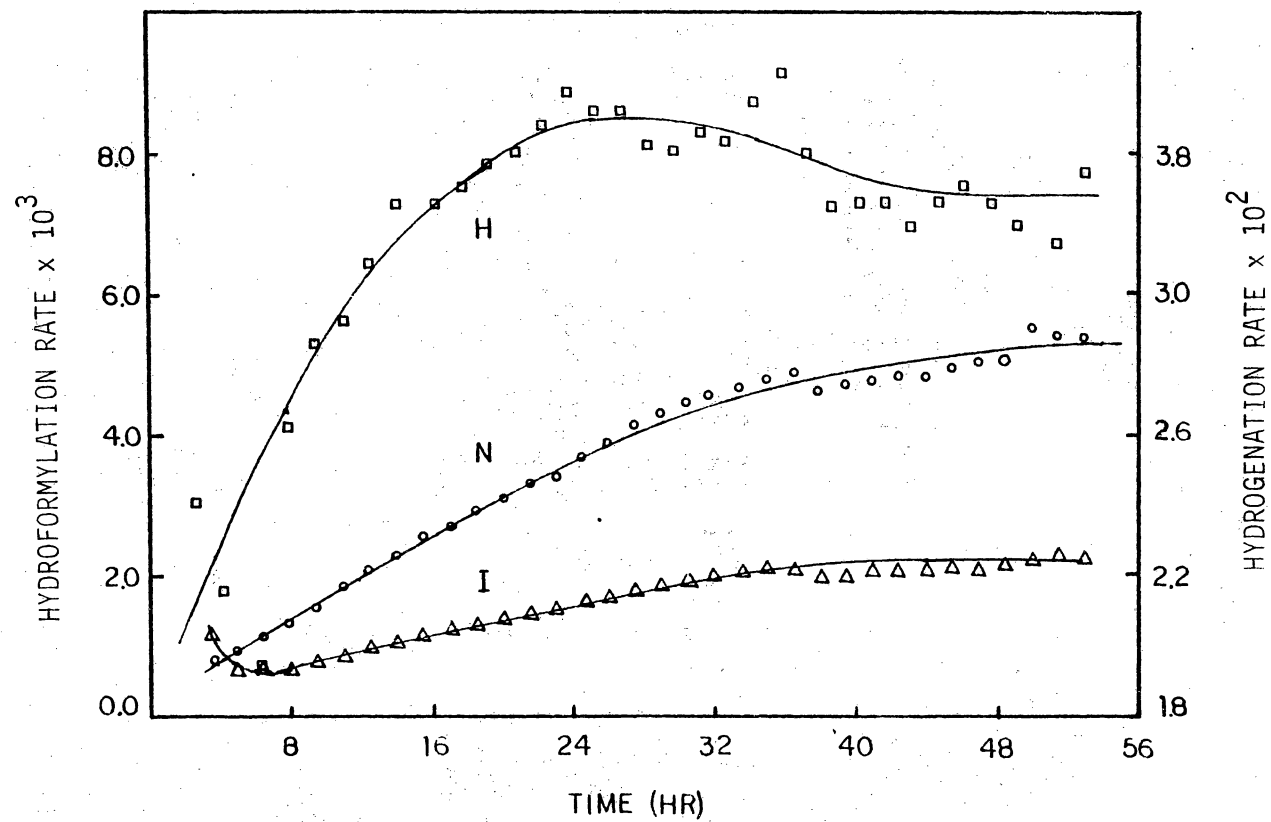
Figure 13: Startup Curve for RhNaY Prepared in Absence of NaCl

NaCl concentration had a pronounced effect on activity. In the absence of NaCl (catalyst EY), the steady state rates were not altered, although it required 56 hours in order to obtain steady state (see Figure 13). Regioselectivity was 2.37. A 0.2N NaCl concentration (catalyst DY) changed the final product distribution. Aldehydes were not detected in the chromatogram, but 2-methyl-3-hexanone and 4-heptanone were observed in a 1:2 ratio.

NaY was washed in 0.1N NaCl at 90°C for several hours, then filtered and dried. A hydroformylation reactant stream bubbling through a 50:50 solution of the two butyraldehydes was passed over the catalyst. The two ketones were observed in the product stream.

In general, the ammine exchanges failed to activate. One method did, however, produce a burst of activity. Catalyst IX was precarbonylated and exposed to reaction conditions for several hours. Roughly 1.0 ml of distilled water was injected into the reactant stream. Immediately, the catalyst exothermed 20°C. A sample taken 5 minutes after this exotherm showed iso- and n-butyraldehyde production. Regioselectivity was 3.0, a significant increase above the values observed for catalyst AY. The catalyst deactivated to zero activity within an hour. A second injection of water again promoted a rise in hydroformylation activity. A third, however, failed to initiate activity.

Catalyst HY was pretreated according to the H_2/N_2 treatment. Whereas this catalyst failed to activate following precarbonylation or the N_2 treatment, this pretreatment activated hydroformylation production. During the first several hours, numerous unidentified products were formed. These were absent after 5 hours. The n/i ratio was only 1.17 while 4-heptanone and 2-methyl-3-hexanone were produced in a 2:1 ratio. The rates for aldehyde and ketone formation were approximately the same as the aldehyde rates for catalyst AY. The total ketone rate was roughly five times the aldehyde production rate.

5.2.2 Side Reactions

A number of other compounds were formed on catalyst AY. During startup of the catalyst, gas chromatograph peaks appeared before and after the aldehydes eluted. At steady state, only compounds with much longer retention times were observed. The product stream was analyzed by online gas chromatograph-mass spectrometry in order to help assign these side products. The mass spectra are shown in Appendix D. Two startup products are 2-propanol (see Figure 49) and 2-pentene (see Figure 50). Mass spectra for several other compounds have not been positively assigned. These products have molecular ion peaks at 84 (2 products), 86, and several

at 100 (see Figures 51-54). As the catalyst approaches steady state, five products other than propane and the two butyraldehydes which are formed are iso-butanol, n-butanol, 2,4 dimethyl pentanone, 2-methyl-3-hexanone, and 4-heptanone (see Figures 55-57).

5.2.3 Partial Pressure Analysis

It was desired to determine the rate dependencies of the partial pressure of propylene, hydrogen and carbon monoxide for catalyst AY. Rates were obtained from propylene and CO partial pressures at 1/3, 2/9 and 1/9 atm, while H_2 was varied twice at 1/3 and 2/9 atm. The catalyst was brought to steady state at 150°C in 20 hours. After steady state, rates were collected at 135 and 120°C. The catalyst was heated back to 150°C and allowed to once again reach steady state. Partial pressures were then adjusted. N_2 makeup gas was used to maintain a constant contact time.

The results of the study are presented in Table 8 . A nonlinear least squares program in SAS was used to calculate the parameter estimates (see Appendix F for the computer program). All three rates are first order dependent on olefin concentration. Hydrogen concentration exponents were 0.30, 0.40 and 0.48 for hydrogenation, iso-butyraldehyde and n-butyraldehyde production rates respectively. CO inhibits

all three rates approximately equally, with the exponent ranging from -0.70 to -0.72.

5.2.4   RhNaX Catalysts

The RhNaX catalysts (AX) prepared from the $RhCl_3 \cdot 3H_2O$ were not subjected to the extensive study as the RhNaY (AY) catalyst. This was due mainly to the inability to satisfactorily reproduce results from one batch of catalyst to the next. At the onset of this study, rate data was collected for AX and AY. The startup curve for catalyst AX appears in Figure 14 . Note that the startup behavior was similar to AY (see Figure 10). The iso-butyraldehyde rate proceeded through a more intense maximum than formed for catalyst AY. Rates for hydrogenation, iso-butyraldehyde and n-butyraldehyde production were 2.8×10^{-2}, 0.8×10^{-3} and 1.6×10^{-3} moles/g-Rh hr respectively. E_A^H, E_A^N and E_A^I were 25.0, 9.7, and 11.7 kcal/mole, respectively. The selectivity and regioselectivity were 11.7 and 2.0. These results were reproduced for this batch of catalyst.

The catalytic activity data obtained from different batches varied widely. Only loadings targeted at 4 wt.% Rh were active. In general, the high activity and selectivities reported above were not attained. Regioselectivities ranged from 0.20-1.68. Parameters which were varied includ-

TABLE 8

Parameter Estimates for the Power Law Model

$$r = Ae^{-E_a/RT}(C_3)^\alpha (H_2)^\beta (CO)^\gamma$$

	r_H	r_I	r_N
A	4.12×10^6	1356.4	1855.4
E_a(kcal/mole)	15.7	10.97	10.75
α	1.01	1.0	0.97
β	0.35	0.40	0.48
γ	-0.713	-0.70	-0.72
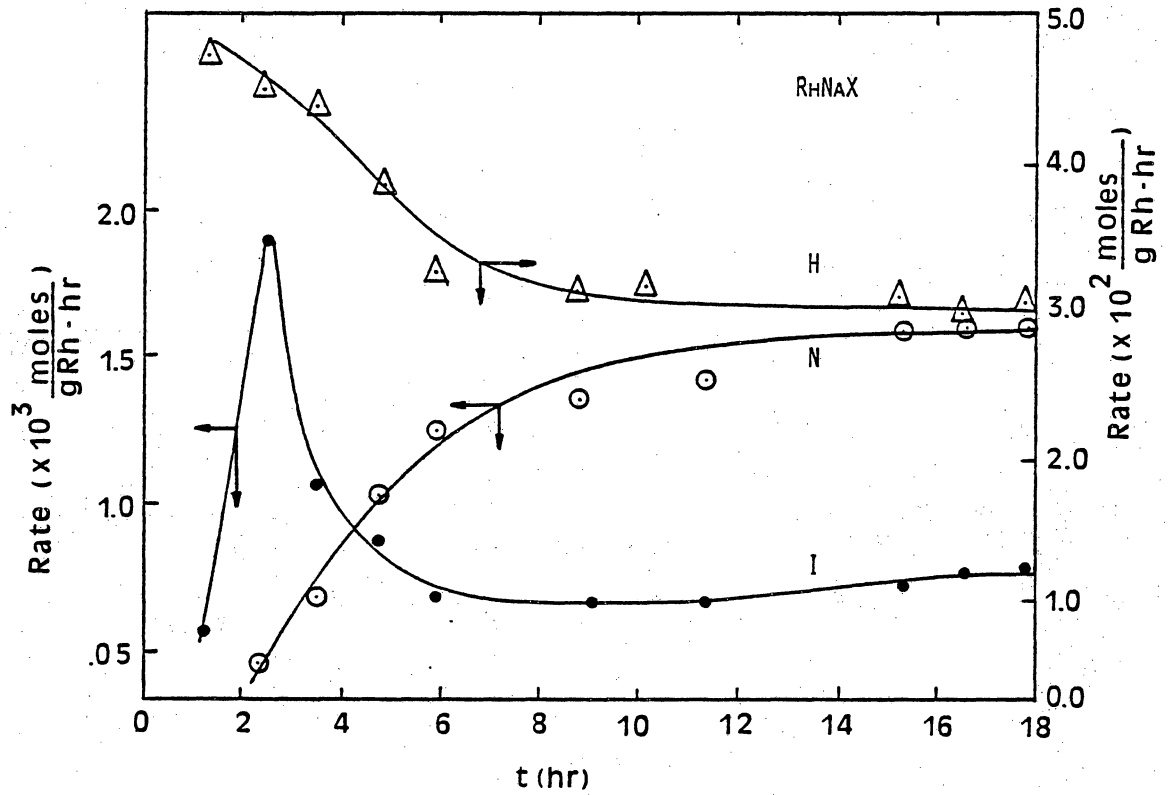
Figure 14: Reaction Rates as a Function of Time for RhNaX

ed washing the zeolite, weight loadings, aging of the cata-
lyst and different pressure used during pelletizing the ca-
talyst.

5.2.5 Rhodium On Silica

Rh was impregnated onto SiO_2 under the conditions shown
for M/SiO_2 and N/SiO_2. Rhodium on silica material was also
obtained from Dr. Robert Burwell of Northwestern University.
(This was made under conditions similar to M). Pellet size
was less than 200 mesh. Only Dr. Burwell's material and ca-
talyst M were active hydroformylation catalysts. Rhodium
supported silica showed behavior similar to the rhodium
zeolite during startup. Regioselectivity and selectivity
were 1.8 and 11.2, respectively. Activation energies were
E_A^I=11.9 and E_A^N=12.9 over 130 to $160^{0}C$ for Burwell's ca-
talyst. Activation energies were not calculated for M/SiO_2.

5.2.6 Inactive Catalysts

Catalysts BX, HX, HY, I-L and N were not active. This
broadly covers all of the ammine exchanges onto zeolites.
As seen from Table 4, these exchanges included variations of
rhodium source, weight loadings, pH, NaCl, zeolite type,
temperature, and time.

Different pretreatments were also attempted. Frequently, O_2, N_2 or air was used at high temperature in order to drive ammonia ligands off the rhodium or to simply dry the zeolite. Attempts using these pretreatments included:

1. drying catalyst KY, 4 wt.% in air at 400°C, then cooling prior to precarbonylation;

2. drying KY in air at 400°C, cooling at 150°C, then starting reaction conditions;

3. heating IY and IX in oxygen at 400°C, then precarbonylating;

4. precarbonylating catalysts KX, KY, LY, (1 wt.% Rh) and 4 wt.% KY;

5. catalyst BX was precarbonylated and heated in air to 250°C prior to precarbonylation.

None of these procedures produced active hydroformylation catalysts.

5.2.7   Phosphine Modified Rhodium Zeolites

Six experiments were performed during which phosphines were added to catalyst AY. Both dimethylphenylphosphine (DMP) and n-hexyldiphenyl phosphine (HDP) were used. Phosphines at approximately 2-3 times the stochiometric amount of rhodium charged into the reactor were injected into the reactant stream. Table 9 summarizes the experimental condi-

tions.   A qualitative description of these experiments is given below.

In experiment A, catalyst AY was precarbonylated and allowed to reach steady state as shown in Figure 10 .   Next, 0.15 ml of HDP was injected into the stream.   No change in product distribution was observed until 3 hours later. Iso-butyraldehyde production was immeasurable, while n-butyraldehyde and n-butanol rates were around one half of their steady state values.   At the same time, production of 4-heptanone and 2-methyl-3-hexanone had tripled.   After several hours, only n-butyraldehyde and 4-heptanone were present in significant quantities.   The 4-heptanone to 2-methyl-3- hexanone ratio was 23:1.   The catalyst then began to deactivate, and was completely unreactive after 10 hours (following the HDP injection).

After steady state was reached with AY, DMP was injected (experiment B).   The reactor exothermed by $2^{\circ}C$ for only 3 minutes.   A sample taken 5 minutes later showed an order of magnitude increase in activity.   Only a slight enhancement of selectivity was observed.   The catalyst was still producing measurable quantities of only n-butyraldehyde and n-butanol 40 minutes after the injection, but completely deactivated within one hour.   A second injection of DMP failed to produce any significant changes.

TABLE 9

Summary of Experimental Conditions for Phosphine Modified
Catalytic Runs

Experiment	Phosphine	T_{inj}	Precarb.	S.S.*	Bubbler
A	DMP	150	Yes	Yes	No
B	HDP	150	Yes	Yes	No
C	DMP	25	No	No	No
D	DMP	25	No	No	Yes
E	DMP	150	Yes	No	No
F	DMP	150	Yes	No	Yes

* steady state

The catalyst was exposed to DMP at 25°C along with reactants in two separate experiments. In experiment C, DMP was injected into a reactant stream. The catalyst was then heated to 150°C under these conditions. N-butanol was the only product observed after 1 hour at 150°C. N-butanol production decreased steadily from its initial rate while iso- and n-butyraldehyde increased. The maximum rates were observed after 5 hours, with n/i<1.0. The catalyst continued to deactivate over 24 hours. No ketones were produced. For the experiment D, DMP was injected in a similar manner, but the reactant stream passed through a DMP bubbler in order to allow continuous contact. After several hours at 150°C, both butyraldehyde and butanols were observed in a 1:1 ratio. The catalyst slowly deactivated over the next 36 hours. No ketones were observed.

Precarbonylated catalyst AY was also treated with DMP (experiment E). Following precarbonylation, the reactor was heated to 150°C under CO flow. At approximately the same time, DMP was injected and reactant flow started. N-butanol was present from the first injection. However, it decreased with time. Only trace quantities of aldehyde were formed.

Following precarbonylation and heating the reactor to 150°C, the reactant stream and DMP flow was started (experiment F). After 2 hours, trace amounts of aldehyde were pre-

sent, but were absent after 3 hours.   At 16 hours of reactant contact time, 2-methyl-3-hexanone and 4-heptanone were produced in a 1:1 ratio.   A breakthrough point for DMP had not been observed after 24 hours.   Therefore, an injection of DMP was made.   Immediately, the ketone production rate jumped by a factor of 30.   2,4-dimethylpentanone was observed in trace quantities.   The rates slowly diminished. After 24 hours, the rates were approximately the same as before the DMP injection A second injection failed to change the rates.

5.3   BATCH IR

Figure 15 shows the infrared spectrum taken for catalyst AY before and after exposure to reactants.   Both spectra were taken by fusing the catalyst with KBr.   In each case, the catalyst was handled in the absence of O_2.   Spectrum A resulted from carbonylating with 30 psig CO, $120^{\circ}C$ for 10 hours.   Bands were present at 2095, a shoulder at 2020, and 1765 cm^{-1}.   Spectrum B was taken after the catalyst had been used in the differential flow reactor.   Following reaction, the catalyst was cooled under CO and N_2 ($\approx 1/9$) flow.   Bands were located at 2095, 2068, 2020, 1765, and 1710 cm^{-1}.

Figure 16 shows the IR for catalysts AX following the same conditions used on catalyst AY.   Spectrum A, which was
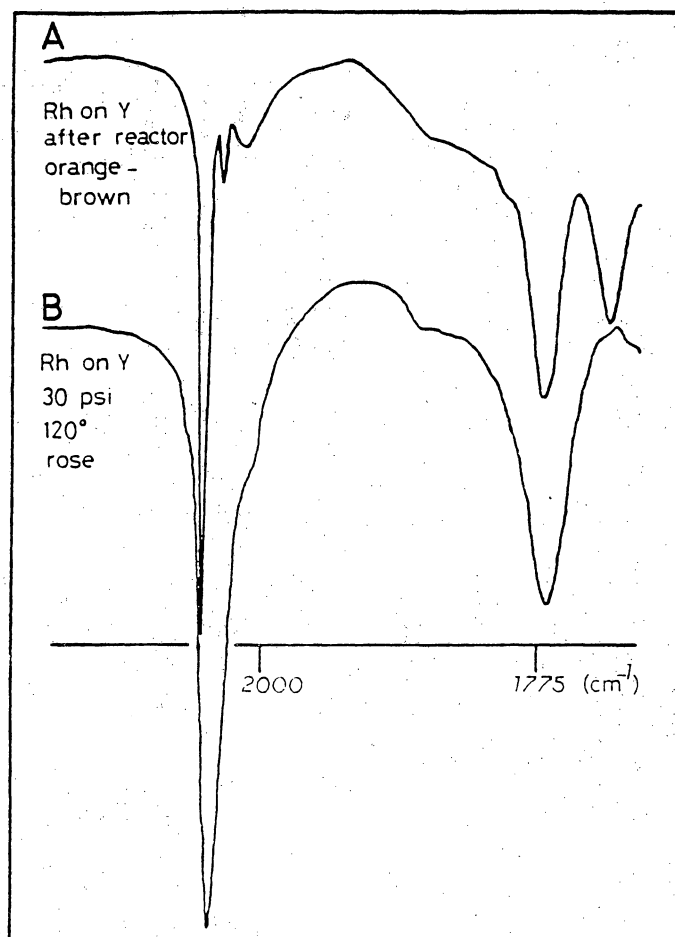
Figure 15: IR of Catalyst AY (50)

a) after carbonylation; b) after reaction conditions
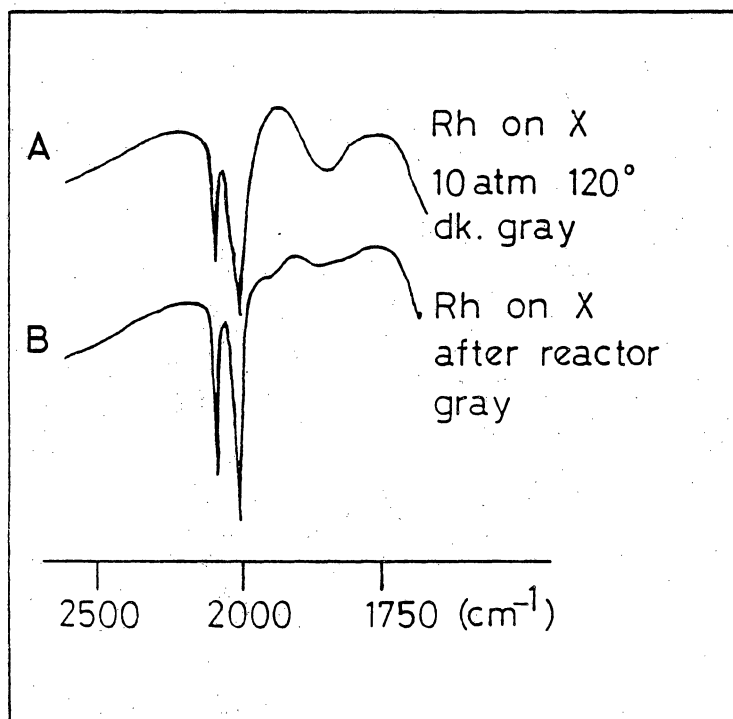
Figure 16: IR of Catalyst AX (50)

a) after carbonylation; b) after reaction
conditions

collected following carbonylation, has bands at 2090 and 2020 cm^{-1}, with a broad, weak band at 1850 cm^{-1}. Following the reaction, spectrum B shows that the same bands remained. The 1900-1000 cm^{-1} region shows only weak bands.

5.4   IN SITU HYDROFORMYLATION IR STUDIES

In situ FTIR experiments were conducted which mimicked the catalyst environments in the reactor. The majority of the experiments were performed on 1 wt.% catalyst AY. Heavier rhodium loadings did not provide adequate resolution above 1900 cm^{-1}. However, study of the 4 wt.% Rh catalysts did show distinct behavior and will be covered.

For convenience, the spectrum was divided into 3 regions, 2150-1750, 1750-1600 and below 1600 cm^{-1}. Subsequently, these will be referred to as regions I, II and III, respectively.

5.4.1   Hydroformylation Conditions Following Different Pretreatments

Figure 17 shows spectra collected over time for the 1 wt.% catalyst AY under reaction conditions. The catalyst had been precarbonylated (resembling Figure 6d). In region I, after one hour exposure to reactants, a band at 2042 cm^{-1} developed. The band at 2021 cm^{-1} became more resolved after 5.5 hours. At 20 hours contact time, numerous weak bands appeared between 2035 and 1900 cm^{-1}.
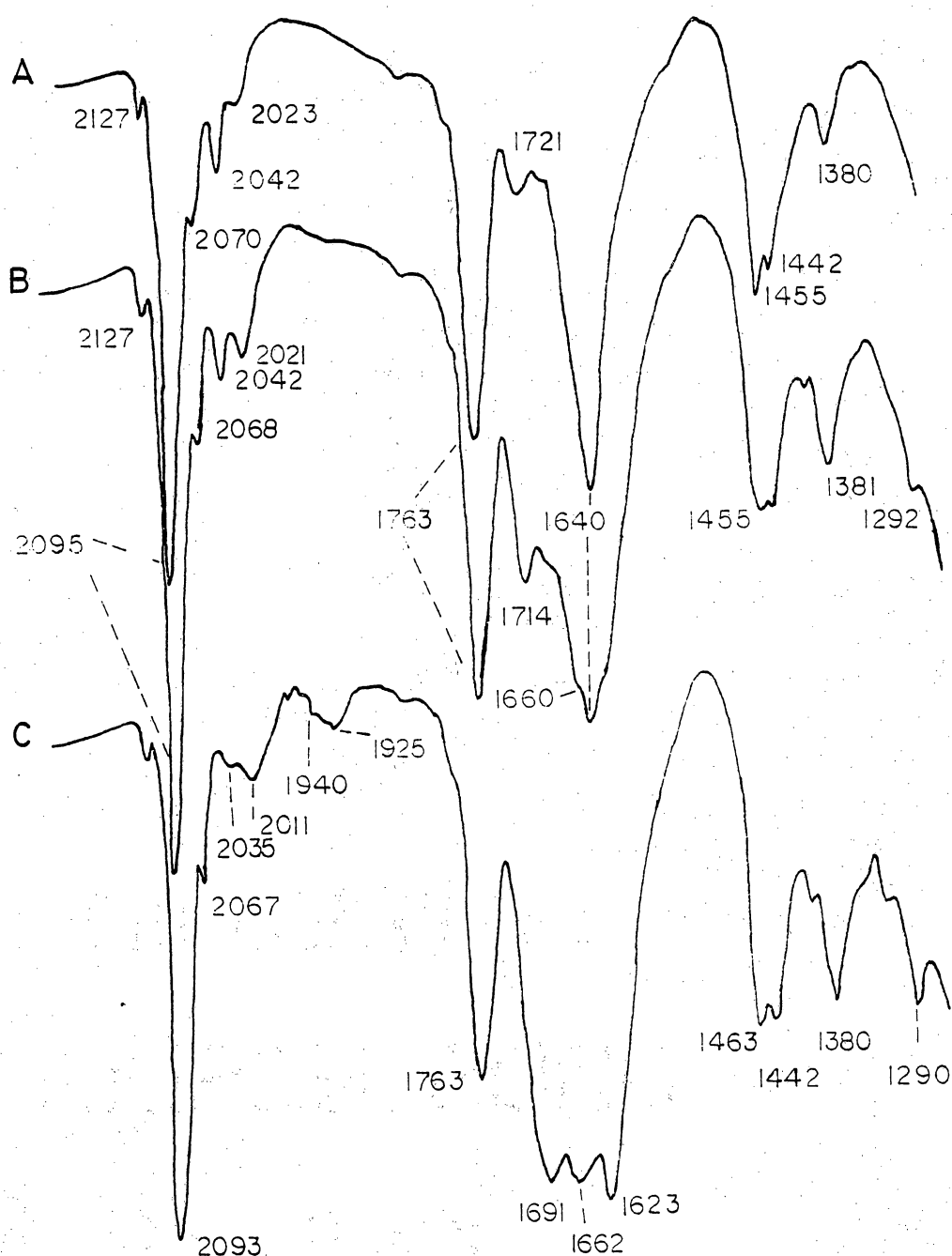
Figure 17:   Precarbonylated 1 wt.% RhNaY under
Hydroformylation Conditions

a) after 1 hour; b) after 5.5 hours; c) after 20
hours

In region II, three bands developed with time. Initially a band at 1721 cm^{-1} appeared, but it shifted downfield to 1691 cm^{-1} within 20 hours. After 5.5 hours, shoulders were present on the 1640 cm^{-1} band at roughly 1660 and 1623 cm^{-1}. After 20 hours time, these shoulders were well resolved into bands at 1662 cm^{-1} and 1623 cm^{-1}.

Region III bands underwent numerous changes also. Immediately after reaction conditions were initiated, the bands at 1455, 1442 and 1380 cm^{-1} were present. Additional bands at 1292 and weaker bands between 1440 and 1400 cm^{-1} were formed after 5.5 hours. In the final spectrum, 1463 cm^{-1} had replaced 1455 cm^{-1} and 1290 cm^{-1} had intensified. No spectral changes were observed beyond 18-20 hours.

Figure 18 presents the series of spectra collected for a 1 wt.% catalyst AY which had been air dried. Spectrum A was taken after 2 hours exposure to CO at 150°C. Strong bands at 2110, 2096, 2042 and 2022 cm^{-1} were present. Spectrum B shows the catalyst after 3 hours under reactant flow. The 1757 cm^{-1} bands had weakened, as had the band at 2096 cm^{-1}. An additional strong band appears at 1719 cm^{-1}. After 10 hours, spectrum C shows the shifts of bands to 2038 and 2015 cm^{-1}. The band at 2109 cm^{-1} was present only as a shoulder. A weak, broad band developed at 1924 cm^{-1}. At steady state, weak bands were present at 2035, 2005, 1990, 1937 and 1918 cm^{-1}.
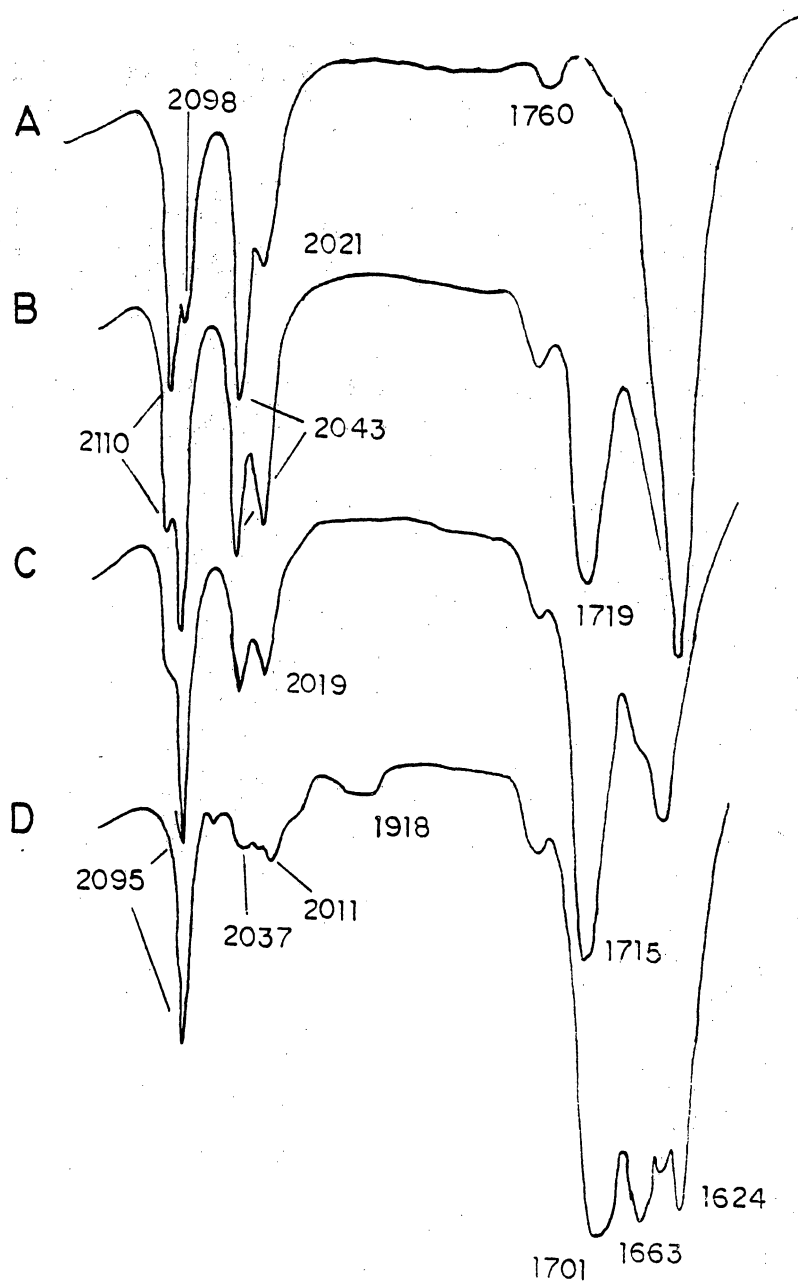
Figure 18: N$_2$ Treated 1 wt.% RhNaY under Hydroformylation Conditions

a) at 120°C for 20 minutes; b) 150°C for 3 hours; c) 10 hours 150°C; d) 22 hours

Region II of Figure 18 underwent similar changes as shown in Figure 17 . After 10 hours, the 1719 cm^{-1} band has shifted to 1714 cm^{-1}, and settles at 1694 cm^{-1} in spectrum D. At steady state, 1663 and 1626 cm^{-1} were resolved at steady state whereas they appeared as shoulders after 10 hours.

The N_2 pretreated catalyst AY under the reaction environment is shown in Figure 19 . This catalyst exhibited the same behavior shown in Figure 17 . At $120^{\circ}C$, 2110 and 2043 were roughly the same intensity, as were 2098 and 2021. Upon heating to $150^{\circ}C$ under reaction conditions, 2019 and 2098 intensified. Following 10 hours reactant contact, 2110, 2043 and 2019 had weakened. At steady state, numerous weak bands appeared between 2150 and 1900 cm^{-1}.

In region II, the 1719 cm^{-1} band was present after 3 hours at $150^{\circ}C$. It shifted with time downfield to 1701 cm^{-1} at steady state. 1660 cm^{-1} appears as a shoulder after 10 hours, and was well resolved along with 1624 cm^{-1} at steady state.

Figures 20, 21 and 22 show the results of identical experiments to those discussed in Figures 17-19 performed on a 4 wt.% RhNaY catalyst. Following region I in Figure 20 with time showed basically the same features developing as with the 1 wt.% catalyst AY. Initially, a 2047 cm^{-1} band ap-
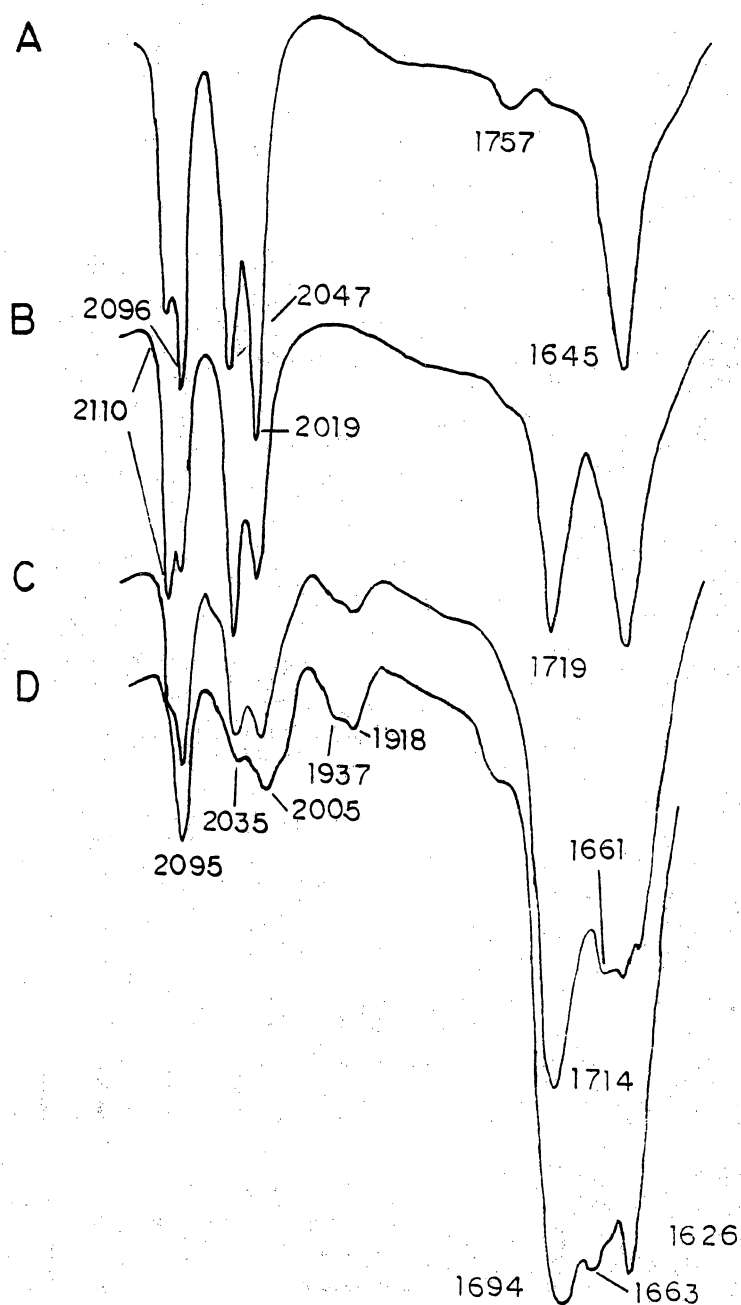
Figure 19: Air Dried 1 wt.% RhNaY under Hydroformylation Conditions

a) CO after 2 hours; b) 3 hours with reactants; c) 10 hours at 150°C, d) after 22 hours

peared but weakened after 9 hours. Weak bands were present at 1925 and 1850 cm^{-1} after 9 hours. At steady state, the weak bands at 1850 cm^{-1} were better resolved into two peaks at roughly 1866 and 1840 cm^{-1}. Region II also exhibited the same behavior. A 1721 cm^{-1} band initially appeared, and with time it shifted to a lower frequency to 1696 cm^{-1}. Bands at 1660 and 1625 cm^{-1} intensified with time.

4 wt.% AY catalysts subjected to air drying and N_2 treatment exhibited similar behavior, and are shown in Figure 21 and Figure 22 . The two doublets between 2110 and 2020 cm^{-1} were initially present. After several hours, the higher frequency doublet was reduced to a 2095 cm^{-1} band. Concurrently, the lower frequency doublets were enveloped by a broad band located at approximately 2030 cm^{-1}.

For the air dried catalyst, a non-Gaussian band at 1679 cm^{-1} has developed after 2 hours, and was present after 9 hours for the N_2 treated catalyst. However, at steady state, this band was absent.

Catalyst HY is shown as a function of time under reaction conditions in Figure 23 . After 30 minutes, features were present which had required 10 hours to develop for the other exchanges. Specifically, these bands are located at 1692, 1661, 1626 and 1290 cm^{-1}. After 4.5 hours, weak bands at 1945 and 1865 cm^{-1} were present. However, bands at 1662,
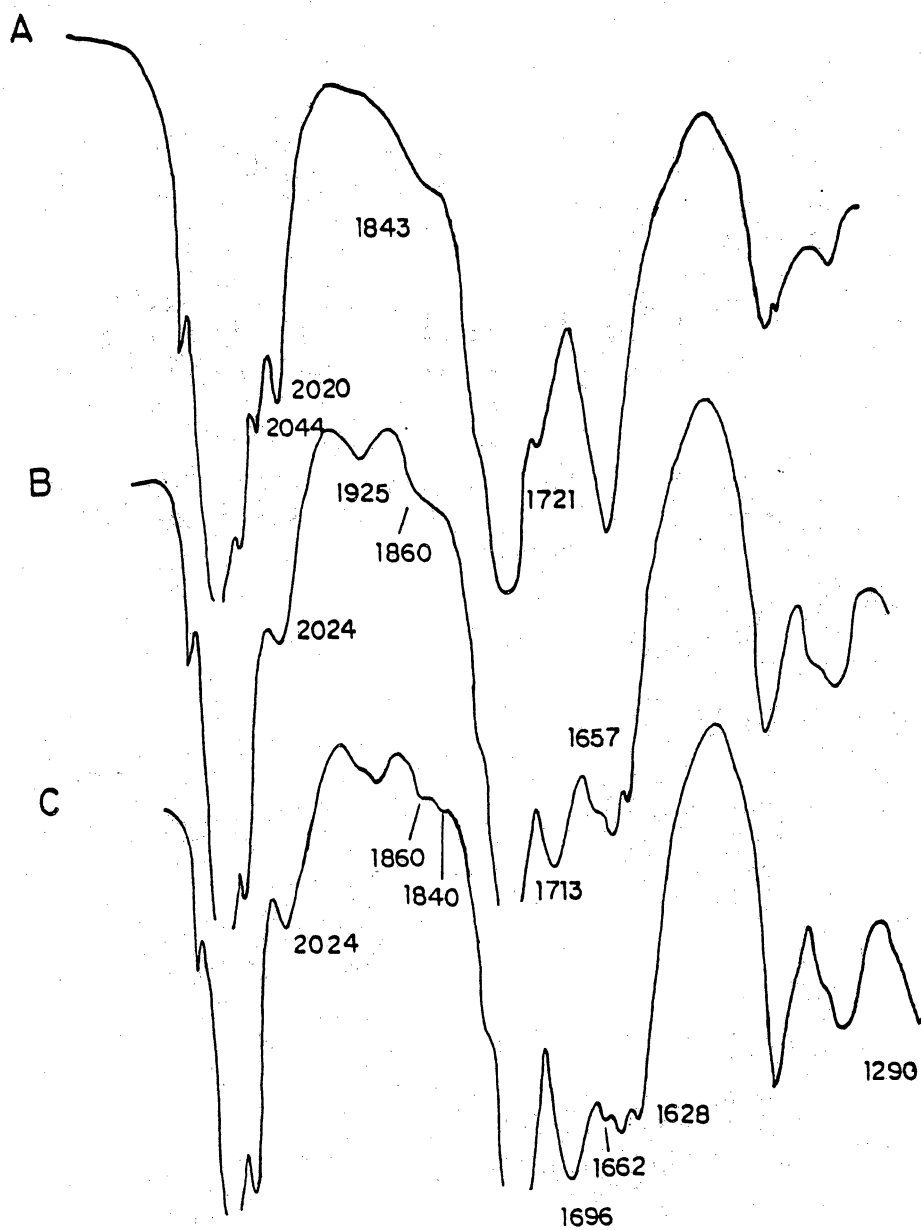
Figure 20: Precarbonylated 4 wt.% RhNaY Under
Hydroformylation Conditions

a) after 1 hour; b) after 9 hours; c) after 22
hours
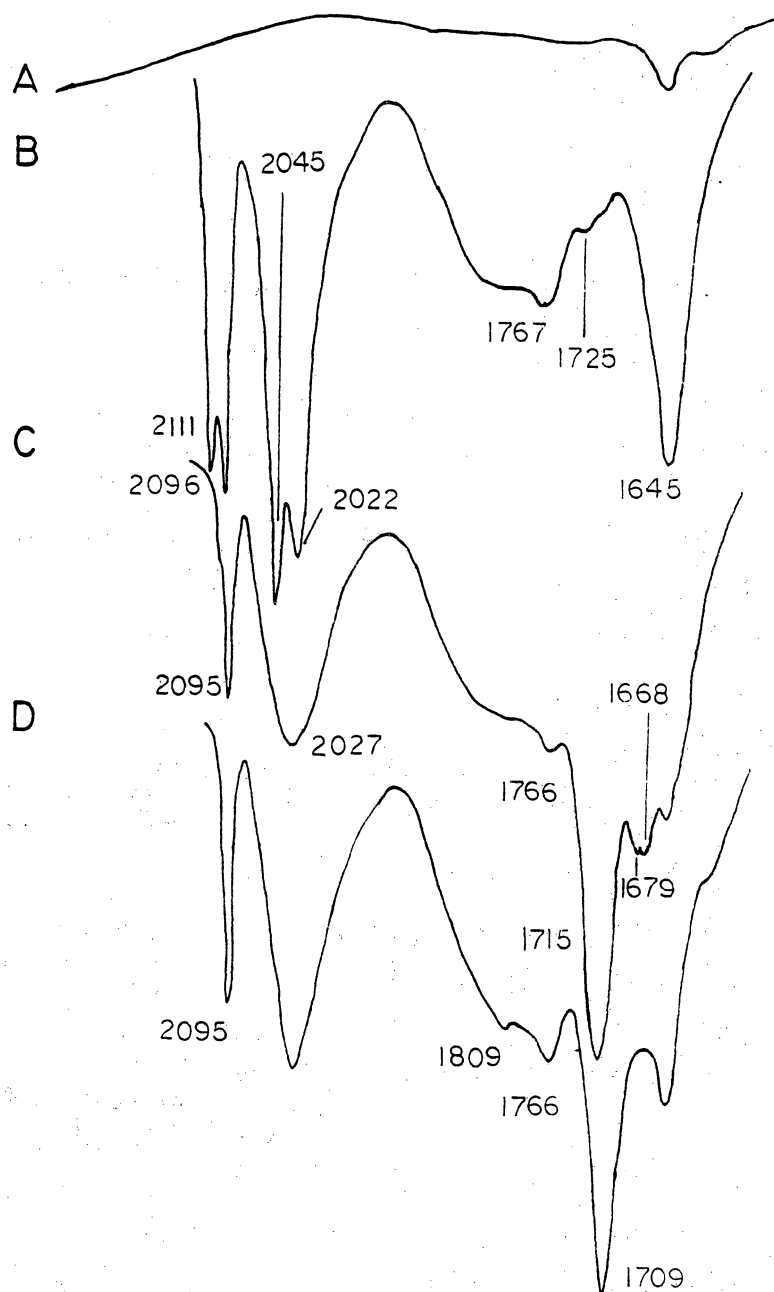
Figure 21: Air Dried 4 wt.% RhNaY Under Hydroformylation
Conditions

a) air dried; b) 15 minutes with reactants; c) 2
hours with reactants; d) 19 hours with reactants
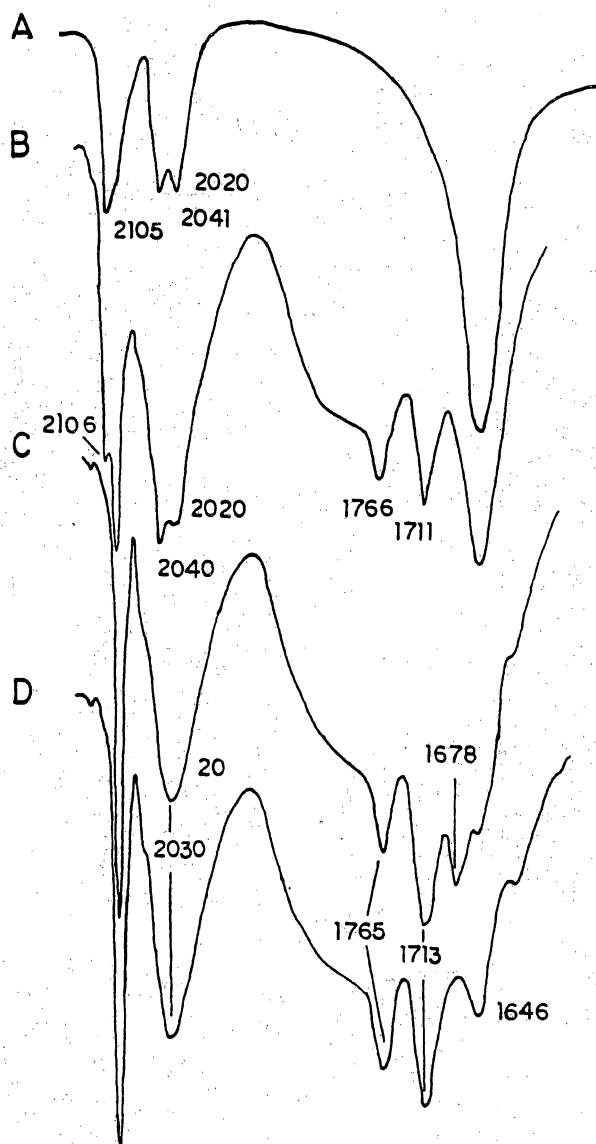
Figure 22:   N$_2$ treated 4 wt.% RhNaY Under Hydroformylation
             Conditions

             a) 10 minutes with reactants; b) 30 minutes with
             reactants; c) 9 hours with reactants; d) 26
             hours with reactants

1626 and 1290 cm^{-1} had disappeared. The 1692 cm^{-1} had moved to 1698 cm^{-1}. No spectral changes were observed from 4.5 hours to 8 hours.

5.4.2   Ethylene Hydroformylation

Figure 24 is a collection of spectra taken of catalyst AY under ethylene hydroformylation conditions. Ethylene partial pressure was 1/3 atm. Spectrum A shows the precarbonylated catalyst. Spectrum B was taken after 11 hours under reaction conditions. In region I, bands were located at 2128, 2095, 2068, 2045, 2019 and 1762 cm^{-1}. In region II, a doublet appeared at 1722 and 1704 cm^{-1}. Region III contained bands at 1462, 1400 and 1383 cm^{-1}. After 24 hours, spectrum C was recorded. Significant changes include the resolved shoulder at 2108 cm^{-1} and the intensified bands at 2041 and 2021. Regions II and III underwent little change, but the bands did grow in intensity.

5.4.3   Catalyst IY with Water Injections

An in situ IR experiment was conducted on the catalyst IY to reproduce the water injection inducement of hydroformylation. Figure 25 shows the IR spectra collected. Spectrum A
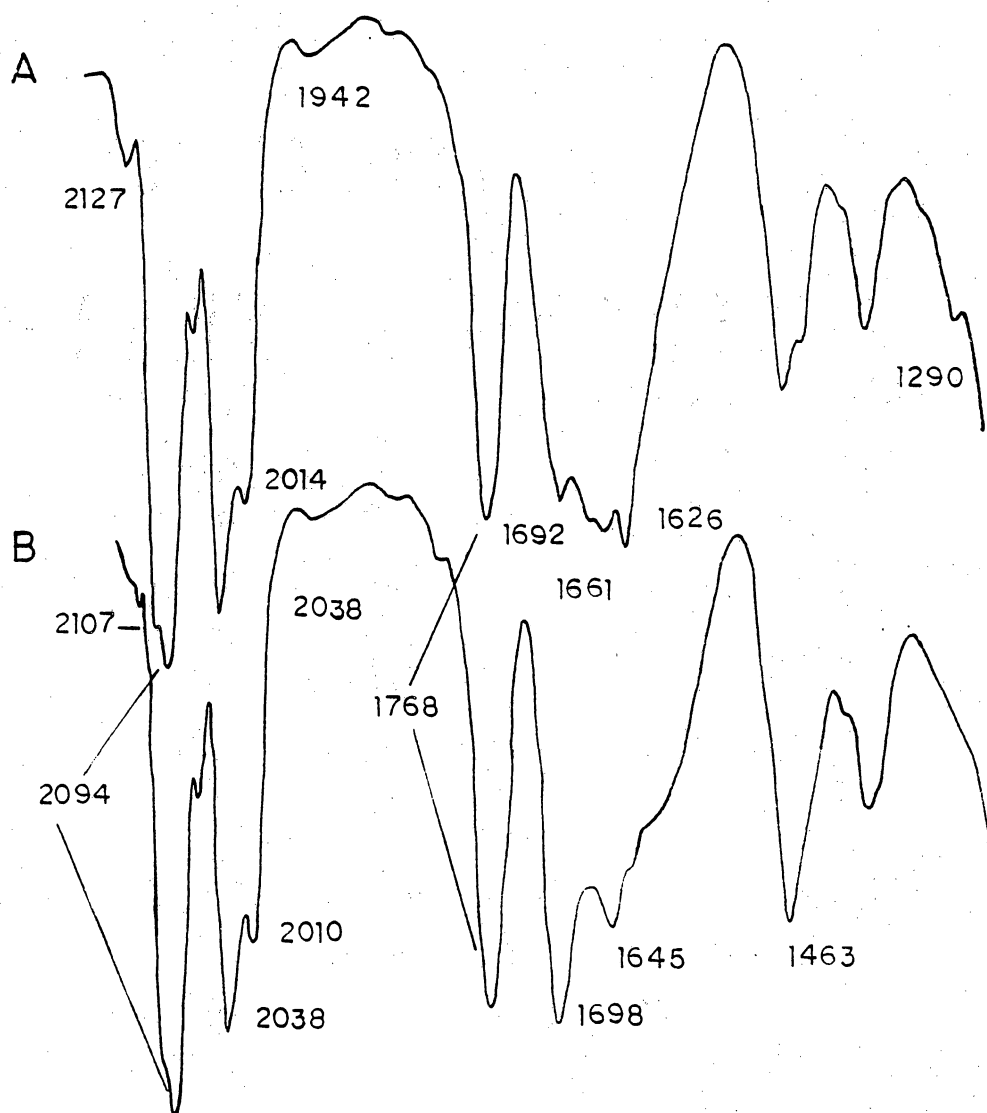
Figure 23: Catalyst HY under Hydroformylation Conditions
a) 30 minutes; b) 4.5 hours
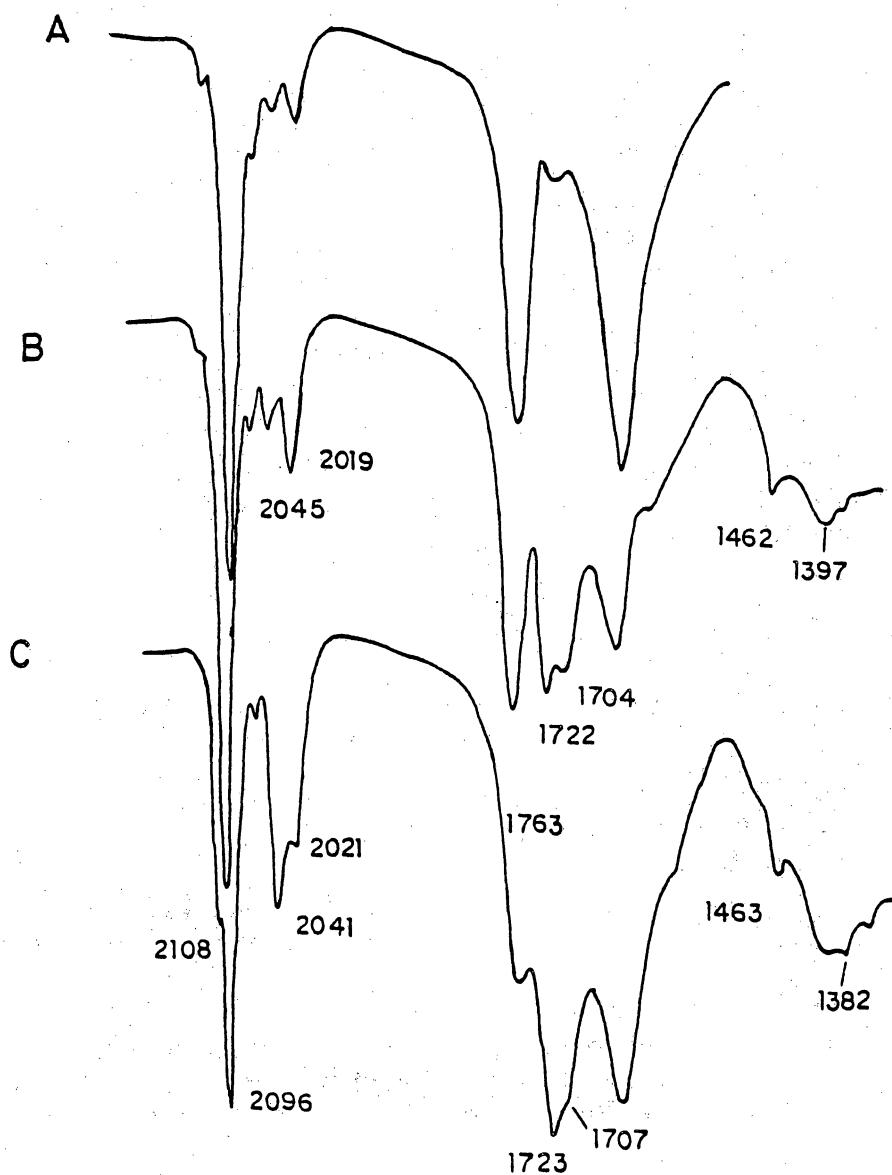
Figure 24:   Catalyst AY under Ethylene Hydroformylation
             Conditions

             a) precarbonylated; b) after 11 hours; c) after
             24 hours

is that of the catalyst evacuated at room temperature. Bands in region III include 1481, 1423 and 1337 cm^{-1}. Spectrum B was taken following precarbonylation.

Typical bands for precarbonylated catalysts are present, but an additional broad band at 1437 cm^{-1} developed. Following 3 hours of reactants, 0.25 ml of distilled H_2O was injected into the cell (spectrum C). Immediately transmission was reduced, and substantial changes occurred in region I. The 2095 cm^{-1} band was a weak shoulder while the 2066, 2042 and 2025 cm^{-1} peaks had intensified. Reactant flow was established after 8 minutes. Five minutes later spectrum D was taken. 2096 cm^{-1} had grown back while only a small, broad shoulder had replaced the 2040-2000 cm^{-1} peaks region. A second water injection removed the bands in region I. Spectrum E was taken after 5 hours with reactants. Only weak bands remained at 2050 cm^{-1}. A weak band also had developed at 1710 cm^{-1}.

5.4.4   Individual Gas Adsorptions

Combinations of propylene, H_2, and CO were admitted into the IR cell in order to help assign bands more specifically. Catalyst AY (1 wt.%) had been precarbonylated prior to experiments for $C_3^=/H_2$ and H_2 additions. Because the precarbonylated catalyst is unstable under vacuum and heat, CO
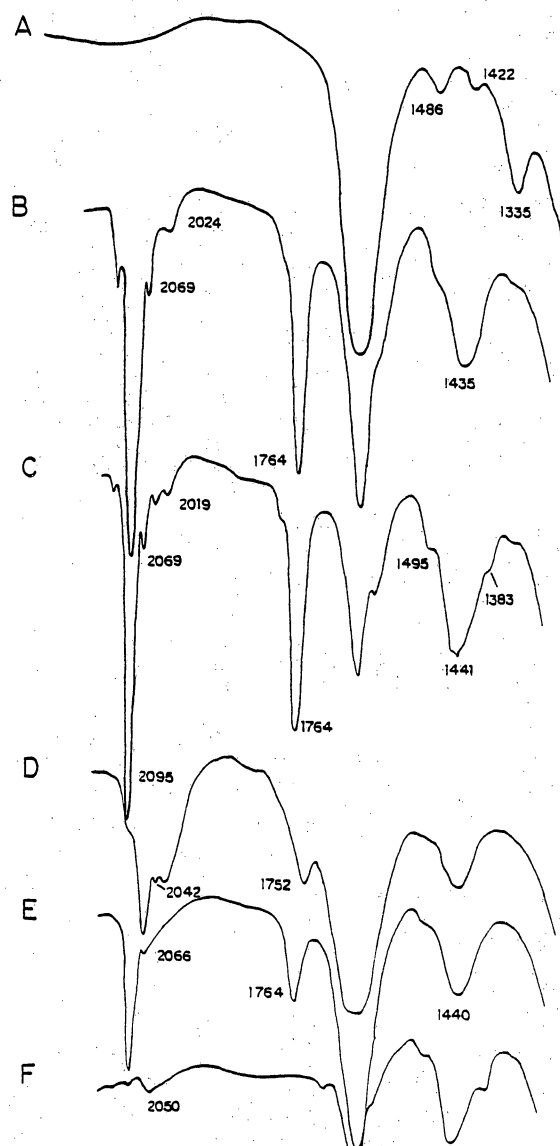
Figure 25: Catalyst IY under Hydroformylation Conditions With H_2O Injections

a)catalyst IY at room temperature; b) RXN conditions for 3 hours; c) precarbonylated; d) after H_2O injection; e) readmitted reactants for 5 minutes; f) 5 hours after second H_2O injection

pressure was retained. Gases were added through port V4 from a premixed bomb.

Figure 26 shows the spectra of the precarbonylated RhNaY (A) before propylene addition, (B) after 2 hours, (C) with propylene and after 20 hours contact. Notice that the bands at 3692 cm^{-1} disappeared after 20 hours. After 2 hours time, a sharp band at 2042 appeared. Propylene bands were evident between 3100 and 2800, and below 1500 cm^{-1}. Slightly resolved bands appeared at 1722 and 1709 cm^{-1}. At steady state, the 2042 band moved to 2037 cm^{-1}. The bands at 1722 and 1712 cm^{-1} combined to form one at 1709 cm^{-1}. The band at 1379 cm^{-1} was more intense than the 1460 cm^{-1} band also.

Figure 27 presents the reaction of the precarbonylated catalyst with H_2 at $150^{\circ}C$. After 35 minutes with H_2 and CO, spectrum A was taken. Bands developed at 2108, 2045, 2021, 1852 and 1716 cm^{-1}. After 23 hours, the intensity of these bands reduced to less than 5% transmission. The 2052 cm^{-1} broad band obscures the 2045 and 2021 bands, and its shoulder extends to 1960 cm^{-1}. Also present is a band at 1371 cm^{-1} which had a shoulder at 1450 cm^{-1}. Weak bands also appear at 2973 and 2937 cm^{-1}.
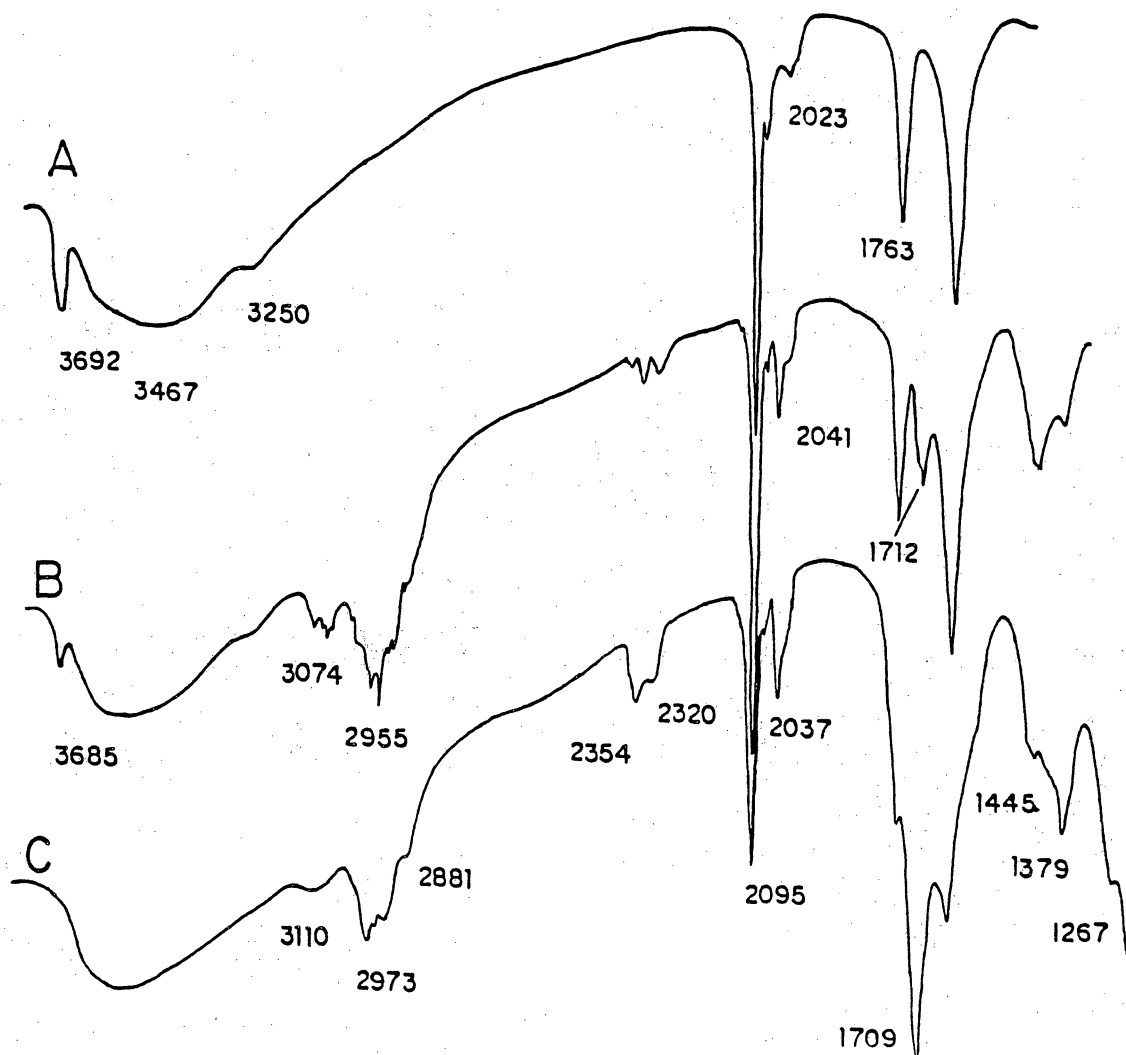
Figure 26: Precarbonylated RhNaY with $C_3^=$ and CO

a) precarbonylation; b) 2 hours; c) 20 hours
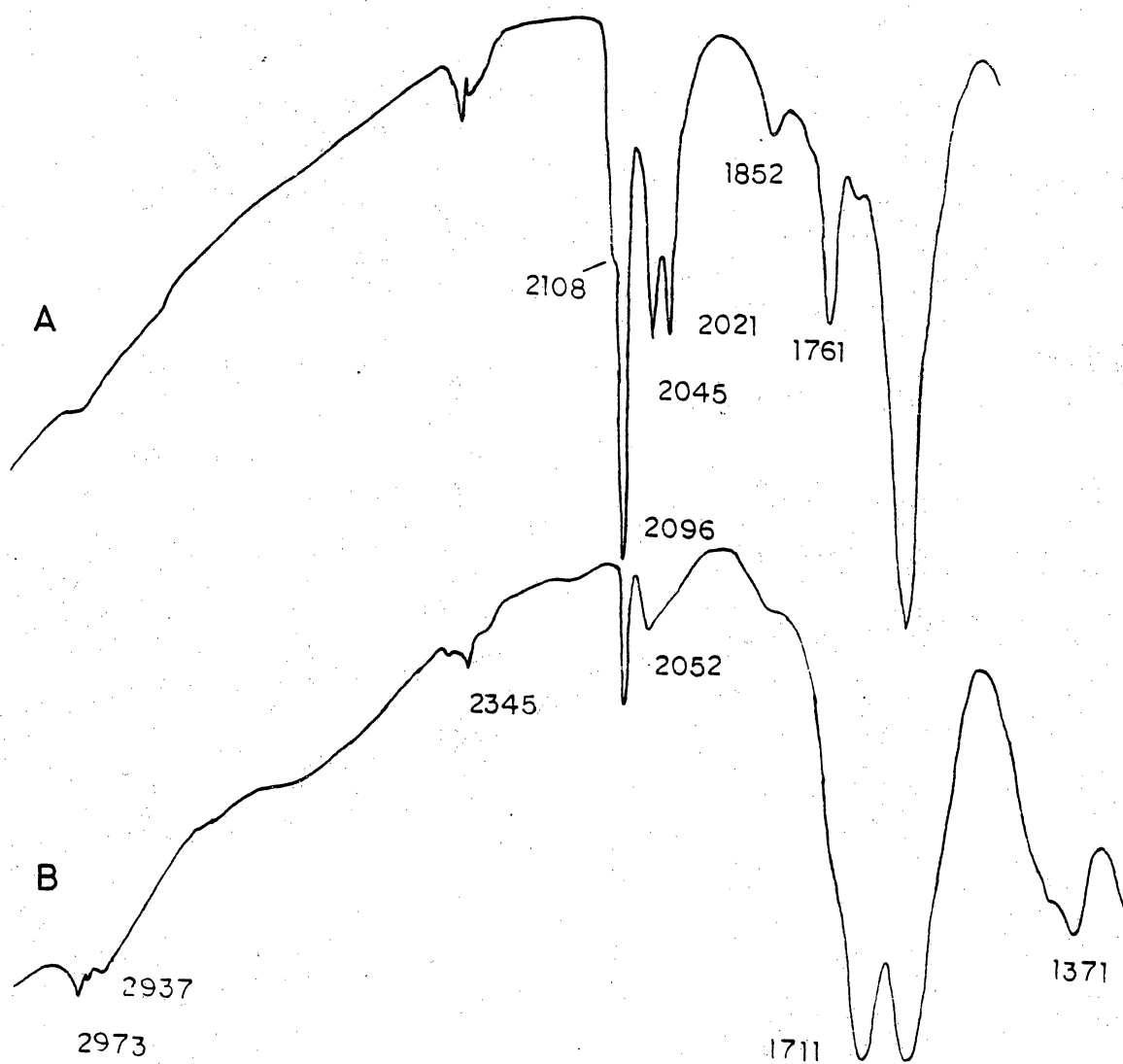
Figure 27: H_2 and CO on Precarbonylated RhNaY

a) after 35 minutes; b) after 23 hours

Propylene and hydrogen were added to an untreated cata-
lyst which was heated to 150°C under N_2. The results are
shown in Figure 28 . Notice again the removal of the 3690
cm^{-1} band.

The bands of gas phase propylene around 2800-3000 cm^{-1} have
weakened significantly. Also, bands developed at 1710, 1463
and 1371 cm^{-1}. It was observed that the cell lost pressure
quickly, eventually down to 10" Hg vacuum.

Appendix B contains numerous spectra of adsorbed gases
and liquids onto zeolites. These include propylene, iso-bu-
tyraldehyde, n-butyraldehyde, propionaldehyde, 2-trans hexe-
nal, 4-heptanone, carbon dioxide and propylene. These spec-
tra will be referred in the discussion as needed.

5.4.5   Catalyst AX

Figure 29 is a collection of spectra taken of catalyst AX
under hydroformylation conditions. The catalyst had been
precarbonylated, and spectrum A was taken five minutes after
reaction conditions were started. New bands developed in
regions II and III only at 1615, 1579, 1455, 1442, and 1374
cm^{-1}. After 1 hour, spectrum B was taken. The band at 1647
cm^{-1} had weakened while 1704, 1578, and 1422 cm^{-1} intensi-
fied. Also, note a shoulder at 2035 cm^{-1}. Spectrum C was
taken after 26 hours under reaction conditions. Shoulders
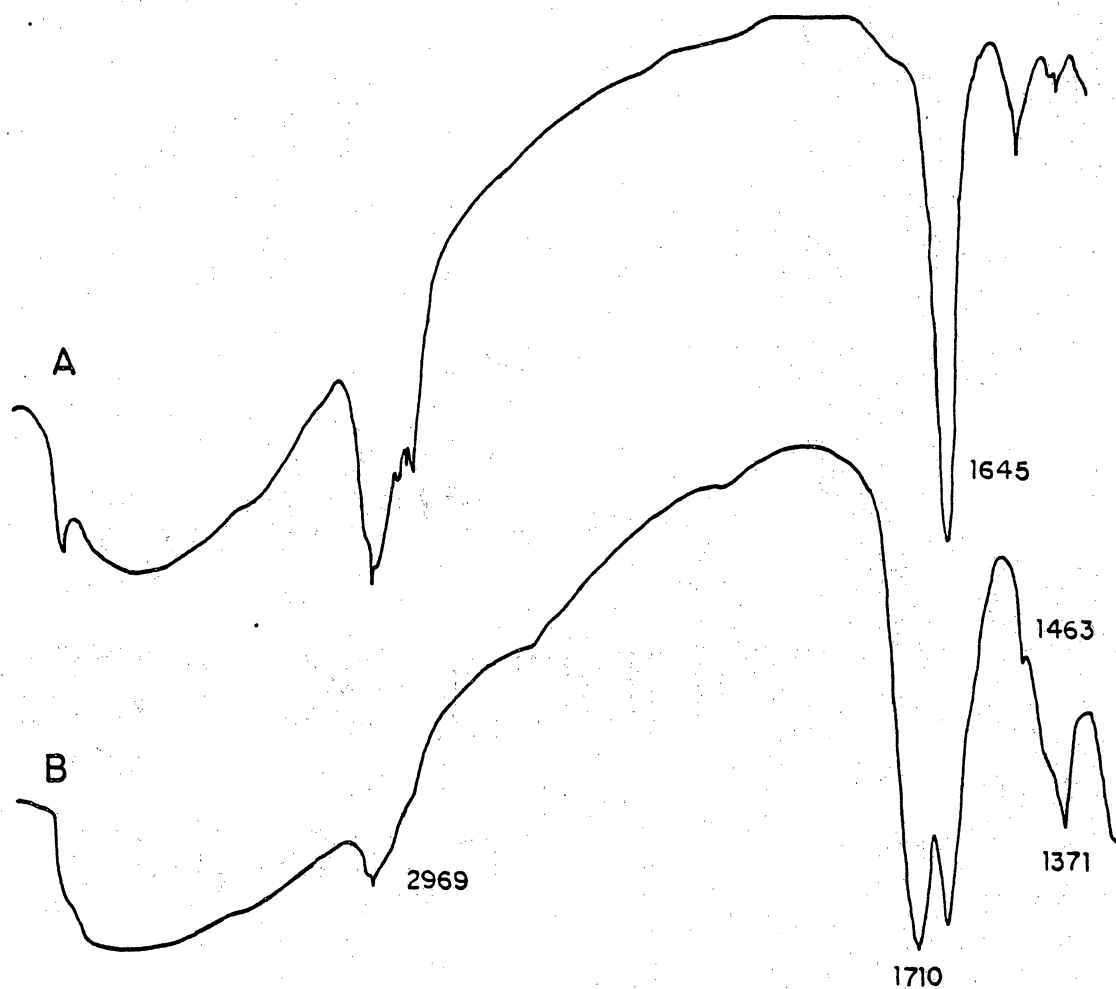
Figure 28: H_2 and $C_3^=$ on Untreated RhNaY

a) at 130°C for 5 minutes; b) at 150°C after 25 minutes

appear at 2100 and 2035 cm^{-1} as does a broad band at approximately 1940 cm^{-1}. The 1704 cm^{-1} band shifted to 1698 cm^{-1}, and a weak band developed at 1666 cm^{-1}.

Figure 30 shows the behavior of batch of catalyst AX which did not have measurable activity. Basically, the same bands developed with time as on the active catalyst (Figure 29).

The band at 2090 cm^{-1}, however, did diminish with time. A shoulder at approximately 1940 cm^{-1} also developed. A band at 1660 cm^{-1} was present after 8.5 hours and remained at steady state. The broad band at roughly 1830 cm^{-1} did not change with time.

5.4.6   Isotopic Substition

D$_2$ and ^{13}CO gases were added to the gas mixture in order to facilitate assignment of various IR bands. Catalysts AY or AX were used.

5.4.6.1   RhNaY

Figure 31 shows the spectra taken of precarbonylated catalyst AY subjected to labelled CO substitutions. Spectrum A is the precarbonylated material. Spectrum B results from the evacuation and subsequent addition of 3"Hg of ^{13}CO. The entire spectrum was shifted downfield by a factor of approx-
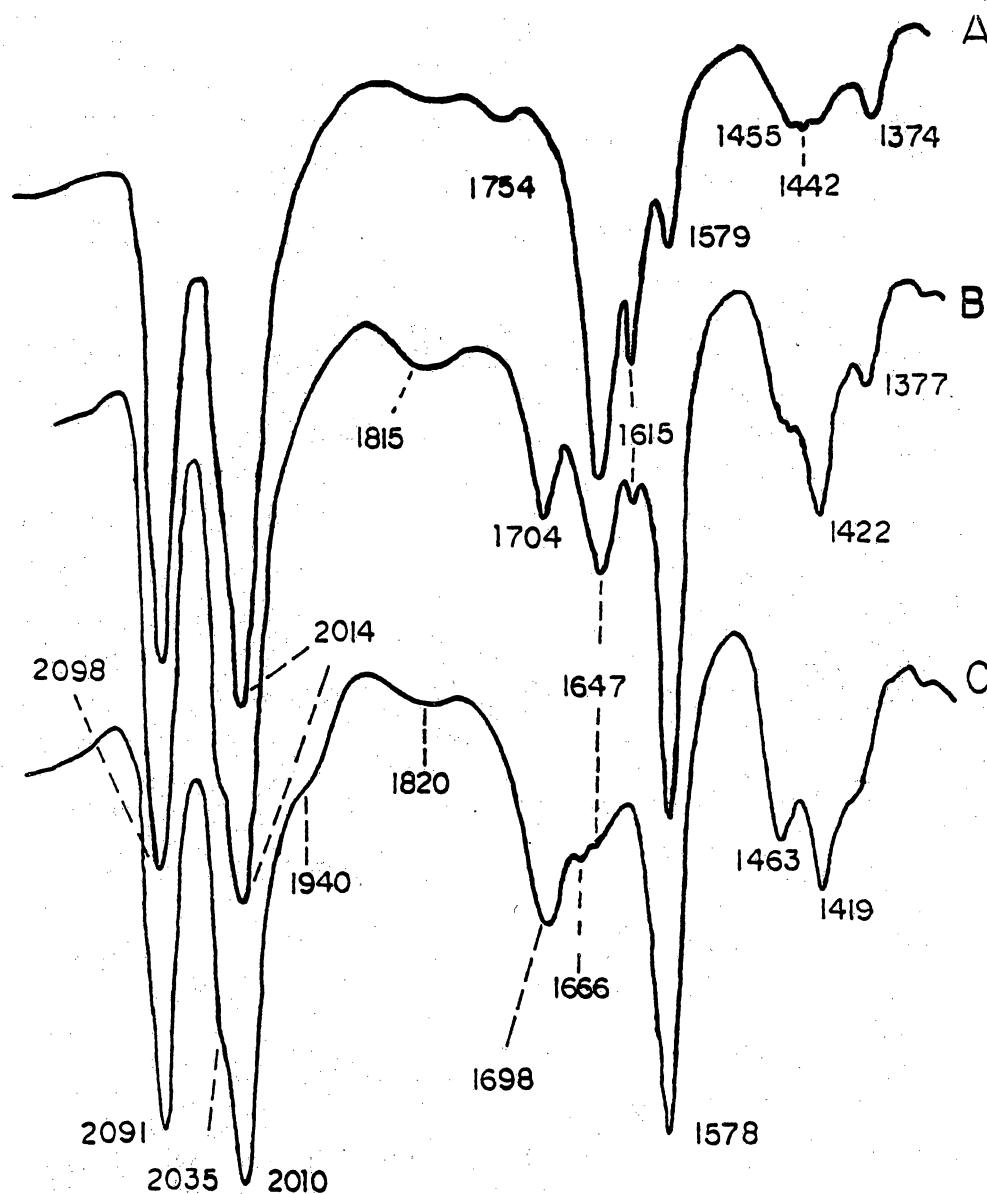
Figure 29:   Catalyst AX under Hydroformylation Conditions

a) 5 minutes with reactants; b) after 1 hour; c) after 26 hours
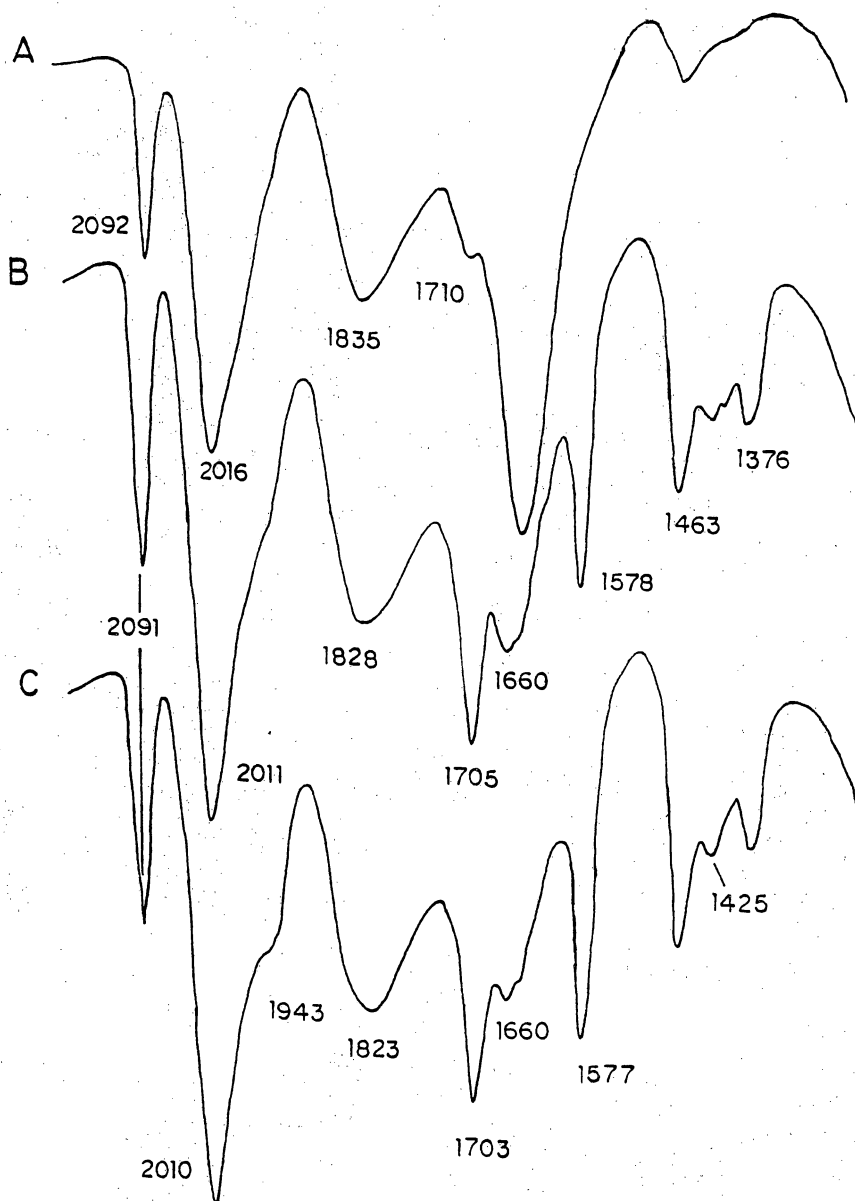
Figure 30: "Inactive" Catalyst AX Under Hydroformylation Conditions

a) after 5 minutes; b) 8.5 hours; c) 18 hours

imately 0.977. Bands are present at 2048, 1997, 1973 and 1723 cm^{-1}. 26"Hg of a premixed gas bomb of propylene/H_2/N_2 in 3:3:2 ratios was added to the cell. Spectrum C is the spectrum taken after 14 hours under these reaction conditions. No additional bands are present in region I. In region II, a shoulder at 1710 cm^{-1} appears. Also, a broad region between 1710 and 1645 cm^{-1} suggests the presence of a band. Region III contains two bands at 1457 and 1378 cm^{-1}.

Attempts to introduce D_2 or ^{13}CO at steady state for catalyst AY were unsuccessful. Bands in region I were very sensitive to partial pressure variation. D_2 was used as a substitute for H_2 in a flowing reactant stream. Catalyst AY was taken to steady state so that bands were present at 2094, 2066, 2037, 2008 and 1938 as shown in Figure 32 a. The spectrum did not change after 1 hour under D_2/$C_3^=$/N_2/CO flow, as shown in spectrum B.

5.4.6.2   RhNaX

Figure 33 contains the spectra taken after treatment of catalyst AX with D_2 and ^{13}CO. The catalyst after 11 hours under reaction conditions is shown in spectrum A. Spectrum B shows the changes which resulted after 30 minutes from the addition of 2"Hg D_2. Only region II significantly changes.
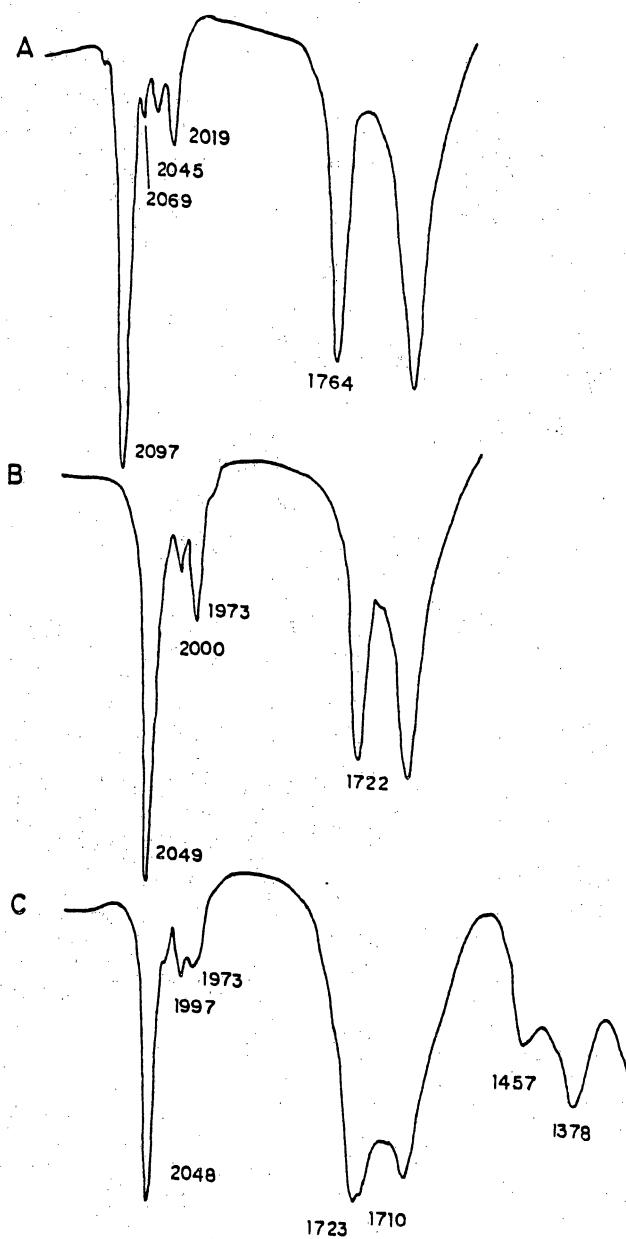
Figure 31: ^{13}CO Substition on RhNaY

a) precarbonylated with ^{12}CO; b) 3" Hg of ^{13}CO at 150°C; c) 14 hours with $C_3^=/H_2/N_2/^{13}CO$
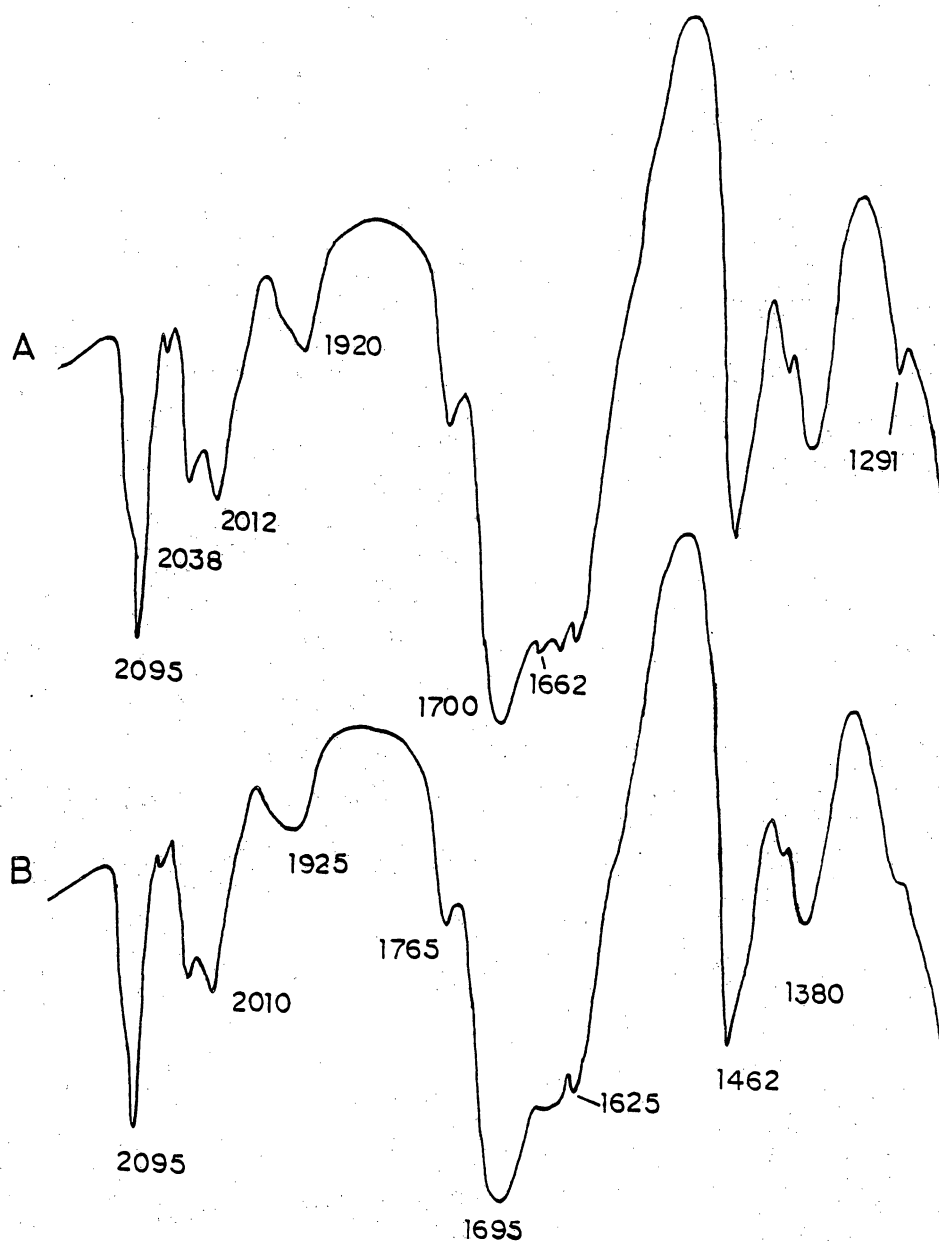
Figure 32: Catalyst AY at Steady State With $D_2/C_3^=/CO/N_2$ Flow

a) steady state with $H_2/C_3^=/CO/N_2$; b) after 1 hour with $D_2/C_3^=/CO/N_2$

The band at 1645 cm^{-1} disappeared while the 1424 cm^{-1} band intensified slightly. A shoulder appears at 1670 cm^{-1}. Spectrum C was taken after 10 minutes with ^{13}CO. The bands at 2098 and 2014 have shifted to 2043 and 1966 cm^{-1}. The band at 1618 cm^{-1} has moved to 1600 cm^{-1}. In region III, only one broad band at 1450 cm^{-1} was present. Spectrum D was taken after H_2 and ^{12}CO had been readmitted to the cell. Additional bands developed below 1750 cm^{-1}. Only bands at 1500 and 1535 cm^{-1} were resolved.

5.4.7   Rhodium Carbonyl Reactions with Phosphines

Catalysts were reacted with dimethylphenylphosphine (DMP) and n-hexyldiphenylphosphine (HDP) after different treatments. Catalysts AX and AY were subjected to phosphine exposure. The phosphines were injected by a syringe through port V4 in Figure 4 .

Figure 34 presents the before and after phosphine exposure spectra for the air treated catalyst. Spectrum A shows the catalyst following drying at 190°C and CO adsorption at 150°C. In spectrum B, 2112 and 2100 cm^{-1} were completely removed. The 2047 cm^{-1} band weakened and was present as a shoulder on 2023 cm^{-1}. A weak band developed at 1964 cm^{-1}. Spectrum C results after exposure of the catalyst with HDP for 17 hours. The two doublets were replaced by two bands at 2108 and 2039 cm^{-1}.
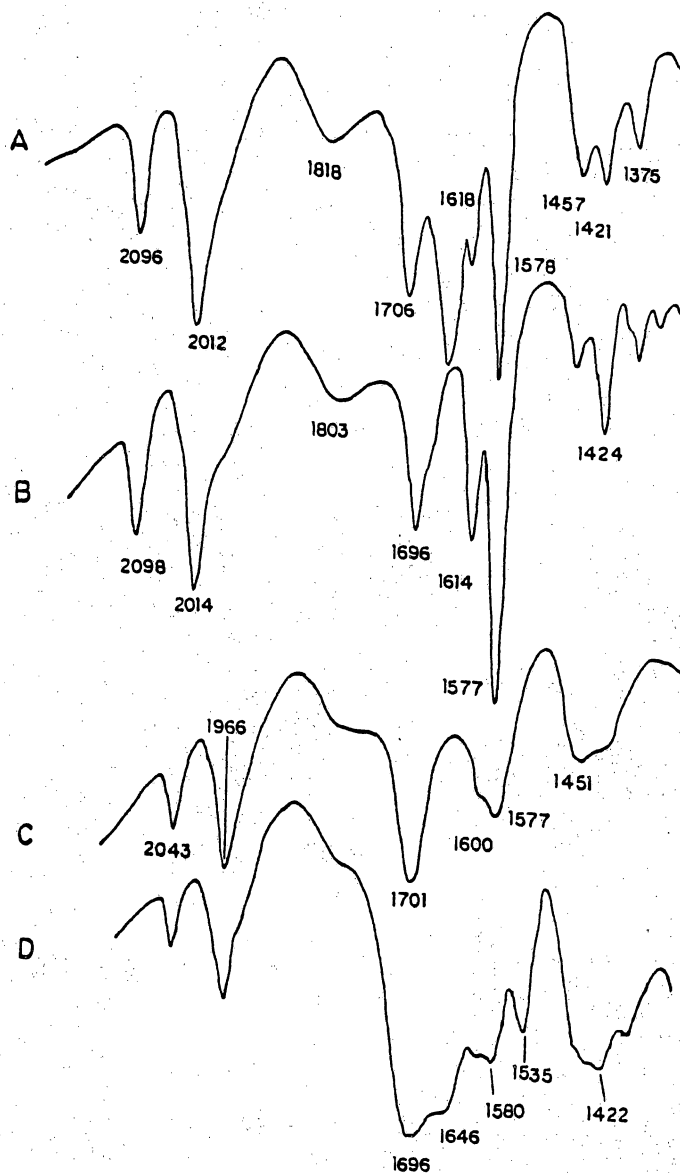
Figure 33: D_2 and ^{13}CO on Catalyst AX

a) under reactants for 11 hours; b) 30 minutes with 2"Hg D_2; c) 10 minutes with ^{13}CO; d) readmitted H_2 and ^{12}CO
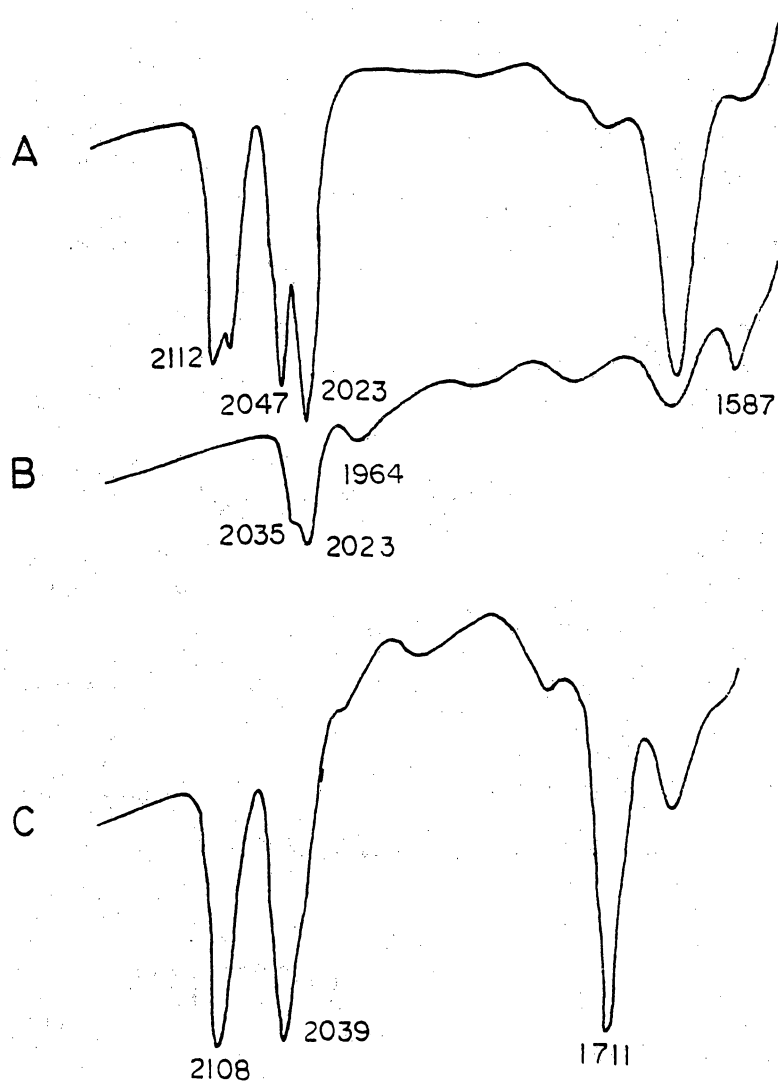
Figure 34:   Air Dried RhNaY with DMP

a) after CO; b) DMP for 15 minutes; c) HDP for 17 hours

The reactions of the precarbonylated AX catalyst are shown in Figure 35 . Spectrum A is the precarbonylated catalyst. Spectrum B was taken after 10 hours with DMP. Bands were present at 2018, 1990, and 1850 cm^{-1}. Additional bands due to phosphine are located below 1600 cm^{-1}. The reaction of AX with HDP is shown in spectrum C. Only a shoulder at 2035 cm^{-1} developed after 12 hours.

Spectrum A of Figure 36 was taken after the precarbony-lated NaY had been contacted with DMP for 16 hours. Bands at 2091 and 1766 cm^{-1} decreased in intensity from the origi-nal material. New bands at 2029, 1959, 1862, 1833 and 1815 cm^{-1} were present. The band at 1640 cm^{-1} decreased signifi-cantly also. Spectrum C was taken after 7 hours contact with HDP. Figures 36 b and c show the before and after spectra of the precarbonylated catalyst AY which had been contacted with HDP for 8 hours. Note that additional bands appear at 2042 and 1712 cm^{-1}.

Catalyst AY was allowed to reach steady state under reac-tion conditions. HDP was injected into the cell. The cell was closed off so that HDP could vaporize and contact the catalyst. Spectrum A in Figure 37 is the steady state spect-rum, and spectrum B shows the changes following 7 hours con-tact with HDP. Bands at 2094 and 1763 cm^{-1} remained un-changed, while the bands at 2037, 1660, 1624, and 1290 cm^{-1} were removed.
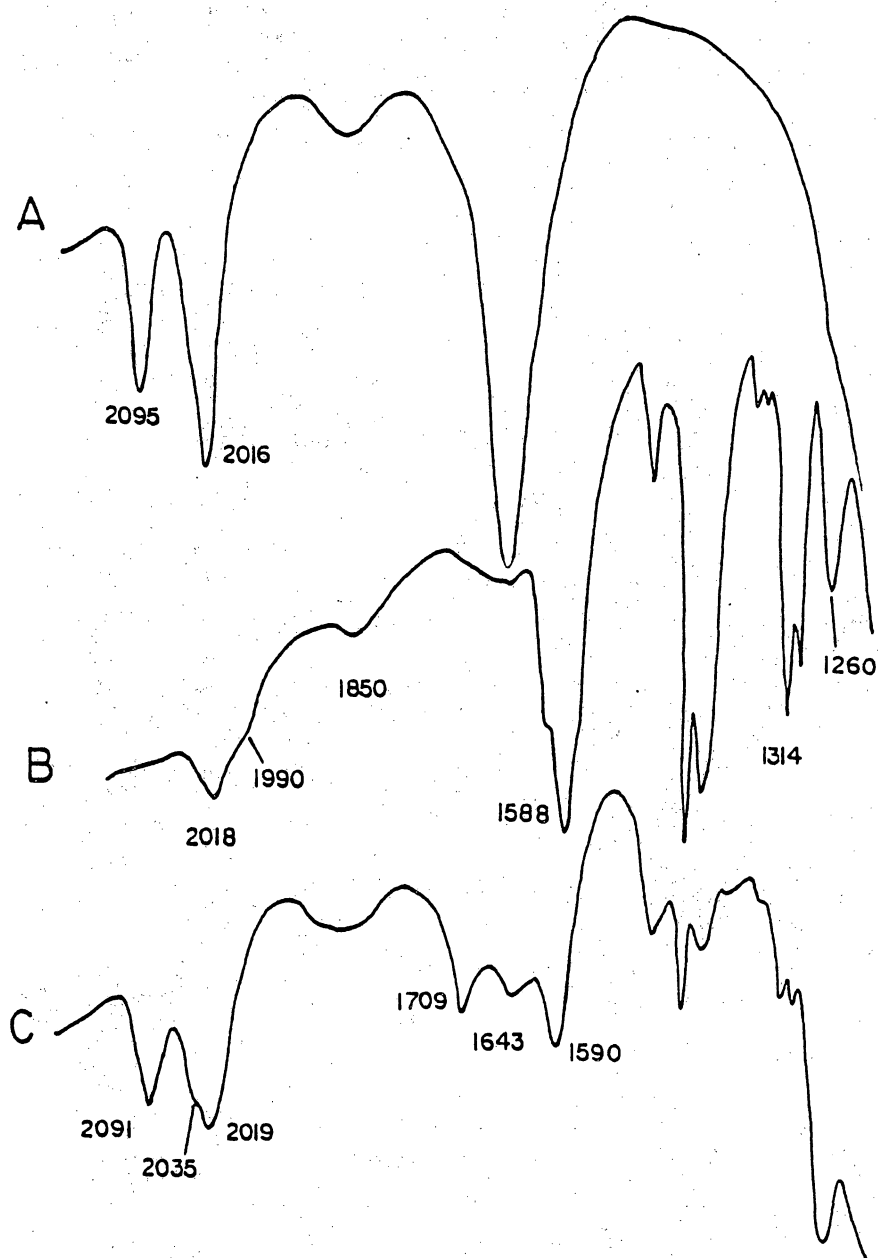
Figure 35: RhNaX Reactions with Phosphines

a) carbonylated NaX; b) after 10 hours with DMP;
c) after several hours with HDP
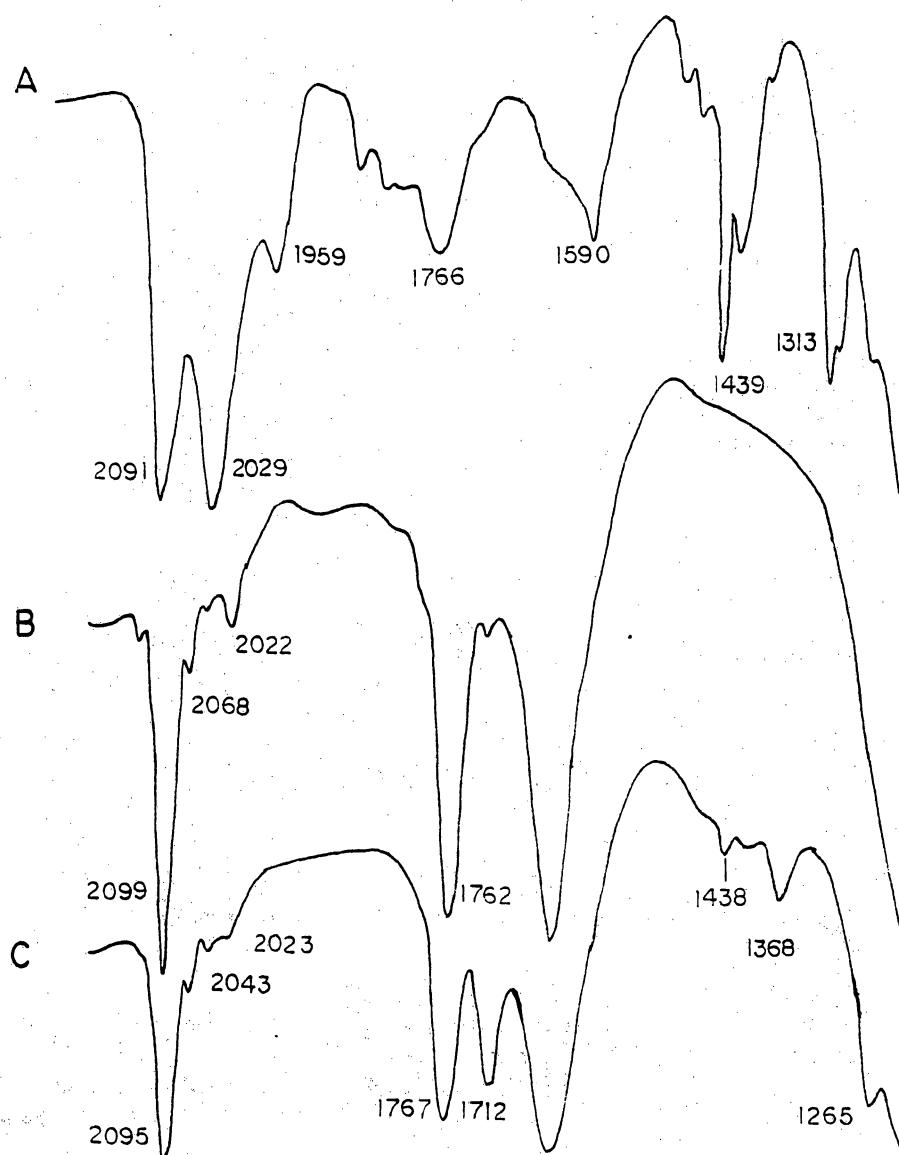
Figure 36: Precarbonylated Catalyst AY with Phosphines

a) carbonylated material reacted with DMP; b) precarbonylated; c) steady state spectrum with HDP for 7 hours
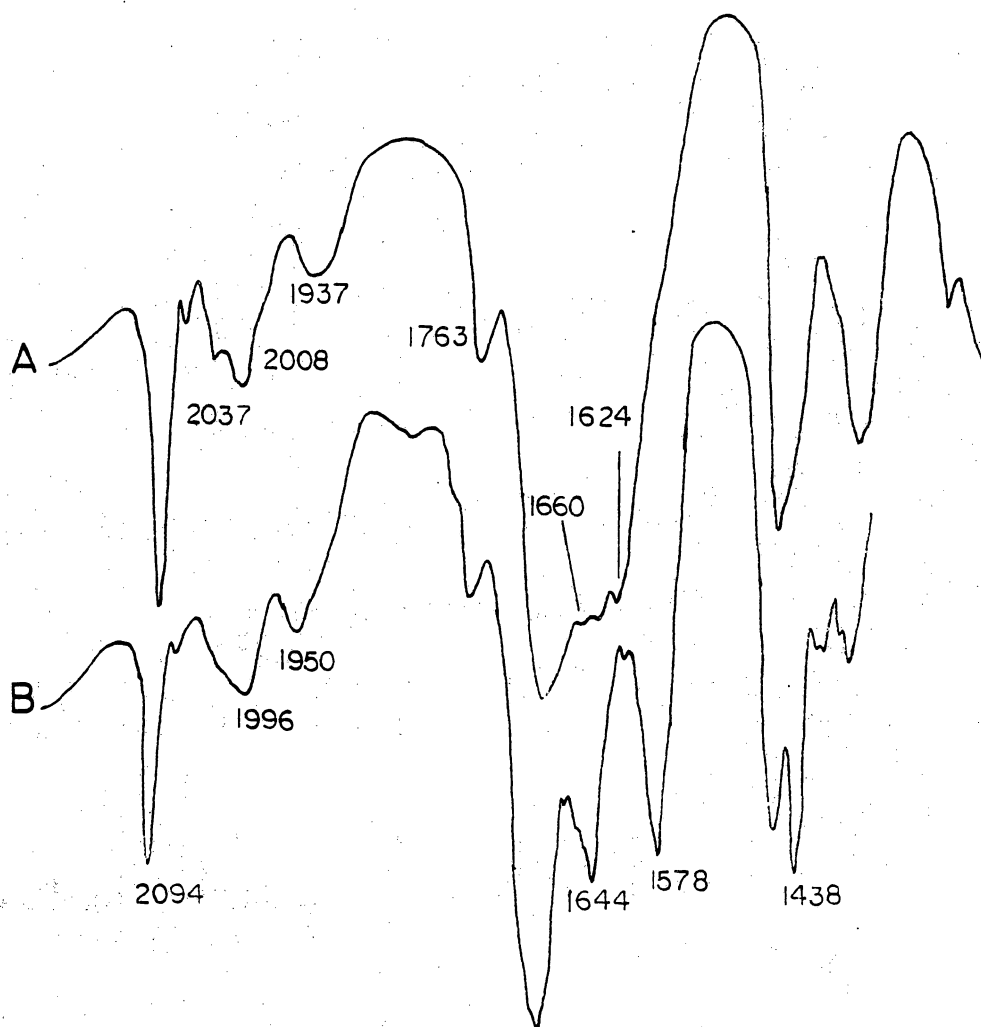
Figure 37:   Catalyst AY at Steady State Reacted with HDP

a) steady state; b) after 7 hours with HDP

Chapter VI

DISCUSSION

6.1   CARBONYL FORMATION

As shown in Figures 15 and 16, the infrared spectra of
the catalyst following precarbonylation and reaction indi-
cated the same species. Thus, no changes were present to
provide any insight to the catalytic behavior. It was also
clear that the NaX and NaY zeolites were supporting diffe-
rent rhodium carbonyls. Hence, in situ IR studies were ini-
tiated in an attempt to understand the carbonyl formation
and the behavior of the catalysts under reaction conditions.

6.1.1   RhNaY

It is evident that several rhodium carbonyl species are
being formed during carbonylation as shown in Figure 6 .
Ultimately, the $Rh_6(CO)_{16}$ cluster is formed on NaY under
precarbonylation conditions (see Figure 6d). The infrared
spectrum for the species is in excellent agreement with re-
sults reported by Mantovani et al. (10) and Gelin et al.
(51). Table 10 provides rhodium carbonyl IR data for vari-
ous compounds. Assignment of the spectrum observed in Fig-
ure 6d to $Rh_6(CO)_{16}$ requires significant shifts of the
bands for free $Rh_6(CO)_{16}$. For example, the triply bridging

carbonyl shifts 40 cm^{-1}. This has been taken to be evidence that the $Rh_6(CO)_{16}$ resides in the supercage (52). Theolier et al. (53) deposited $Rh_4(CO)_{12}$ onto alumina and silica, and obtained IR bands at 2068 and 1840 cm^{-1} for alumina, 2080, 2051, 1840, and 1800 cm^{-1} for silica. Thus $Rh_4(CO)_{12}$ is a strong candidate for the intermediate giving a bridging carbonyl at 1834 cm^{-1}. This is consistent with the known synthesis of $Rh_6(CO)_{16}$ from $Rh_4(CO)_{12}$ in solution (54).

It has been proposed by Primet et al. (55) that the following reactions take place to form $Rh(I)(CO)_2$-NaY:

$$Rh(III) + CO \rightarrow Rh(III) - CO$$

$$Rh(III)-CO+2CO+H_2O \text{ (or OH groups)} \rightarrow Rh(I)(CO)_2 +CO_2 +2H^+$$
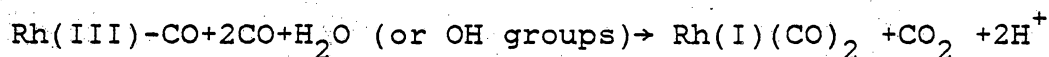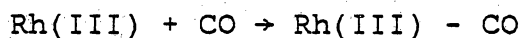
In a separate experiment, Theolier et al. (53) have proposed the following scheme to produce silica supported clusters:

$$2Rh(I)(CO)_2 \xrightarrow[\text{(CO}_2 + 2H^+)]{H_2O/CO} 2Rh^\circ(CO)_m \xrightarrow{CO/\text{high } H_2O \text{ conc.}} Rh_4(CO)_{12}$$

$$\downarrow \begin{smallmatrix}CO/low \\ H_2O \\ conc.\end{smallmatrix} \qquad\qquad\qquad 2Rh^\circ(CO)_m \downarrow$$

$$Rh_z(CO)_T \qquad\qquad\qquad Rh_6(CO)_{16}$$
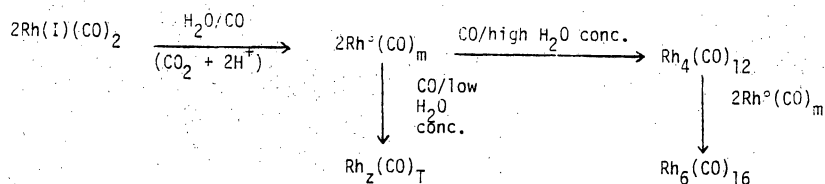
TABLE 10

Literature Values for Various Rhodium Carbonyls

Complex	Support	ν_{CO}	Reference
$Rh_6(CO)_{16}$	NaY	2095, 2045, 2020	51
$Rh_6(CO)_{16}$	nujol	2075s, 2025w, 1800m	56
$Rh_6(CO)_{16}$	NaY	2095vs, 2080sh, 2060w, 1765s	10
$Rh_6(CO)_{16}$	NaY	2099, 2069, 2020, 1765	this work
$Rh_4(CO)_{12}$	alumina	2068, 1840	55
$Rh_4(CO)_{12}$	silica	2080, 2051, 1840, 1800	55
$Rh(III)CO$	NaY	2172	55
$Rh(CO)_w$	NaX	2046, 1987	50
$Rh(CO)_2^+$	NaX	2099, 2017	50
$Rh(CO)_2^+$	NaX	2085, 2014	39
$(Rh(CO)_2Cl)_2$	KBr	2105, 2089, 2035, 2003	---
$Rh(CO)_2O_zH_2O$	NaY	2110, 2040	57
$Rh(CO)_2(O_z)_2$	NaY	2095, 2020	57
$Rh(CO)_2O_zH_2O$	NaY	2110, 2047	this work
$Rh(CO)_2(O_z)_2$	NaY	2096, 2022	this work

In this example, $Rh(I)(CO)_2$--SiO_2 was generated by O_2 oxidation of $Rh_6(CO)_{16}$--SiO_2 formed by impregnation of $Rh_4(CO)_{12}$ in a hydrocarbon solvent with subsequent decomposition to the higher nuclearity cluster. Our results are consistent with these proposed reactions. Although the presence of $Rh(III)CO$ and $Rh(I)(CO)_2$ is not obvious in the spectra shown in Figure 6, they may be obscured by the broad peaks in the 2200-2000 cm^{-1} region.

The important role of the zeolite water is exemplified by the results presented in Figure 7 . Catalyst AY dried in air produced the $Rh(I)(CO)_2$--NaY species (see Figure 7a). The four bands are attributable to two dicarbonyl species.
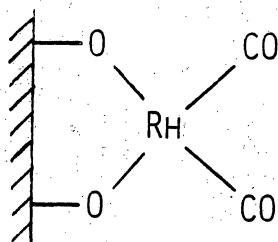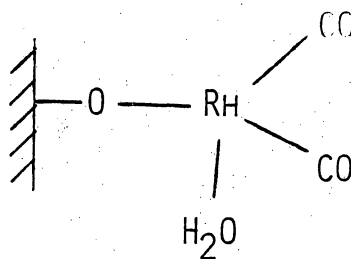
Species I   Species II

Species (I) $Rh(CO)_2(O_z)_2$ (O_z is lattice oxygen), yields IR bands at 2096 and 2022 cm^{-1}. Species (II) has the formula $Rh(CO)_2(O_z)(H_2O)$, where the rhodium is tethered to the zeolite by only one bond. The IR bands for this species are at

2110 and 2047 cm^{-1}. The same spectra as that for dried AY is produced from dried catalyst IY as shown in Figure 7 b. One additional band at 2167 cm^{-1} is assigned to the Rh (III)-CO species (55). Catalyst IY precarbonylated without drying produced the $Rh_6(CO)_{16}$-NaY as seen in Figure 7 c. Hence these experiments indicate that a dehydrated zeolite inhibits the sequence proposed by Theolier et al. (53). The reaction stops once $Rh(CO)_2$-NaY is formed. Rh clusters form only on RhNaY at low pressure in the presence of water.

Several studies on the formation of zeolite supported mononuclear and polynuclear carbonyls are reported in the literature. No explanation has been given for the inconsistencies among these reports. Experimental differences included rhodium source ($RhCl_3$, $(Rh(NH_3)_5Cl)Cl_2$, $Rh(NH_3)_6Cl_3$), and pretreatments (air, oxygen, nitrogen, or CO/H_2). The results shown here indicate that the degree of zeolite hydration is the controlling factor. Gelin et al. (51), Primet et al. (55), and possibly Arai and Tominaga (31) dried the catalyst prior to CO adsorption. They all reported dicarbonyl formation. Mantovani et al. (10) dried their catalyst only at room temperature. Therefore, there was sufficient water present to form the $Rh_6(CO)_{16}$ cluster.

Evidence for the mobility of cations in zeolites is given in Figure 38 . It is shown that the self-diffusion coeffi-
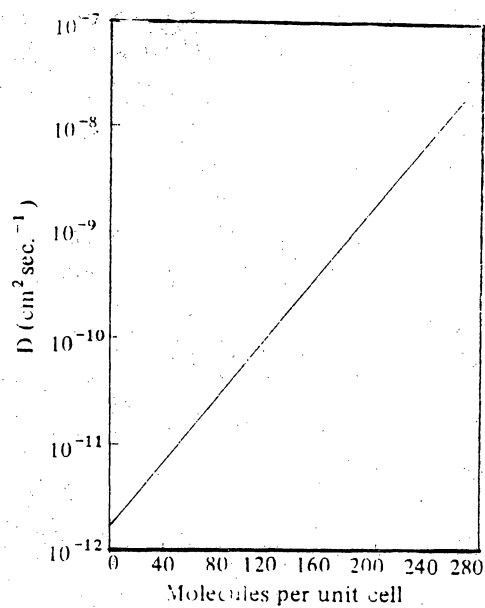
Figure 38: Dependence of Self-Diffusion of Na$^+$ in NaX at 25°C on Number of Water Molecules per Unit Cell (48)

cient of Na$^+$ in NaX at 25°C is strongly related to the degree of hydration. The self-diffusion coefficient increases by 3 orders of magnitude over the range of 40 to 240 water molecules per unit cell (48). Recall that 240 water molecules are close to the value in the stochiometric formula for NaX. Similar behavior has been observed for NaY. Since the RhNaY is hydrated when the precarbonylation begins, rhodium ions should have considerable mobility. However, drying the zeolite at 190°C possibly restricts the rhodium mobility. Hence, only mononuclear species are formed. For RhNaX, mechanisms other than ion mobility as a result of hydration must account for the absence of cluster formation.

The carbonylation of catalyst HY produced all three of the species discussed above (see Figure 8). The presence of $Rh_6(CO)_{16}$ is evidenced by the triply bridging band at 1762 cm^{-1}. The intense carbonyl stretching mode at 2095 cm^{-1} for the cluster is obscured by the bands assignable to the two dicarbonyls. The carbonylation intermediate species are also slightly different. However, it is believed that this catalyst follows the mechanism outlined above.

The differences between catalyst AY and HY are that for catalyst HY the pH was allowed to drop to 4 (no addition of base is required for this exchange) and no NaCl is present. Since the ion exchange process involve replacing 3Na$^+$ with

one Rh^{+3}, or Na^+ with one H^+, it appears that the sodium ion may be controlling the degree of dispersion and/or location of ion exchange of the Rh. A competitive exchange reaction may exist as follows:

$$3Na_s^+ \longleftrightarrow 3Na_z^+ \longleftrightarrow Rh^{+3} \qquad (3)$$
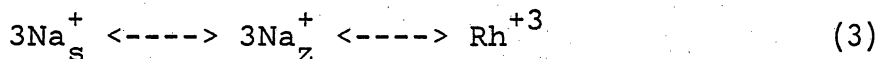
where subscript s and z denotes solution and zeolite species, respectively. These equilibria could exist for each ion exchange site in the zeolite. In the absence of this competitive exchange during preparation of catalyst HY, it is apparent that the Rh is exchanged into different sites.

6.1.2 RhNaX

The carbonylation of RhNaX (see Figure 9) is not nearly as complex as that for RhNaY. The $Rh(I)(CO)_2$-NaX species is dominant while some multinuclear species, $Rh_x(CO)_y$ where $x \geq 2$, is also present. The band positions correspond with the literature values as shown in Table 10 . By analogy to the IR band positions of the two types of dicarbonyl species, the dicarbonyl is assumed to be the bidentate structure (species I). Unlike the RhNaY, only one species is observed on RhNaX.

The fact that the NaX and NaY predominately support mononuclear carbonyls and polynuclear carbonyls, respectively,

is an excellent example of the differences in intrazeolitic chemistry for these two zeolites. While the topology for these two zeolites is identical, structural differences include cation positions and number, cation distribution, framework charge, and Si/Al ordering. The differences in cation exchange behavior has been studied extensively (48). However, properties at near full exchange capacity have been studied with little emphasis on the low loadings. Evidence indicating differences between NaX and NaY include diffusion and heats of adsorption. Table 11 presents a comparison in the heats of adsorption for various molecules. In general, higher activation energies for diffusion exist on NaX, as well as higher heats of adsorption. This data suggest that molecules have more restricted mobility in NaX than in NaY. Since a high degree of mobility is required to form polynuclear rhodium clusters, the NaY support would be the more likely candidate of the two zeolites for supporting such species. The difference between the electrostatic potentials for NaX and NaY may also result in stronger rhodium-zeolite bonds in NaX than NaY. A stronger metal-support interaction on NaX may prevent the agglomeration of rhodium atoms necessary to form polynuclear carbonyls.

TABLE 11

Heats of Adsorption Data For NaX and NaY (48)

	NaX	NaY
H_2O	22.7 kcal/mole	19.5 kcal/mole
NH_3	16	13.9
CO_2	11	7.3
C_2H_4	9.2	7.6
CO	5.63	5.4

6.2 RHODIUM CARBONYL LOCATION

The primary objective of the reaction with the two phosphines was to locate the carbonyls on the zeolite. Evidence of the addition of a phosphine ligand to a rhodium complex is a decrease of a carbonyl stretching frequency. Reactions with HDP were used to indicate that the species resides on the exterior of the zeolite, while it was expected that DMP would be able to react with carbonyls positioned throughout the crystal.

It has been pointed out previously that the shift in the bridging band at 1760 cm^{-1} for $Rh_6(CO)_{16}$-NaY is taken as evidence for the cluster residing in the alpha cage. Additional evidence is shown in Figure 36 b and c. No changes in these spectra indicate that the cluster does not react with HDP. Therefore, the cluster is located in the α-cage. Reaction with DMP produced the strong band at 1959 cm^{-1}. Reduction in the intensities of 2091 and 1766 cm^{-1} also indicate the decompostion of $Rh_6(CO)_{16}$.

RhNaY precarbonylated to produce the two dicarbonyl species exhibits interesting behavior (see Figure 34). The two dicarbonyl species react quickly with DMP. The higher wavenumber stretching frequencies completely disappear along with the development of a weak 1964 cm^{-1} band, indicating that only monocarboyl species are present. Spectrum 34B

shows that rhodium carbonyl phosphine complexes of the form NaY-Rh(CO)(PPhMe$_2$)$_n$ have been formed. DMP also consumed H$_2$O to produce phosphate. The P=O stretching bands, located at 1313 and 1305 cm^{-1}, intensified as the 1640 cm^{-1} water band decreased. HDP reacts only with the bidentate structure. Only bands indicative of the species II are present. Also, a slight shoulder appears at 1950 cm^{-1}.

The Rh(CO)$_2$-NaX reacts similarly to Rh(CO)$_2$-NaY with the DMP (see Figure 35). The antisymmetric stretch is removed and replaced by a weak band at 1990 cm^{-1}. Note also that virtually all the H$_2$O was reacted to form phosphate. However, the HDP failed to change the dicarbonyl bands. The weak additional band at 2035 cm^{-1} may indicate reaction with some surface rhodium but the majority of the dicarbonyl appears to be located inside the zeolite. Also no bands were seen below 2000 cm^{-1}.

The reactions of the dicarbonyl on RhNaX and RhNaY with the two site discriminating phosphines illustrate the power of chemical probes. Whereas Lefebvre and Ben-Taarit (57) proved the existence of the two dicarbonyls, their techniques were not adequate to determine location. Here it is shown that for RhNaY, the bidentate structure is located at the surface while the Rh(CO)$_2$(H$_2$O)O$_z$ is inside the alpha cage. Interestingly, the Rh(CO)$_2$(O$_z$)$_2$-NaX is located inside the zeolite crystal.

6.3   CATALYTIC ACTIVITY

Rhodium zeolites are active for hydroformylation of propylene, although the conditions for catalyst preparation are very restricted. In general, the activity of rhodium zeolites in this study compares favorably with the results of Ichikawa (6) and Arai and Tominaga (31). The rates are faster than those reported by Takahashi and Kobayashi (Table 2). The activation energies agree with values of Takahaski and Kobayashi, and Ichikawa, but are significantly different than the values from Arai and Tominaga. Since E_A^I is higher than E_A^N, the trend in regioselectivity is that it increases with decreasing temperature. This is observed in homogeneous cases as well (58).

The catalyst required an activation temperature of 150°C. Scurrell and Howe (37) reported the same temperature requirement to activate RhNaX for methanol carbonylation. They postulated that 150°C was required to reduce Rh(III) to Rh(I). Since catalysts AY had been pretreated at 120°C with CO, this reduction process has already occurred. In fact, the in situ rhodium carbonyl formation studies indicate that roughly 80-90°C was the reduction temperature. Therefore, the activation temperature cannot be attributed to this process. One possibility is that this temperature is required to form a rhodium hydride.

The long time required to reach steady state can be attributed to two processes. Time may be needed to build up the concentration of active sites. Secondly, it has been illustrated that startup time for ethylene hydroformylation could be reduced by roughly one third by preadsorption of propionaldehyde (32). Hence in our case, some time is required to saturate the support with butyraldehyde.

The maximum in iso-butyraldehyde rate could be ascribed to the loss of rhodium carbonyls from the exterior of the catalyst. Since 150°C may volatilize certain rhodium carbonyls, untethered rhodium might be able to vaporize into the product stream. This loss of rhodium may also account for the increased sharpness of the IR bands of the catalyst following reaction. Atomic absorption analysis of the catalyst before and after reaction did not indicate a difference in zeolite rhodium content.

Due to the low activation energies for hydroformylation, it was suspected that the rates may be mass transfer limited. This possibility is partly disallowed by the fact that the Arrhenius plots are linear over the 80-150°C range. Also, Ichikawa's studies were performed on larger pore supports and he obtained similar values. One report on rhodium zeolite hydroformylation (31) contained values of 8.7 and 7.3 for E_A^N and E_A^I, respectively. This deviates from the

relative values seen here. The discrepancies may be due to their off-line sampling technique, and the mass transfer effects due to larger pellet size (-10/+20 mesh).

The assumption of a differential reaction for rate calculation was substantiated by results shown in Figure 12 . Since the conversion was linear with W/F, the differential conversion analysis was valid.

Rates reported at 150°C can skew the impressions of selectivity for the catalysts. Thermodynamically, the hydrogenation path is preferred at 150°C compared to the hydroformylation. If the rates were reported at 100°C, selectivity would be around 1.0 or less (see Figure 11).

As mentioned in Chapter II, most supported rhodium catalysts have a regioselectivity around 2.0. This is twice the homogeneous catalyst value. These catalysts then may be considered to be zeolite-modified rhodium carbonyls, i.e., the framework serves as a ligand for rhodium rather than simply a support. Hence, the effect of the zeolite may be similar to the role of phosphorous compounds as ligands. It is evident then that the role of the support is due to steric and/or electronic influences. Molecular sieving is disallowed since the pore size of NaX and NaY zeolite are large enough to allow diffusion of both reactants and products. The fact that M/SiO_2 also produced $n/i \simeq 2.0$ supports these conclusions.

Rhodium metal is known to be an excellent hydrogenation catalyst. By pre-reducing the catalyst in H_2 at $100^{\circ}C$, propylene was completely converted to propane. However, under hydroformylation conditions, the CO adsorption inhibits hydrogen adsorption and the rate of hydrogenation was reduced by a factor of 100 and no hydroformylation activity was observed. Thus, it is believed that hydroformylation is not taking place on rhodium metal.

The decrease in hydrogenation activity while the aldehyde rate increases can be interpreted as a possible interconversion of active species. Initially, hydrogenation species dominate, but are replaced by the hydroformylation active species.

Since it is possible to form different rhodium carbonyls on zeolites, the activity of these species as catalytic precursors was studied. It is apparent from the results in Table 6 that different carbonylation methods did not have a strong effect. Only the pre-reduction with 10% H_2 in N_2 altered the selectivity. The regioselectivity decrease to 1.37 was also observed by Takahashi and Kobayashi (32). This trend toward the homogeneous regioselectivity is not fully understood. One explanation could be the presence of active sites on the edges of large rhodium rafts. These rafts have been observed for Rh/Al_2O_3 systems (59). It has

been shown that addition of CO to these rhodium rafts alters the Rh-Rh bond length (60). Hence, the raft is allowed to expand, (or "breath") (61). The rafts collapse following CO desorption. If the hydroformylation is conducted on this surface, the effects of the zeolite may be blocked. Thus, the selectivity could approach homogeneous values.

It is interesting to note that catalyst HY activated only by the H_2/N_2 pretreatment. Rates and selectivities agree well with Takahashi and Kobayashi (see Table 2 and Table 6). However, catalyst AY pretreated in this manner had slightly higher regioselectivity than HY.

The production of 2-propanol during start-up can be rationalized by two synthetic routes. Formation of lower alcohols via hydration of olefins readily occurs in the presence of acid. The second route is a two step process. It has been shown that rhodium can catalyze aldehyde formation via water addition to olefins. The propionaldehyde then would be hydrogenated to propanol. Takahashi et al. (62) have shown the propionaldehyde desorbs from NaY to produce pentene. It is not possible to define the actual path. However, the Wacker-type mechanism is supported by the fact that pentene is observed. No propionaldehyde has been detected in this study.

The other start-up products shown in Figures 51-54 have not been identified. The molecular weights are relatively high compared to the corresponding molecular weights and retention times of known compounds (note Table 20 in Appendix C).

The formation of ketones is not typically considered as a side reaction of the rhodium based hydroformylation process. The three C_7 ketones are the result of the rhodium zeolite acting as a bifunctional catalyst. The fact that aldehyde vapor passed over NaY (which had been refluxed in 0.1N NaCl at 90°C) with normal hydroformylation reactants yielded the three ketones indicates that the zeolite is performing the following reactions:
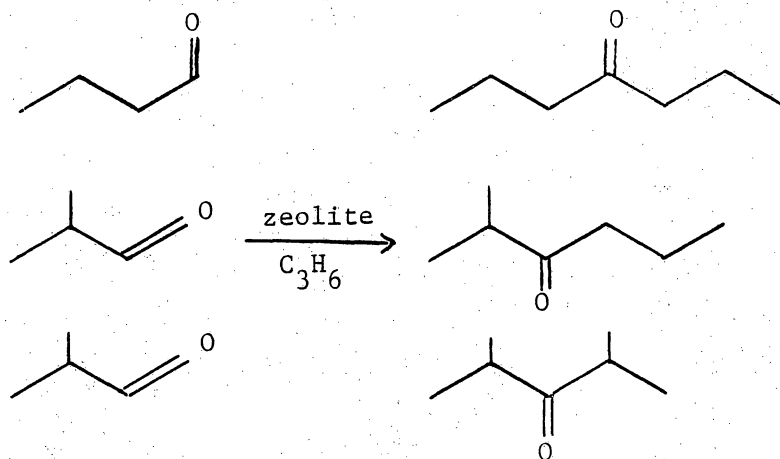
Catalyst preparation and pretreatment affect the ketone production. Catalyst AY converts less than 5% of the aldehyde to the ketone. It is significant that the 4-heptanone

to 2-methyl-3-hexanone ratio is 2:1. 2,4-dimethylpentanone occurs only during startup. This is the same selectivity shown for aldehyde production. The 0.2N NaCl prepared catalyst showed 100% conversion of butyraldehyde to ketone in the same 2:1 ratio. It was initially thought that some NaCl may be occluded within the zeolite. However, XPS and silver nitrate tests did not show an increase of chloride. Catalyst HY pretreated by the 10% H_2 in N_2 method also showed enhanced selectivity for ketone formation in the same 2:1 ratio. This exchange method does not have any NaCl present. Therefore, the occluded NaCl must not promote ketone production.

6.4   IDENTIFICATION OF REACTION INTERMEDIATES

6.4.1   RhNaY

The general approach to assigning the infrared bands resulting under hydroformylation conditions was to look for those species which are present in homogeneous systems. This required elimination of all bands due to the products adsorbed on the zeolite. Individual gas adsorptions and combinations of reactant gases were used to identify intermediates.

Metal hydride (M-H) and metal carbonyl stretching frequencies appear in the same region (2100-1600 cm^{-1}). This

overlap makes positive assignment of the bands difficult. Isotopic substition experiments, the most frequently used technique to separate bands, were only moderately successful due to the complex spectra. These limitations will be pointed out below.

Precarbonylated 1 wt.% catalyst AY (see Figure 17) under reaction conditions will be analyzed thoroughly since it provides the best resolution.

Bands in region III for spectrum A are attributed to adsorbed propylene. Adsorption of propylene and CO onto NaY at $120^{\circ}C$ produced the same bands (see Figure 41 in Appendix B). Table 12 lists the IR frequencies for propylene in the gas phase and on the zeolite NaY. The shifts of the CH_3 group asymmetric and symmetric deformation band suggests the adsorption of $C_3^=$ in a partially hydrogenated state (an alkyl group). Similar observations have been reported (63). The asymmetric bands are lowered to 1455 and 1442 cm^{-1} also. In the gas phase, the double bond stretch for propylene is located at 1645 cm^{-1}. No intensity changes in this region support the conclusion that the double bond character is diminished when adsorbed on the zeolite.

The stretching frequency of the carbonyl group of liquid aldehyde occurs in the range 1740-1720 cm^{-1} (49). Hence, the 1721 cm^{-1} band in spectrum A is attributed to adsorbed product aldehyde (see Figure 43 in Appendix B).

TABLE 12

IR Bands for Propylene

Gas	NaY	Assignment
1647	---	C=C stretch
1472	1456	CH_3 asym deform
1448	1442	CH_3 asym deform
1416	1420	CH_2 deformation
1399	1380	CH_3 sym deform
1287	---	CH bending

The 2042 cm^{-1} band is taken as evidence for the following species:

$$O - Rh \overset{\displaystyle\diagup CO}{\underset{\displaystyle| \atop C_3H_6}{- CO}}$$

$$| \atop Z$$
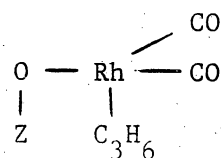
This is supported by the results of propylene and CO adsorbed onto Rh$_6$(CO)$_{16}$-NaY at 150°C as shown in Figure 26 . Initially, the band appears at 2041 cm^{-1}, but after 20 hours, it shifts to 2037 cm^{-1}. Following this band in Figure 17 with time shows the same behavior under reaction conditions. Lefebvre and Taarit (57) reported that addition of ethylene to the dicarbonyl (species I) produced the above structure with carbonyl frequencies at 2110 and 2042 cm^{-1}. With propylene, a shoulder on the high frequency side of 2095 cm^{-1} peak hints that this band is present, but it is obscured by the 2093 cm^{-1} of Rh$_6$(CO)$_{16}$. King et al. (64) identified C$_2$H$_5$Rh(CO)$_4$ under homogeneous hydroformylation conditions by in situ IR. The complex featured carbonyl stretches at 2115, 2037, and 2019 cm^{-1}. Assignment was based by similarities of the IR for CH$_3$Co(CO)$_4$. (The fact that this assignment assumes the presence of mononuclear carbonyls will be addressed in more detail below).

Changes in spectrum B are largely attributable to buildup of product on the catalyst. The shift of 1721 cm^{-1} to 1714

cm^{-1} results from the higher coverage of the zeolite and the shift in selectivity to n-butyraldehyde. This trend is shown in Figures 42 and 43 in Appendix B. The intensification of 1380 cm^{-1} is also due to the aldehyde.

The deformation band of a $=CH_2$ group appears at 1480-1440 cm^{-1} for aliphatic hydrocarbons. This mode of vibration shifts to 1430-1415 cm^{-1} for a metal alkyl group ($M-CH_2$) (49). The rocking mode for $\equiv CH$ group occurs at 1340 cm^{-1}. By analogy to the CH_2 deformation shifts, a metal alkyl of the form M-CH would be subjected to a shift to around 1300 cm^{-1}. Based on these shifts, the 1292 cm^{-1} in spectrum B is assigned to a rhodium isopropyl species. An additional argument is the displacement of rocking deformation to 1265 cm^{-1} for the species, $M-CH=CH_2$ (49). Although the bonding is sp^2 (compared to sp^3 above), the assigned species represents an intermediate effect due only to the metal

The 1623 cm^{-1} band is tentatively assigned to the stretching frequency of propylene adsorbed onto the zeolite. Interactions of the double bond with Na^+ ions result in the shift to lower frequencies. The magnitude of the shift is cation dependent, but has been shown to be at 1625 cm^{-1} for NaY (65). The adsorption of propylene was reported as reversible (65). However, the 1625 cm^{-1} band on our catalyst at steady state was not removed under vacuum. ^{13}CO substi-

tution (see Figure 31) did not produce the 1625 cm^{-1} nor a corresponding band at 1560 cm^{-1}. Hence, it does not appear to be due to the carbonyl species.

It is perplexing that neither the 1292 or the 1623 cm^{-1} bands are observed during the adsorption of propylene onto plain NaY zeolite. Possibly, the support is exposing different adsorption sites under reaction conditions.

The steady state spectrum was collected after 20 hours. It is significant that no spectral changes had been observed for several hours. This is approximately the same time required for the catalyst to reach steady state in the reactor (see Figure 10). This result provides evidence that the IR flow cell does in fact mimic the behavior of the reactor system.

It has been shown that the bands around 1720-1700 cm^{-1} are due to butyraldehyde adsorption. Further shifts to 1695 cm^{-1} also result from the adsorption of 4-heptanone (see Figure 44 in Appendix B).

The assignment of the 1660 cm^{-1} band is difficult since several species are likely candidates. It has been proposed that the rate determining step of the homogeneous rhodium carbonyl mechanism is the hydrogenolysis of the acyl complex. If this is correct, then it is expected that the acyl concentration would be higher than other intermediates. The

metal acyl has been identified through a downfield shift of the carbonyl stretching frequency. Literature values range from 1720-1650 cm^{-1} as shown in Table 13 . The assignment is not clear as seen by the scatter in Table 13 . Generally, it has been assigned at either one of two positions in the literature at 1725 -1720 cm^{-1} and at 1675-1650 cm^{-1}.

One product which adsorbs at approximately 1660 is an α, β-unsaturated aldehyde. Such a compound would be formed from an aldol condensation reaction between two aldehydes with subsequent dehydrogenation. 2-trans-hexenal was adsorbed onto NaY to approximate the aldol condensation compound, and produced a band at 1680 cm^{-1} (see Figure 44 in Appendix B). Therefore, the dehydrogenated aldol condensation product can be eliminated as the source of the 1660 cm^{-1} band.

Since no other products of the hydroformylation reaction adsorb in this region, the band at 1660 cm^{-1} is assigned to the rhodium acyl, Z-O-Rh(COPr)L_2, where L=CO or O_z. Several additional arguments for this assignment follow.

One argument for this assignment is from analogy to aldehyde and ketone carbonyl band positions. In Table 14, values for ν_{CO} are shown as a function of alkyl group size. Note that there exists a 36 cm^{-1} reduction between methyl-propyl ketone and methyl-ethyl ketone. A 29 cm^{-1} reduction

TABLE 13

Literature Values for Acyl Carbonyl Frequencies

compounds	$\nu_{CO}cm^{-1}$	Reference
$(NEt_4)(Rh_6(CO)_{15}(COPr)$	1655-1670	66
$Rh(COCH_3)$ I-NaX	1720	39
CH_3CO $Mn(CO)_5$	1661	67
$NaX-ORh(COCH_3)I$	1724	68
$(C_8H_{17}CO)Co(CO)_4$	1720	69
$(CH_3CO)Co(CO)_4$	1720	14
$(nBuCO)Co(CO)_4$	1720	77
M-CO-X, X=Halide	1640	70
C_2H_5CO $Ir(CO)_3P-i-Pr_3$	1671	71
$(C_2H_5CO)Co(CO)_3PBu_3$	1676	71

is observed between diethyl ketone and ethyl-propyl ketone. The carbonyl band position drops 35 cm^{-1} between the acetaldehyde and pentanal. By changing the olefin under hydroformylation conditions, the acyl would occur at different positions. The steady state spectrum for catalyst AY under ethylene hydroformylation conditions contains a 1700 cm^{-1} band, but not one at 1660 cm^{-1}. This 1700 cm^{-1} band is assigned to the rhodium acyl for propionaldehyde production.

Finally, the behavior of catalyst HY provides yet another argument for the acyl band assignment. This catalyst initially was active, but deactivated after several hours. As shown in Figure 23, the acyl intermediate appears earlier than for catalyst AY, but then is absent after 5 hours. If this were an adsorbed product, the band would remain. Finally, attempts to remove the 1660 cm^{-1} by replacing reactants with CO/H_2 for other stable catalysts did not alter the band intensity or position. This is taken as indirect evidence for the stability of the acyl.

The remaining bands to be assigned are the groups between 2050 and 1900 cm^{-1}. Terminal metal carbonyl and metal hydride stretches appear in this region. Positive assignment of these bands to ν_{Rh-H} or ν_{Rh-CO} bands was difficult. Theoretically, substitution of H_2 with D_2 would be located at $\sqrt{1/2}\ \nu_{Rh-H}$. If $\nu_{Rh-H}=2040$ cm^{-1}, ν_{Rh-D} would be 1440

TABLE 14

Carbonyl Band Positions for Aldehydes and Ketones (72)

Aldehydes	ν_{CO}
Formaldehyde	1754, 1724
Acetaldehyde	1730
Propionaldehyde	1724
Valeraldehyde	1695

Ketones	
Methyl propyl ketone	1694
Methyl ethyl ketone	1730
Ethyl ketone	1724
Ethyl propyl ketone	1695

cm^{-1}. This region is complex at steady state. Unfortunately, the bending mode for partially deuterated water (HOD) is also located at 1425 cm^{-1}. Therefore, any growth in band intensity in the mid-1400 cm^{-1} region is due to DOH, not Rh-D. Figure 33 shows this band develops while the H_2O bending mode at 1640 cm^{-1} decreases. Attempts to replace zeolitic water with D_2O were not successful. Temperatures up to 500°C would be required to dehydrate the zeolite. This was not done since it would be too far removed from actual operating procedures. Similar difficulties were encountered with ^{13}CO substitutions. Terminal carbonyl bands of both $Rh(CO)_2$-NaY and $Rh_6(CO)_{16}$ shift to 2040 cm^{-1} with ^{13}CO ($\sqrt{12/13}$ x ν_{Rh-CO}). Similar overlapping difficulties in the 1700- 1500 cm^{-1} region made isotopic substitution difficult to interpret.

An added experimental difficulty was the extreme sensitivity of the 2050-1900 cm^{-1} bands to CO and H_2 partial pressure. The flow D_2 experiment (see Figure 32) was designed to circumvent this problem. Since no changes were observed after 1 hour of D_2 flow, it was concluded that these species were due to carbonyl bands. Flow ^{13}CO experiments are cost prohibitive.

The $Rh_6(CO)_{16}$ cluster was fully exchanged with labelled CO at 150°C as shown in Figure 31 . Since all of the bands

shifted and maintained the same shape, all bands above 1700 cm^{-1} after precarbonylation are due to rhodium carbonyls. This provides more evidence that the 2040 cm^{-1} band is not due to a rhodium hydride stretch.

Under reaction conditions with ^{13}CO few changes took place. The region between 1723 and 1640 cm^{-1} is lower in intensity without a resolved band. This may be due to product aldehydes or ketones with ^{13}CO substitution $(0.977(1710)=1670 \ cm^{-1})$.

Spectra resulting from the addition of individual gases to catalyst AY show different behavior than the catalyst exposed to a complete hydroformylation environment. In each case, (Figures 26-28), a band at approximately 1710 cm^{-1} indicates the formation of an oxygenate. In Figures 26 and 28, gas phase propylene bands between 3100-2800 cm^{-1} decreased concurrently with the 3690 cm^{-1} peak while the 1710 cm^{-1} band intensified. It is proposed that propionaldehyde is formed from propene and water. Notice also that gas phase CO_2 bands at 2354 and 2320 cm^{-1} are present under $C_3^=/CO$ environment (Figure 26). CO_2 is probably produced from the water gas shift reaction:

$$CO + H_2O \underset{\leftarrow}{\rightarrow} H_2 + CO_2 \tag{4}$$

As a result of hydrogen formation, the flow cell contains all the hydroformylation reactants. Therefore, the 1710 cm^{-1} may also be due to the presence of butyraldehyde. It is significant that no CO_2 bands are present following H_2 and $C_3^=$ addition (Figure 28). In Figure 27, the appearance of bands in the 2900-3000 and 1300-1500 cm^{-1} regions indicate the conversion CO/H_2 to hydrocarbons and oxygenates. Carbon dioxide is also formed under the H_2 and CO atmosphere.

6.4.2   RhNaX

The RhNaX does not lend itself to the same detailed analysis as performed on RhNaY. The positions of the dicarbonyl bands, 2098 and 2014 cm^{-1} obscure the 2035-1950 cm^{-1} region. However, other important features are present. The shoulders on the high frequency sides of the dicarbonyl bands at 2100 and 2035 cm^{-1} are also present. The broad shoulder at 1940 cm^{-1} in spectrum C overlaps the region where many bands are present on RhNaY.

Aldehyde adsorption onto NaX is considerably different than on NaY due to the difference in silica and alumina content. Over time, a shift in aldehyde band is observed, although the initial band is 1704 cm^{-1}. The band is not as intense as on NaY. This is due to adsorption of

n-butyraldehyde in a carboxylate fashion. Bands at 1578 and 1419 cm^{-1} are due to the asymmetric and symmetric stretch of the following carboxylate group:

$$
\begin{array}{ccc}
\underline{\quad\quad} C & \overline{\underline{}} & O \\
\| & & \| \\
\underline{\quad} O & \underline{\quad} Al \underline{\quad} & O
\end{array}
$$
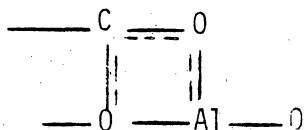
Hair and Chapman (73) performed IR adsorption studies with benzaldehyde on silica, alumina, and silca-alumina at various compositions. Only the alumina rich material allowed this type of adsorption. On silica, no carboxylate bands appeared.

Labelled CO experiments for RhNaX were more informative than on RhNaY. As seen in Figure 33, the shoulder at 1940 cm^{-1} moves without loss of intensity with the dicarbonyl bands. The shift of the broad, weak 1800 cm^{-1} band also indicates that it is a bridging carbonyl. The band at 1615 cm^{-1}, near the band assigned to adsorbed propylene on NaY, moves to 1600 cm^{-1}, indicating that it is a carbonyl stretch. The shift, however, is only by a factor of 0.989. Carbonyl group bonding through both carbon and oxygen possess an IR stretch around 1650 cm^{-1} (74). Also, hydrogen bonding with the carbonyl group can lower the frequency to

1610 cm^{-1} (49). As was observed for RhNaY, the region between 1700 and 1645 cm^{-1} is intense but unresolved due to isotopically labelled product oxygenates. Further evidence for this carbonyl assignment is the band at 1535 cm^{-1}. This band corresponds to the labelled aldehyde adsorbed in a carboxylate fashion.

6.4.3   RhNaX vs. RhNaY

Figure 39 shows the steady state spectra for catalysts AX and AY. This figure illustrates the similarities and differences between the two catalysts. Each catalyst indicates the presence of rhodium alkyl and acyl complexes. A direct comparison of the 2050-1900 cm^{-1} region is not possible, although the broad shoulder at 1940 cm^{-1} on catalyst AX suggests the presence of similar intermediates. Based on these observations, it is believed that the support is not influencing or altering the reaction mechanism.

Since the hydroformylation startup, regioselectivity, and activation energies are nearly the same for catalysts AX and AY, it is postulated that the active species for hydroformylation is the same for each catalyst. Although no Rh-H band was observed in the IR, it is believed that the active species contains a hydride because of what is known from homogeneous systems. The following reactions are postulated to give the active species:
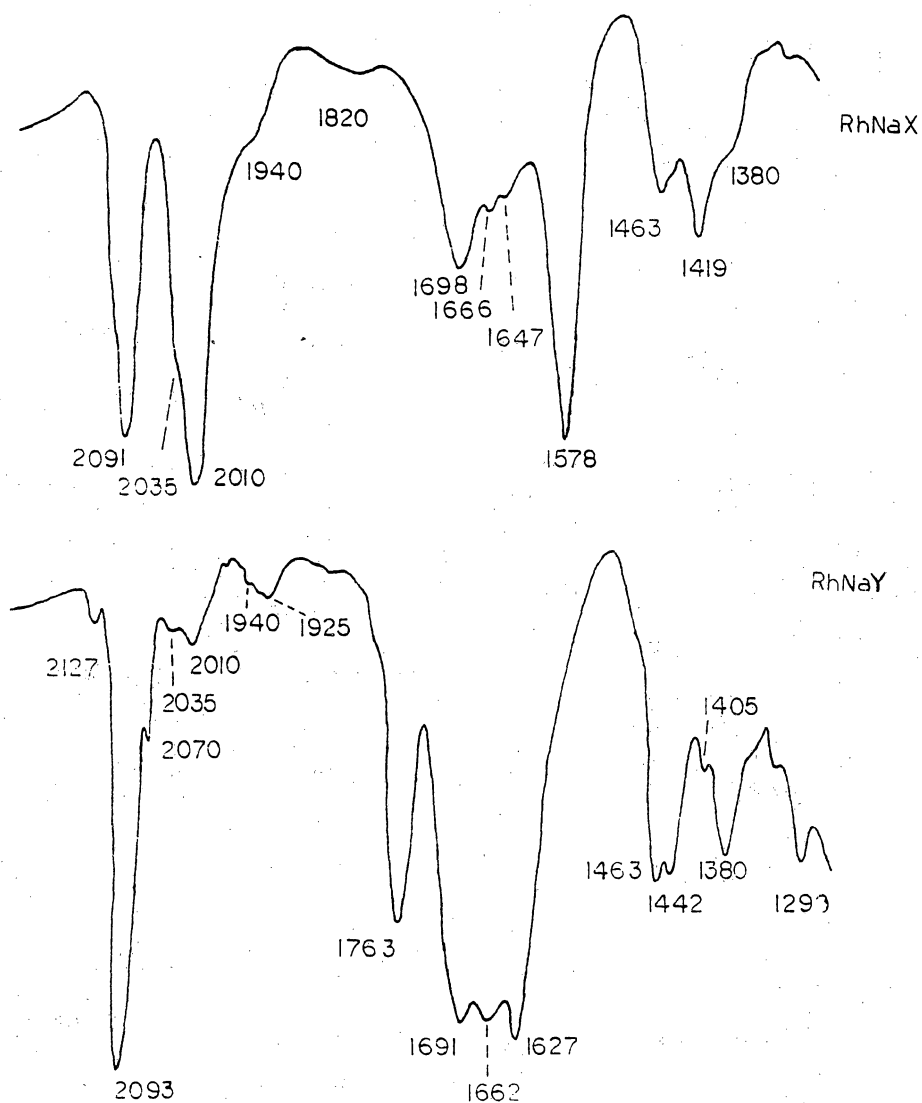
Figure 39:   Comparison of Catalyst AX and AY at Steady State

a) catalyst AX; b) catalyst AY

$$Rh(CO)_2\text{-NaX} \rightleftarrows HRh(CO)_x\text{-NaX} + H^+\text{-NaX} \qquad (5)$$

$$Rh_6(CO)_{16}\text{-NaY} \rightleftarrows Rh(CO)_2\text{-NaY} \rightleftarrows HRh(CO)_x\text{-NaY} \qquad (6)$$
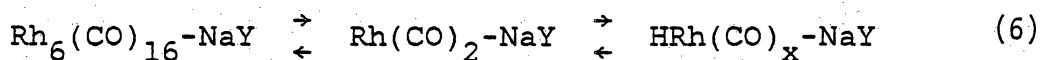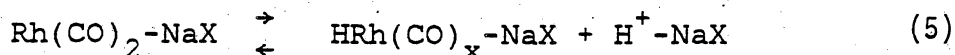
It was not possible to determine accurately whether the $Rh_6(CO)_{16}$-NaY or the $Rh(CO)_2$-NaX were decomposing. Transmission through the wafer decreased as the zeolite saturated with products. Therefore, a simple comparison of the before and after spectra is not possible. (Further comments on rhodium utilization are given below.) The equations for hydride formation are written as equilibria. Although the partial pressure of H_2 is three times that of CO, the total pressure may not be high enough to drive the equilibria toward the large production of hydride.

6.4.4   Active Site

Figure 40 is a collection of the steady state IR for catalyst AY as a function of pretreatment. Spectrum A is spectrum D of Figure 18 . Spectrum B is the spectrum D of Figure 19, and spectrum C is spectrum C of Figure 17 . This composite illustrates the catalyst similarities as a function of pretreatment. Obviously, pretreatment has little effect on the final spectrum. This is not surprising since the different pretreatments had no effect on catalytic performance.
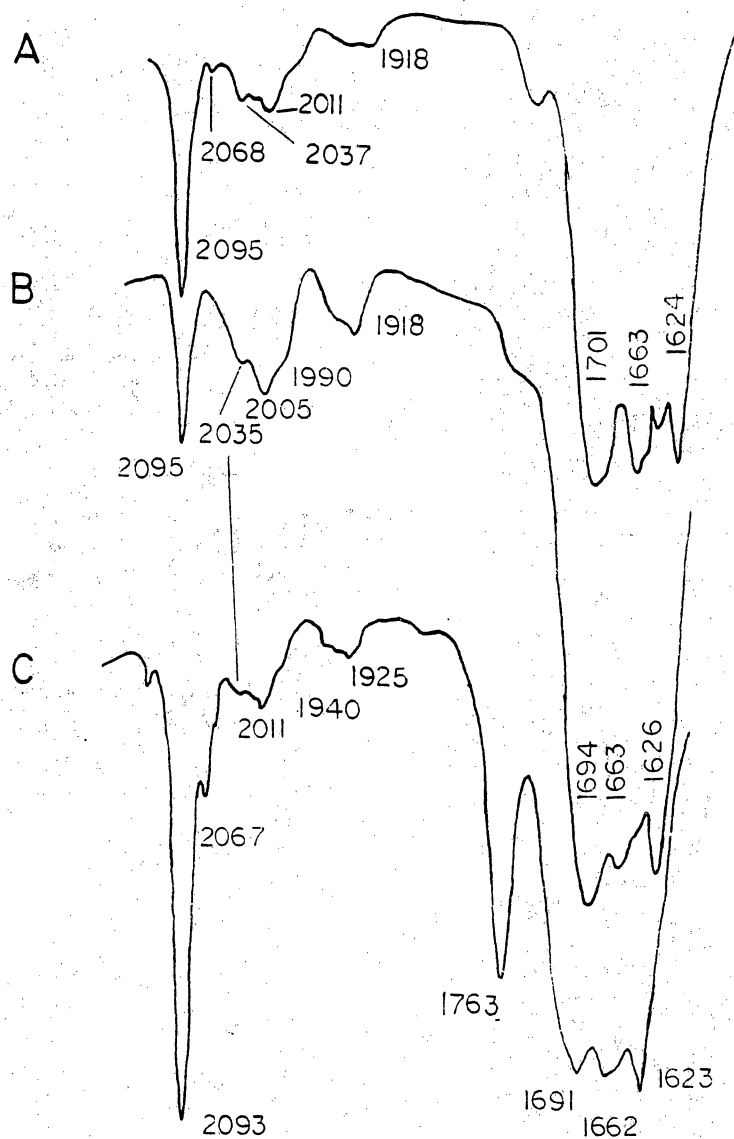
Figure 40: Steady State Spectrum of Catalyst AY Following Different Catalytic Pretreatment

a) air dried at steady state; b) N_2 treated at steady state; c) precarbonylated at steady state

Note that all three spectra contain $Rh_6(CO)_{16}$ bands at 2095 and 1763 cm^{-1} in varying intensities. The fact that spectrum C indicates that $Rh_6(CO)_{16}$ is the most abundant species and that the activity of this catalyst is essentially the same as with other pretreatments suggests that the cluster is not the active site for the hydroformylation of propylene. Rather, it appears that it is merely a rhodium sink. This does not preclude the possibility that the clusters may act as a rhodium source by decomposition under H_2. H_2 reacts with the cluster to produce dicarbonyl species and CO_2 (see Figure 27). Recall that the partial pressure of H_2 is three times that of CO. Because of this large amount of rhodium occupied in the cluster, it is apparent that only a small fraction of the metal is involved in catalysis. Hence, the combination of catalytic activity and in situ IR studies leads to the conclusion that rhodium utilization is poor for hydroformylation at 1 atm total pressure.

As shown in Figure 37 catalyst AY reacts with HDP to form rhodium phosphine complexes. However, the bands assigned to various intermediates are removed. Specifically, the rhodium alkyl bands at 2037 and 1292 cm^{-1}, the acyl at 1660 cm^{-1}, and the adsorbed propylene at 1623 cm^{-1} are not present after treatment with HDP. Also, the injection of HDP on the catalyst slowly poisoned the catalyst. These results imply

that the catalysis is taking place on the external surface of the zeolite. Note that $Rh_6(CO)_{16}$ bands were unaltered by HDP.

As mentioned in Chapter II, there is debate in the literature concerning the hydrogenolysis of the acyl species. Aldehyde production is proposed to proceed (i) via H_2 addition to the acyl with subsequent hydride insertion to yield aldehyde and the metal hydride, or (ii) via a binuclear elimination step. The spectra collected on the 4 wt.% catalyst provide some insight into these final steps of the mechanism. Under all pretreatment conditions, the acyl band at 1665 cm^{-1} appears within the first 5 hours, but is absent at steady state for the N_2 and air dried catalysts and is weak on the precarbonylated material. Each steady state spectrum contains some bands in the 1800 cm^{-1} region, with the precarbonylated catalyst having resolved bands at 1860 and 1840 cm^{-1}. By combining this information with the 1 wt.% catalyst spectra, it is plausible to propose that either one or both of the proposed aldehyde elimination steps is occurring. The 1 wt.% catalyst is probably better dispersed than the 4 wt.% catalyst and if a binuclear elimination step is occurring, then the probability of site-site interaction is lower for the 1 wt.% catalyst than for the 4 wt.%. This would result in a higher concentration of rhodium acyl spe-

cies on the 1 wt.% material. The likelihood of binuclear elimination is enhanced on the 4 wt.% catalyst. The binuclear elimination step would supposedly have $Rh_2(CO)_8$ as a by-product. The bands at 1860 and 1840 cm^{-1} are close to the 1852 and 1832 cm^{-1} bands reported for this dimer. However, some caution must be exercised here due to the extreme volatility of $Rh_2(CO)_8$ and by the fact that this compound cannot be isolated. It is felt that the reason for the appearance of the acyl band in spectrum C is that a large portion of the rhodium is tied up in $Rh_6(CO)_{16}$ which would reduce the availability of rhodium-rhodium intermediates. Alternatively, since the cluster completely fills the α-cage, diffusion of the reactants may be blocked or slowed.

Collman et al. (75) performed an investigation on Rh-silica which found that activity was linear with catalyst dispersion (or site-site interaction). The catalysts with higher dispersions were the least active. This was taken as evidence that binuclear elimination was the product elimination step.

6.5   HETEROGENEOUS VERSUS HOMOGENEOUS MECHANISM

It is illustrative to compare the steady state positions of the IR bands with those reported in the literature. No heterogeneous data is available. IR for homogeneous intermediate species for cobalt and rhodium are shown in Table 15 . It is noteworthy that IR frequencies seen in this study are similar to those observed in homogeneous catalytic systems. Homogeneous reaction intermediates give bands with values ranging from 1993 to 2114 cm^{-1}. This overlaps closely with those observed on the rhodium zeolite. However, there are no equivalent bands in the homogeneous studies as low as 1920 cm^{-1}.

Comparison of the observed species with the proposed intermediates of the Heck-Breslow mechanism reveals that the heterogeneous rhodium carbonyl catalyst could be following the same path as the homogeneous rhodium carbonyl analogue. Those species which are not observed are the hydrido-rhodium species, and the coordinated olefin. Absence of IR bands for these species is not surprising considering their instability and their position in the catalytic cycle. The coordinated olefin to metal alkyl transition would be fast at 150°C. This reaction consumes one hydrido species. The oxidative addition of H_2 prior to aldehyde elimination is believed to be the rate determining step. Therefore this

TABLE 15

Literature IR Values for Hydroformylation Intermediates

	ν_{CO} cm^{-1}	Reference
$HCO(CO)_4$	2114, 2053, 2032, 1993	(76)
$RCo(CO)_3$	2105, 2035, 2018	(15)
$MeCo(CO)_4$	2105, 2036, 2019	(14)
$RCOCo(CO)_3$	2108, 2010	(15)
$RCOCo(CO)_4$	2103, 2044, 2022, 2003, 1720	(77)
$RRh(CO)_4$	2115, 2037, 2020	(64)

dihydride would have a relatively short life span as well. There is evidence for the alkyl and acyl species, both of which implies the presence of hydride complexes. The data which presents the possibility of binuclear elimination is also consistent with homogeneous catalysis.

The partial pressure dependencies provide additional evidence for the similarities between the homogeneous and heterogeneous mechanisms. In general, a positive rate dependence for olefin and hydrogen and a negative rate dependence for carbon monoxide have been observed for homogeneous systems (78). No data at our reaction conditions exist in the literature for the homogeneous unmodified rhodium carbonyls thus, a direct comparison is not possible. However, the trends shown here correspond with the homogeneous data. Arai reports first order dependencies for H_2 and $C_3^=$, and a -0.6 dependence for CO for rhodium carbonyls supported on phosphinated silica which were shown to hydroformylate propylene similarily to homogeneous rhodium-carbonyl-phosphines (79) These parameters were determined under reaction conditions virtually identical to this study, i.e., 150°C, 3:3:1 mix of $C_3^=/H_2/CO$, and 1 atmosphere total pressure. Based on these similarities, it is concluded that the heterogeneous rhodium catalysts are following a mechanism similar to the homogeneous analogue.

6.6   INACTIVE CATALYSTS

6.6.1   Effect of Ion Exchange Conditions

Numerous experiments were performed in order to determine the ion exchange conditions which were critical to the production of an active hydroformylation catalyst.   The approach was to consider the exchange conditions for catalyst AY as the baseline, and to bracket those values of exchanges time, pH, and NaCl.   This series of experiments leads to the set of parameter windows shown in Table 16 .   The importance of these values is not fully understood, but some significant information was obtained which allows speculation on the physical processes occurring.

Catalysts AY, BY, and CY probed the role of solution pH. Below pH=6, the catalyst was inactive.   It was suggested by Shannon et al.   (46) that at pH 3.5-5.0 sufficient OH^- ions would be present to allow formation of $(Rh(H_2O)_{6-m}(OH^-)_m{}^{3-m}$.   Since there exists an equilibrium in solution between these rhodium aquo complexes, the zeolite may be discriminating among complexes.   This introduces the possibility that three differently charged rhodium complexes can be exchanged into the zeolite.   However, it has been shown that Rh^{+3} exchanges for 3 Na^+ in NaX quantitatively (80).   Therefore, it can be argued that only Rh^{+3} species are exchanged into the zeolite.   If a Rh^{2+} species was ex-

TABLE 16

Ion Exchange Conditions for Active Rhodium Zeolite Catalysts

$T > 80^{\circ}C$

pH > 6

5 < t < 24 hours

$NaCl \leq 0.1N$

$RhCl_3 \cdot 3H_2O$ - only source

changed, then a net charge balance necessitates a Rh^{4+} exchange, which is not possible. Shannon et al. showed that only $Rh(H_2O)_6^{+3}$ was exchanged into NaY. (This argument holds only for the rhodium trichloride exchanges since some ammine complexes are Rh^{2+}). Thus the lack of activity as a function of exchange pH suggests that initial placement of the Rh is central to activity.

One other exchange (catalyst HY) was performed at low pH. The catalytic activity of catalyst HY was probably due to the creation of acid sites within the zeolite. This postulate was verified by obtaining a similar product distribution from a plain NaY zeolite refluxed in a pH=4 solution. Comparing the activity of catalysts BY and HY suggests that the NaCl concentration is important. As mentioned above, there exists an equilibrium between solution Na^+ and H^+ ions. A high concentration of acid sites was probably not formed on catalyst BY due to the high concentration of Na^+ ions. This suggests that the competitive exchange reactions of Na^+ and H^+ for zeolite Na^+ ion favor Na_s^+-Na_z^+ exchange even at low pH.

With the pH maintained at 6, the salt concentration was varied between 0.0 and 0.2 N. Catalyst EY, AY, and DY were prepared in 0.0, 0.1, and 0.2 N solutions, respectively. The different behavior of these catalysts implies an influ-

ence of the solution Na$^+$ ions. In the absence of NaCl, startup time was almost tripled, while the excess of NaCl promoted the formation of ketones from butyraldehyde and propylene. The rhodium exchanged zeolites did not occlude NaCl. Silver nitrate tests and XPS failed to verify the presence of Cl$^-$. Hence, the possibility of occluded NaCl being a promotor is eliminated.

The variation of time at 90°C is the last parameter studied. Only catalysts under heat for 5 hours activated. The degree of exchange was not affected by the duration of exchange. Even catalyst GY, which was quenched immediately following Rh addition, was fully exchanged.

Collectively, the underlying implications of this sequence of experiments is that the zeolite is highly selective for certain rhodium ions. The catalytic properties of these exchangeable rhodium species are altered by temperature, pH, and salt concentration.

6.6.2   Ammine Preparations

The fact that all of the ammine preparations fail to produce an active hydroformylation catalyst is not understood. As is discussed above, the ion exchange process is very complex and directly influences activity. Although the same extensive battery of experiments was not performed, different pretreatments were studied.

Various ammine catalysts were dried in oxygen, air, and nitrogen as attempts to remove the NH_3 ligands prior to reaction conditions or precarbonylation. Primet et al. (55) reported that $350°C$ in O_2 was sufficient to remove NH_3. Scurrell et al. (37) reported $400°C$ in N_2 was also adequate to perform the same task. Temperatures up to $400°C$ were used, but none affected the catalytic activity.

The precarbonylation of the ammine exchanged catalysts go through similar processes as does catalyst AY. In Figure 25 the band at 1337 cm^{-1} is indicative of NH_3 ligands. During precarbonylation, this band weakens and disappears as a broad band at 1437 cm^{-1} intensifies. This is due to the formation of NH_4^+. For the ammine exchanges, either 5 or 6 NH_4^+ are produced per dicarbonyl species, or, 25 or 30 NH_4^+ ions are produced for each cluster formed. These ions then can potentially block the zeolite pores or occupy positions normally available for active sites. Heating of these catalysts in air prior to carbonylation is intended to prevent NH_4^+ formation by removal of NH_3. However, these catalysts are not active with or without ammonium ions. Therefore, it is felt that these ammonium ions are not the catalyst poison.

Following ion exchange, the important characteristics are 1) the predominant form of the metal, and 2) the location of

the metal. The EXAFS study by Denley et al. (45) showed that rhodium oxides were present for $RhCl_3 \cdot 3H_2O$ exchanged onto NaX. The ammine exchanges produced rhodium aquo complexes on NaX with better dispersion than $RhCl_3 \cdot 3H_2O$ prepared materials. It is not clear cut why the ammine catalysts are inactive. It may be due to the binuclear elimination step discussed earlier. A catalyst with higher dispersion would be less active if this is the mechanism (75).

The infrared experiments which duplicated the water injection onto catalyst IY did not reveal the source of activity (see Figure 25). The inactivity for catalyst IY was verified in the IR by the lack of bands at 1710 and below 1500 cm^{-1} (spectrum B). Water injection altered rhodium carbonyl bands by deteriorating the $Rh_6(CO)_{16}$. The cluster was quickly reformed as shown in Figure 25d. The subsequent H_2O injection removed all carbonyl bands. No product bands were observed. It was proposed that the NH_4^+ ion could become involved through the following reaction sequence:

$$NH_4^+ + H_2O \underset{\rightarrow}{\leftarrow} NH_3 + H_3O^+ \qquad (7)$$

$$RhNaY + CO + H_3O^+ \underset{\rightarrow}{\leftarrow} RhH(CO)_n + H_2O \qquad (8)$$
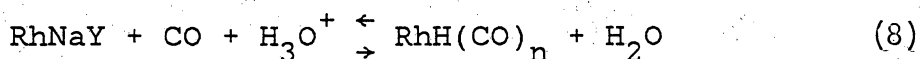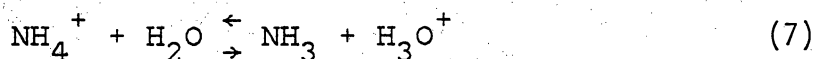
However, this was not substantiated since the NH_4^+ band at 1457 cm^{-1} did not change in intensity throughout the experiment. Bubbling reactants through H_2O so that a continuous excess of H_2O was present failed to maintain activity.

6.6.3 RhNaX

The difficulty in consistently forming an active RhNaX catalyst can be explained by two different arguments. The infrared spectra collected under reaction conditions for "inactive" catalysts show the existence of the same intermediates as the "active" catalysts, while the ammine preparation under reaction conditions (shown in Figure 25) did not show any additional bands indicative of product or intermediates. One order of magnitude decreases in rate would be immeasurable by the differential reactor system. Therefore, it appears that the "inactive" A-X catalysts were in fact active but at a very low rate. A second explanation is based on the binuclear elimination argument. As shown earlier, there is less cation mobility on NaX as a result of higher bond strengths. This restricted mobility may slow the rate of aldehyde production due to the inability to undergo binuclear elimination.

6.7 PRELIMINARY RESULTS FOR PHOSPHINE MODIFIED RHODIUM ZEOLITES

The addition of phosphines to the rhodium zeolite catalysts significantly alters the reactivity. A clear cut explanation for the behavior has not been reached. Primarily, these experiments were to initiate the study of the effects of phosphine in rhodium zeolites.

In general, the addition of DMP shifted the catalytic activity toward the production of linear compounds. N-butanol was the sole product formed initially in experiments C and E (see Table 9). However, the catalysts rapidly deactivated. Providing a constant partial pressure of DMP (Exp D and F) did not have a profound effect, although the rate of deactivation did appear to decrease.

Injection of DMP onto the catalyst produced an intense burst of activity in experiments B and F. In either case was the selectivity was not altered. This may be due to the reaction of DMP with H_2O to produce phosphates. Liberation of some hydrogen may be responsible for initial hydride formation, which could create active species. The exact cause of deactivation is not known at this time.

The addition of HDP to catalyst AY at steady state did reveal the location of the active site. Since this phosphine is too large to diffuse through the zeolite pores, any reaction with rhodium would be at the catalyst surface. The

catalyst deactivated after several hours. This result com-
bined with the removal of all intermediate bands in the
steady state IR (see Figure 37) lead to the conclusion that
the hydroformylation is occurring at the surface.

Chapter VII

CONCLUSIONS

The following conclusions can be drawn from this study of
the hydroformylation of propylene on rhodium zeolites:

1. Rhodium zeolites formed stable hydroformylation cata-
   lysts at 1 atm and 80-150°C. The selectivity to n-
   butyraldehyde was twice that of homogeneous rhodium
   carbonyls.

2. It was found that the catalyst activity was sensitive
   to the ion exchange variables of solution pH, salt
   concentration, temperature, and rhodium source. Only
   the rhodium trichloride exchanged materials were ac-
   tive.

3. It was shown that the degree of zeolite hydration in-
   fluenced the formation of rhodium carbonyls. A hyd-
   rated RhNaY supported polynuclear carbonyl species,
   while a dried RhNaY allowed only mononuclear carbonyl
   production.

4. Zeolite NaX supported the formation of the mononu-
   clear rhodium carbonyls under all conditions.

5. The location of the rhodium carbonyls were determined
   by reaction with phosphines. It was shown that
   $Rh_6(CO)_{16}$ and $Rh(CO)_2(O_z)(H_2O)$ were located within

the zeolite cages, and the $Rh(CO)_2(O_z)_2$ species was located on the surface.

6. NaX supports the rhodium dicarbonyl in the form $Rh(CO)_2(O_z)_2$. It was formed inside the zeolite cages exclusively.

7. The pretreatment of the catalyst had little effect on catalyst performance except for the partial reduction with hydrogen.

8. Reaction intermediates identified by in situ FTIR were similar to those observed during homogeneous rhodium hydroformylation. The partial pressure dependence of the rates on propylene, hydrogen, and carbon monoxide agreed with those reported in the literature for homogeneous catalyst. Based on these observations, it was proposed that the heterogeneous rhodium carbonyl catalyst appeared to follow the homogeneous mechanism. Reaction intermediates identified on RhNaX and RhNaY indicated that the hydroformylation was following the same mechanism on each catalyst.

9. Reactions of the rhodium carbonyls with n-hexyldiphenylphosphine indicated that the active site was located at the zeolite surface.

10. The addition of dimethylphenylphosphine to the RhNaY altered catalysts selectivity toward the linear product. Exposure to DMP at room temperature prior to reaction conditions initially produced n-butanol only. Continuous contact with phosphine reduced the rate of catalyst deactivation.

Chapter VIII

RECOMMENDATIONS

The following recommendations are made for the continued study of rhodium zeolite hydroformylation catalysts:

1. Higher pressures should be used to try to activate the "inactive" materials, i.e., the ammine exchanges and catalyst AX.

2. Questions concerning the importance of the various ion exchange parameters may be studied via _in situ_ UV-spectroscopy during the rhodium exchange.

3. The study of rhodium phosphine complexes as catalysts should be extended to other phosphines.

4. The role of water needs to be established in relation to the phosphine addition.

5. Deactivation studies can be performed by _in situ_ IR.

REFERENCES

1. Grubb, R.H., and L. C. Knoll. _J_. _Am_. _Chem_. _Soc_., 93, 3062, (1971).

2. Bailey, D. D., and S.H. Langer. _Chem_. _Rev_, 81, 109, (1981).

3. Whitehurst, D.D. _Chemtech_, 10, 44, (1980).

4. Pittman, C. U. Jr. in "Comprehensive Organometallic Chemistry", Ch. 55, G. Wilkinson, F.G.A. Stone, E.W. Abel, eds., Pergamon Press, (1982).

5. Allum, K. G., R. D. Hancock, I. V. Howell, R. C. Pitkethly, and P. J. Robinson. _J_. _Organomet_ _Chem_, 87, 189, (1975).

6. Ichikawa, M. _J_._C_._S_. _Chem_. _Comm_., 566, (1978).

7. Ichikawa, M. _J_. _Catal_., 59 67, (1979).

8. Ichikawa, M. _Bull_. _Chem_. _Soc_. _Jap_., 51, 2268, (1978).

9. Allum, K. G., R. D. Hancock, I. V. Howell, T. E. Lester, S. Mckenzie, and P. J. Robinson. _J_. _Catal_., 43, 331, (1976).

10. Mantovani, E., N. Palladino, and A. Zanobi. _J_. _Mol_. _Catal_., 3, 285, (1977/78).

11. Falbe, J. "Carbon Monoxide in Organic Synthesis", Springer-Verlag, Berlin, (1970).

12. Cornils, B., R. Payer, and K. C. Traenckner. _Hydro_. _Proc_. 83, 1975.

13. Johnson Matthey and Sons, Private Communication 1984.

14. Marko, L. in "Aspects of Homogeneous Catalysis", Vol. 2, R. Ugo, Ed., Dordrecht, Reidel, (1973).

15. Alemdaroglu, N. H., J. L. M. Penninger, and E. Oltay. _Monatshefte_ _fur_ _Chemie_, 107, 1153, (1976).

16. Osborn, J. A., J. F. Young, and G. Wilkinson. _J_. _Chem_. _Soc_. _Chem_. _Comm_., 17, (1965).

17. Oliver, K., F. B. Booth. Hydrocarbon Processing, 49, 112, (1970).

18. Masters, C. in "Homogeneous Transition Metal Cataly-sis", Chapman and Hall, London, (1981).

19. Pruett, R. L.. Adv. Organometal Chem., 17, 1, (1979).

20. Paulik, F. E., K. K. Robinson, and J. F. Roth. Monsan-to Co., U.S. Pat. 3,487,112, (1969).

21. Paulik, F. E., J. F. Roth, and K. K. Robinson. Monsan-to Co., French Pat. 1,150,961, (1969).

22. Hershman, A., K. K. Robinson, J. H. Craddock, and J. F. Roth. Ind. Eng. Chem. Prod. Res. Dev., 8, 372, (1969).

23. Chemical Engineering, 110, March, (1977).

24. Tjan, P. W. H. L., PhD Thesis, Delft, Netherlands: (1976).

25. Gerritsen, L. A., W. Klut, M. H. Vreugdenhil, J. J. F. Scholten. J. Mol. Catal., 9, 257, (1980).

26. Scurrell, M. S.. in "Catalysis", Vol. 2, C.Kembeall and D. A. Dowden, eds., Royal-Chem. Soc., London, 215, (1978).

27. Murrer, B. A., and M. J. H. Russell. in "Catalysis", Vol. 6, G.C. Bond and G. Webb, eds., Royal-Chem. Soc., London, 169, (1983)..

28. Fowler, R., H. Connor, R. A. Baehl. Chem. Eng., 110, (1977).

29. Hjortkjaer, J., M. S. Scurrell, and P. Simonsen. J. Mol. Catal., 10, 127, (1981).

30. Rony, P. R., and J. F. Roth. Elsevier Amsterdam, 497, (1975).

31. Arai, H., and H. Tominaga. J. Catal., 75, 188, (1982).

32. Takahashi, N., M. Kobayashi. J. Catal, 85, 89, (1984).

33. Centola, P., R. Terzaghi, R. Del Rosso, and I. Pasquon. La Chime.Industria, 54, (9), 775, (1972).

34. Christensen, B., and M. S. Scurrell. J. Chem. Soc., Faraday Trans. I, 73, 2036, (1977).

35. Yashima, T., Y. Orikana, N. Takabashi, and N. Hara. J. Catal., 59, 53, (1979).

36. Gelin, P., Y. B. Taarit, and C. Naccache. In "New Horizons in Catalysis", T. Seiyama and K. Tamale, eds., Elsevier Scientific Pub. Co., vol. 7, 898, (1981).

37. Scurrell, M. S., and R. F. Howe. J. Mol. Catal., 7, 535, (1980).

38. Yamanis, J., K. C. Lien, M. Caracotsios, and M.E. Powers. Chem. Eng. Comm., 6, 355, (1981).

39. Yamanis, J., and K.C. Yang. J. Catal., 69, 498, (1981).

40. Takahashi, N., Y. Orikasa, and T. Yashima. J. Catal., 59, 61, (1979).

41. Nefedov, B. K., E.M. Shutkana, Ya. T. Eidus. Izv. Akad. Nauk USSR, Ser. Khin., 3, 726, (1975).

42. Nefedov, B. K., N. S. Sergueva, T. V. Zueva, E. M. Shutkina, and Ys. T. Eidus. Izv. Akad. Nauk USSR, Ser. Khin.; 3, 582, (1976).

43. Davis, M. E., E. J. Rode, B. E. Hanson, and D. Taylor. J. Catal., 86 67, (1984)

44. Rabo, J. A.. "Zeolite Chemistry and Catalysis", American Chemical Society, (1976).

45. Denley, D. R., R. H. Raymond, and S. C. Tang. J. Catal., 87, 414, (1984).

46. Shannon, R. D., J. C. Vedrin, C. Naccache, and F. Lefebvre. J. Catal., 88, 431, (1984).

47. Haynes, H.W. Cat. Rev., 17, 273, (1978).

48. Breck, J.. "Zeolite Molecular Sieves", Wiley: New York, (1974).

49. Socrates, G. "Infrared Characteristics Group Frequencies", Wiley-Interscience: Great Britain, (1980).

50. Hanson, B. E., M. E. Davis, D. Taylor, E. Rode. *Inorg. Chem.*, 23, 52, (1984).

51. Gelin, P., Y. B. Taarit, and C. Naccache. *J. Catal*, 59, 357, (1979).

52. Gelin, P., F. Lefebvre, B. Elleuck, C. Naccache, and Y. B. Taarit. in "Intrazeolite Chemistry", G.D. Stucky and F.G. Dwyer, eds., Vol 28, Am. Chem. Soc., Washington, 455, (1983).

53. Theolier, A., A.D. Smith, M. Leconte, and J.M. Basset. *J. Organomet. Chem.*, 191, 415, (1980).

54. Chini, P., and S. Martinengo. *Inorg. Chem.*, 3, 315, (1969).

55. Primet, M., J.C. Vedrine, and C. Naccache. *J. Mol. Catal.*, 4, 411, (1978).

56. Beck, W., K. Lottes. *Chem. Ber.*, 94 (1961).

57. Lefebvre, F., and Y. B. Taarit. *Nouv., J. Chem.*, 8, (6), 387, (1984).

58. Royo, M., F. Melo, A. Manrique, L. Oro. *Transit. Met. Chem.*, 7, 44, (1982).

59. Yates, D. J. C., L. L. Murrell, and E. B. Prestridge. *J. Catal.*, 57, 41, (1979).

60. Van't, Bilk, H.F.J., I.B.A.D. Van Zon, T. Hulzinga, J.C. Vis, D.C. Koningsberger, and R. Prins. *J. Phys. Chem.*, 87, 2264, (1983).

61. Yates, D.J.C., L.L. Murrell, E.B. Prestridge. In "Growth and Properties of Metal Clusters", Bourdon, J. Ed., Elsevier: Amsterdam, 37, (1980).

62. Takahashi, N., Y. Sato, M. Kobayashi. *Chem. Lett.*, 1067, (1984).

63. Pliskin, W.A., R.P. Eischens. *J. Chem. Phys.*, 24, 482, (1956).

64. King, R. B., Jr., A. D. King, and M. Z. Iqbal. *J. Amer. Chem. Soc.*, 101, 4893, (1979).

65. Forster, H., and J. Seebode. *Zeolites*, 3, 63, (1983).

66. Chini, P., S. Martinengo, and G. Garlaschelli. *J.C.S.*, *Chem. Comm.*, 709, (1972).

67. King, R.B., A.D. King, Jr., M.Z. Iqbal, C.C. Frazier. *J. Am. Chem. Soc.*, *100*, 1687, (1978).

68. Huang, T., J. Schwartz, and N. Kitajima. *J. Mol. Catal.*, *22*, 389, (1984).

69. Whyman, R. *J. Organomet. Chem.*, *81*, 97, (1974).

70. Collman, J. P., and L. S. Hegedus. "Principles and Applications of Organotransition Metal Chemistry", University Science Books, Mill Valley, CA, (1980).

71. Whyman, R. *J. Organomet. Chem.*, *94*, 303, (1975).

72. "Atlas of Spectal Data and G/Physical Constants for Organic Compounds", J.G. Grasselli, Ed., CRC Press: Cleveland, (1973).

73. Hair, M.L., I.D. Chapman. in "Proc. Third Int'l Cong. on Catalysis", W.M.H. Sachtler, G.C.A. Schuit, P. Zwietering, eds., NOrth Holland, 1091, (1965).

74. Braterman, P.S. "Metal Carbonyl Spectra", Academic Press: London, (1975).

75. Collman, J. P., J. A. Belmond, and J. I. Brauman. *J. Am. Chem. Soc.*, *105*, 7288, (1983).

76. Bor, G. *Inorg. Chem. Acta.*, *1*, 81, (1967).

77. Marko, V. L., G. Bor, G. Almasy, and P. Szabo. *Brennstoff-Chemie*, *44*, 58, (1963).

78. Pino, P., F. Piacenti, M. Bianchi. in "Organic Syntheses via Metal Carbonyls", I. Wender and P. Pino, Eds. Wiley: New York, 180, (1977).

79. Arai, H. *J. Catal.* *31*, 135, (1978).

80. Caracotsios, M. Masters Thesis, Universtity of Kentucky, (1981).

81. Dietz, W.A. *J. Gas Chrom.*, Feb., 69 (1967).

Appendix A

MATERIALS OF EQUIPMENT SPECIFICATIONS

A.1   EQUIPMENT

A.1.1   Reactor System

Gas Chromotgraph- Perkin-Elmer model 3920, dual flame ionization detectors.

MMD-1- Mini-micro design, E and L Instruments.

Integrator- AutoLab 6300 digital integrator.

Digital Thermometer- Omega Engineering Co., Model 412A-J.

Fluidized bed- Tecam, Inc., Model SBL-2D.

Controller- Tecam, Inc., Model TC4D, PID type.

Testing- 1/4" OD, 316ss, William and Co.

Thermocouple- Omega Engineering, 1/8" OD, Icon/Constantan.

GC Columns- 15' x 1/8", 8% Carbowax 20M, Spherosil XOBO30, 80/100 mesh; Porasil C, 6' x 1/4" ss.

Sampling Valve- 10 port, ss, low temperature and low pressure, Valco Instruments, A60 air actuator.

Rotameters- Matheson Co., 601 tubes, with #3 high accuracy valves.

GC- Hewlett-Packard, Model 5790A.

Mass Spectrometer- Hewlett-Packard, Model 5970 series, mass selective detector.

Capillary Column- Supelco Co., 2-4035, Fused Silica Capillary, SPB-5, 30M, 1.0μm, 0.25 mm ID.

Hydraulic Press- Manufactured by Dake, Model 44225.

A.1.2   IR System

Infrared Spectrometer- IBM Instruments, Model IR/32.

Flow Cell- Home made design, O-rings, Viton, 1" x 3/4" x 1/8", Dominion Seal and Packing.

Gasket- Copper, 2" x 1 3/4" x 0.080".

Fire Rods- Watlow Corp., 2" x 1/8", 100 w, Model #C2A5.

Floppy Disks- 8", double sided, double density, soft sectored.

IR Windows- IRTRAN-2, 25 mm x 2 mm, circular disks.

Back Pressure Regulator- Conoflow, Model H-588, 0-125 psig.

A.2   MATERIALS

Hydrogen- Airco, Industrial Gas, grade 4.5.

Nitrogen- Airco, Industrial Gas, zero grade.

Air- Airco, Industrial Gas, Breathing Air.

Carbon Monoxide- Matheson Co., UHP, grade 99.8%.

Propylene- Matheson Co., 99.8% grade.

Deuterium- 99.99% pure, Airco Products.

Rhodium- Johnson-Matthey, $RhCl_3-3H_2O$.

Zeolites- Strem Chemical, powder form, NaX, NaY

<u>Platinum</u> <u>Catalysts-</u> United Catalyst, Inc., Cat. No.:
G-43.

<u>Silica</u> <u>Gel-</u> Grade 42, 6-16 mesh, Davison Chemical.

<u>Molecular</u> <u>Sieve-</u> 5A, Davison, grade 522, 8-12 mesh.

<u>N-hexyldiphenyl</u> <u>Phosphine-</u> Strem Chemical.

<u>Dimethyl</u> <u>Phenylphosphine-</u> Strem Chemical.

Appendix B

ADSORPTIONS ONTO ZEOLITES

There were several compounds which needed to be adsorbed onto the zeolite support individually so that the IR bands could be assigned. In this section, the IR spectra collected for these compounds are shown.
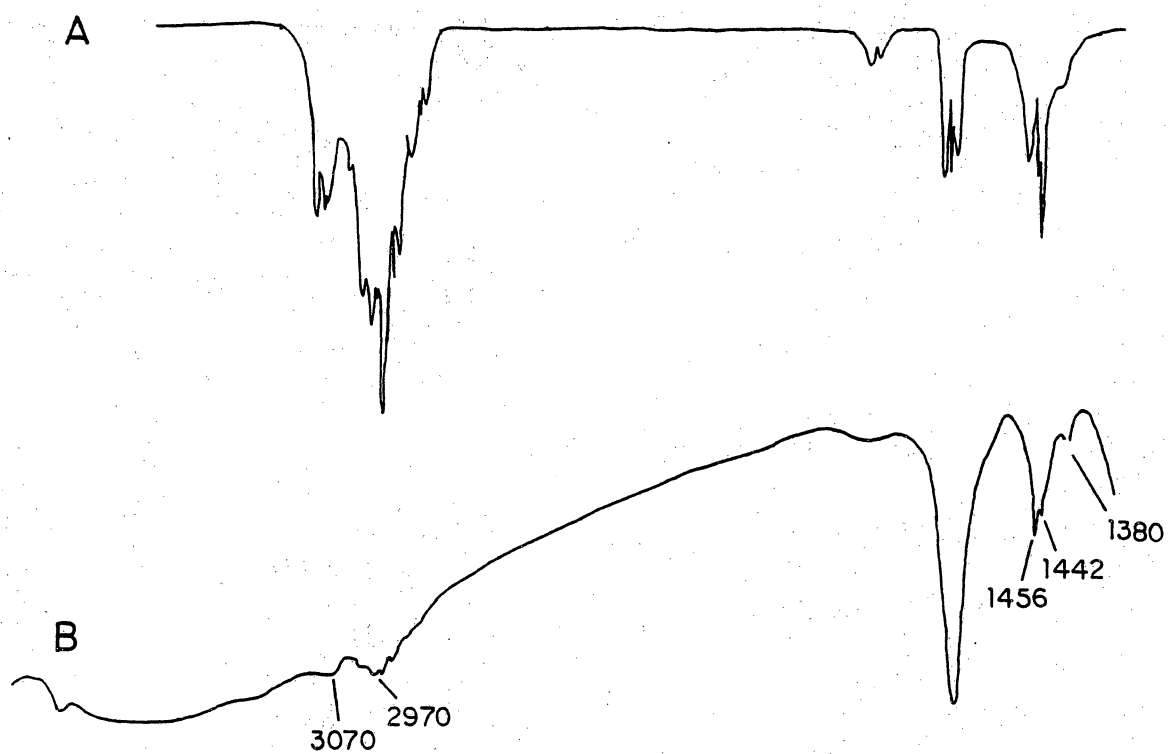
Figure 41: Propylene Adsorbed Onto NaY

a) gas phase; b) gas phase + NaY at 120°C
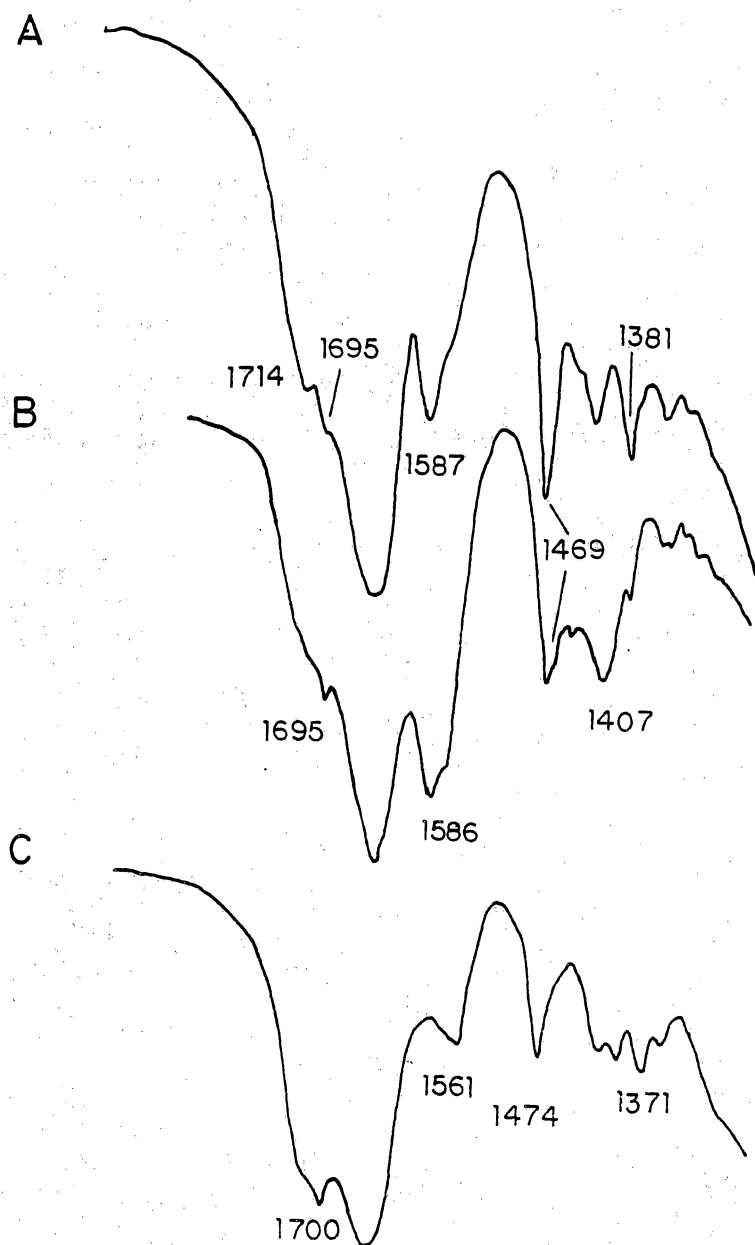
Figure 42:   Butyraldehydes On NaX

a) n-butyraldehyde at room temperature; b) n-butyraldehyde at 150°C; c) iso-butyraldehyde at 150°C
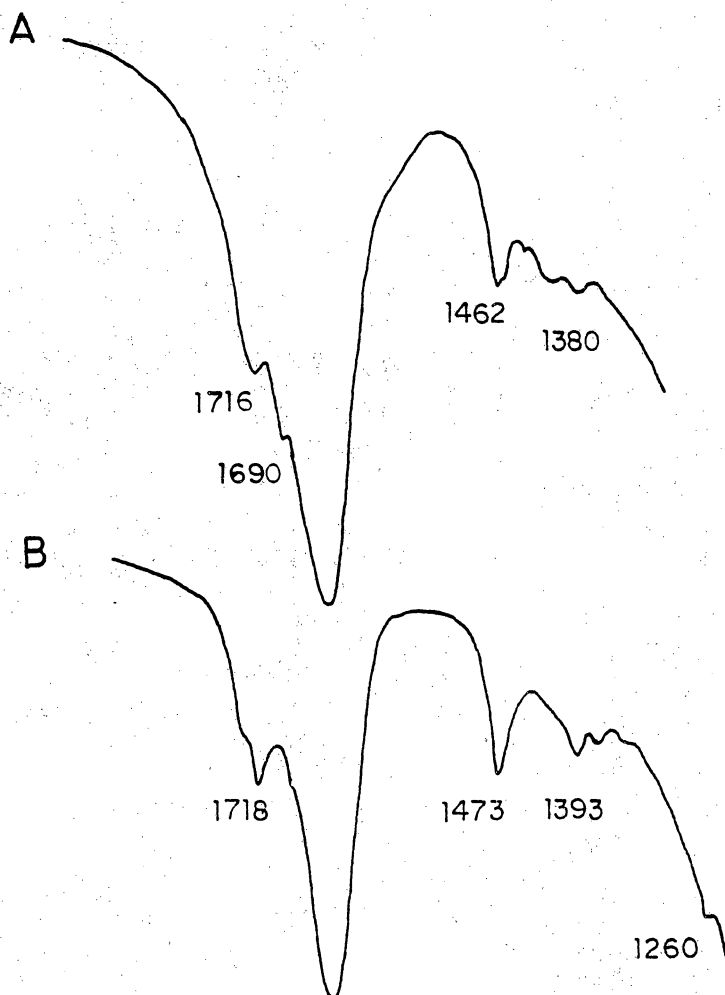
Figure 43: Butyraldehyde On NaY

a) n-butyraldehyde   at   150°C;   b)   iso-
butyraldehyde at 150°C
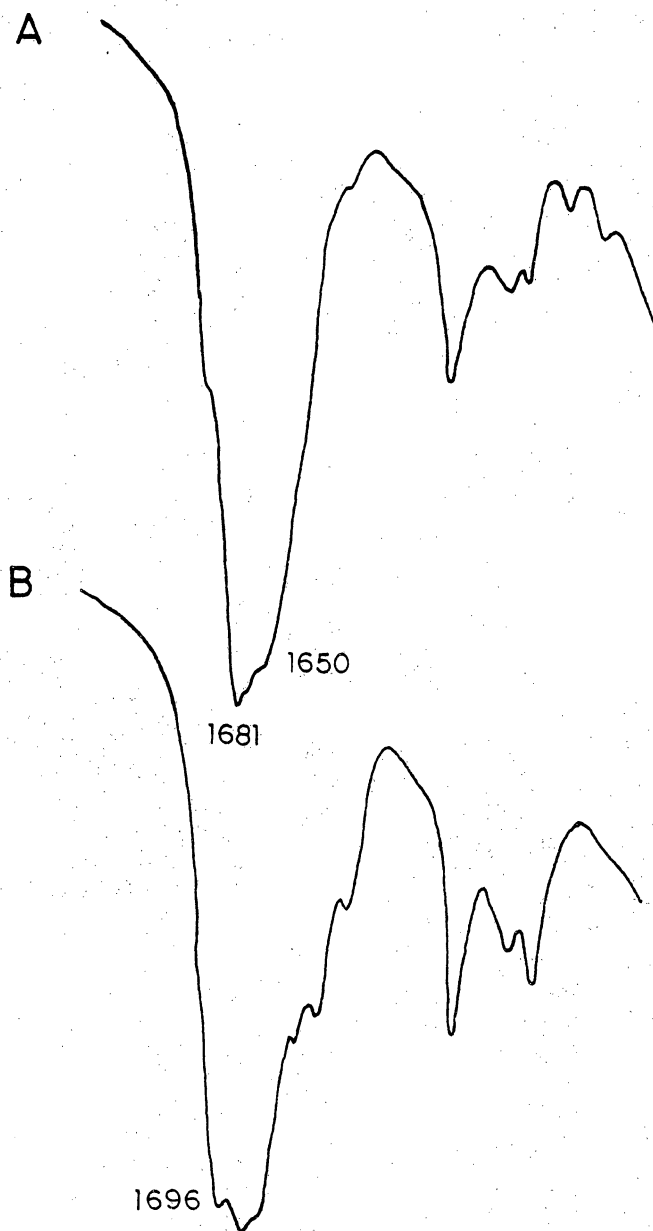
Figure 44:   2-t-Hexenal And 4-Heptanone On NaY

a) 2-trans-hexenal at 150°C; b) spectrum A +
4-heptanone at 150°C
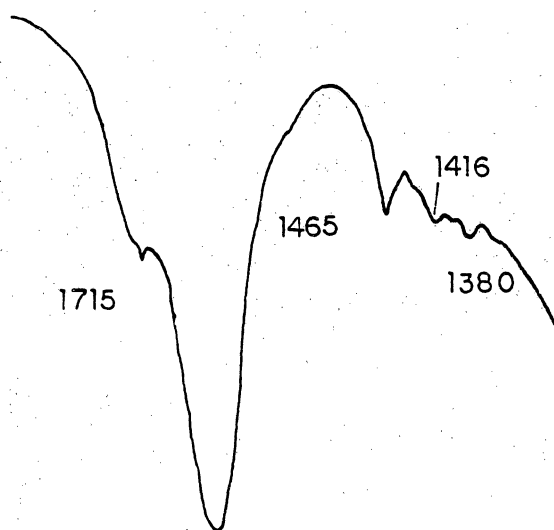
Figure 45: Propionaldehyde On NaY at 150°C
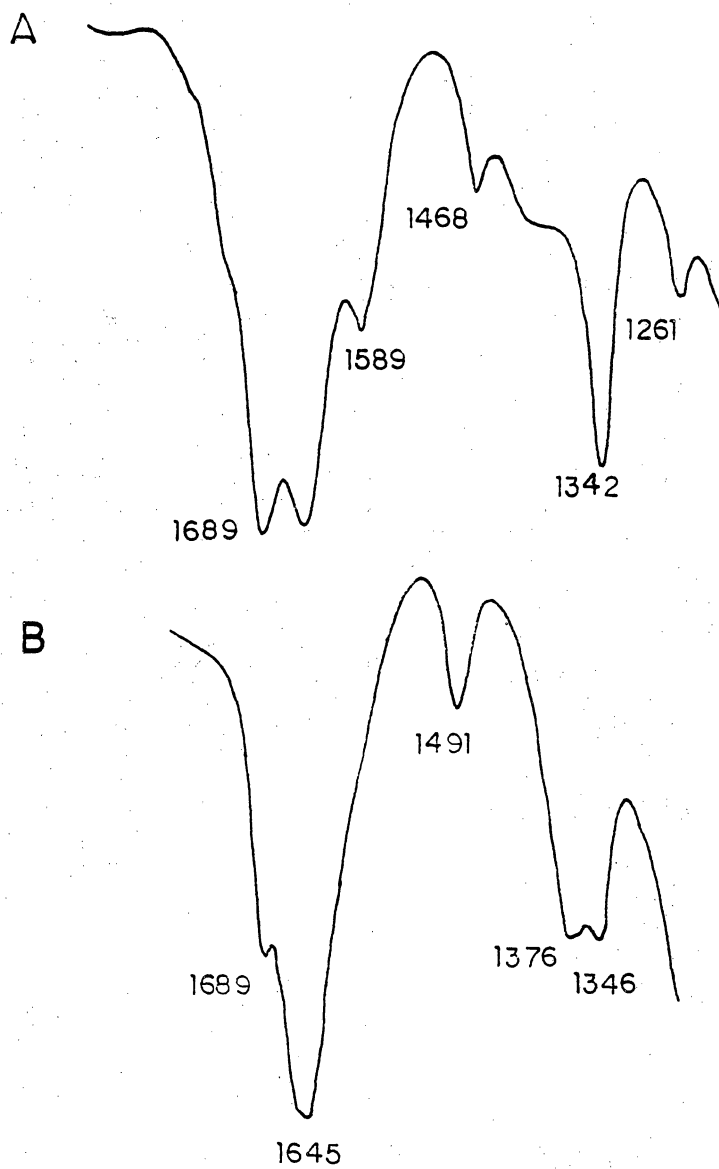
Figure 46: Carbon Dioxide On NaX and NaY

a) NaX at 150°C; b) NaY at 150°C

Appendix C

OPERATING PROCEDURES

C.1   REACTOR SYSTEM OPERATION

C.1.1   Reactor Loading

   Catalyst was compacted without binder under 10,000 psig.
The material was then screened through a 40 mesh Tyler ser-
ies sieve onto a 70 mesh sieve.   Typically, 0.5-0.8 g of ca-
talyst was loaded into the reactor.   Plugs of glass wool
held the powder in place.   The reactor was a 1/4" x 4"
stainless tube.   Check valves were located at the entrance
and exit of the reactor section.   This allowed removal of
the reactor without the catalyst being exposed to air.   This
reactor section was small enough to fit into the dry box so
that the catalyst could be handled in an inert atmosphere.

C.1.2   Gas Sampling and Product Analysis

   The gas composition was measured by gas chromotography.
The Porasil C column was used to separate propane and proy-
lene.   The Spherosil column separated the C_3 fraction from
the aldehydes and iso-butyraldehyde from n-butyraldehyde.
The column system required two flame ionization detectors
and two integrators.   Two samples were required also, one
for each column.   Figure 47 shows the configuration for the

10-port sampling valve. The idle mode is shown in part A. The product gas flows continuously through the 500 µl loop (sample loop 2) while carrier gas flushes the 20 µl loop (sample loop 1). When a sample is taken, the N_2 carrier gas flushes the 500 µl loop into column A and the product gas is sent through the 20 µl loop. It was determined that 2 minutes was required to allow pressure equilibration before the valve is switched back to position A.

The sampling valve was operated either manually or automatically. The MMD-1 was used as a programmable timer. By changing logic levels at certain addresses the 24V power supply was activated. The power supply controlled solenoid valves which regulated house air pressure to the valve activator. Figure 17 contains the assembly language program for the MMD-1. Table 18 shows the addresses and values which change sampling intervals. Sampling intervals of 0.5, 1.0, 1.5, and 2.0 hours were used.
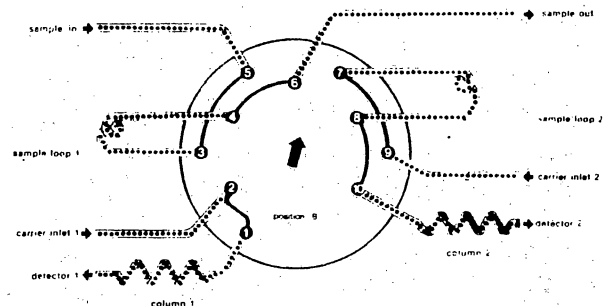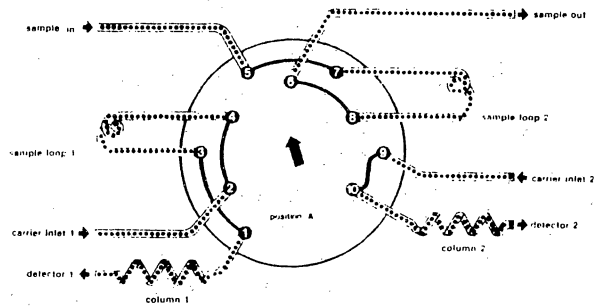
Figure 47:   Connections For 10 Port Sampling Valve

TABLE 17

Assembly Language Program For MMD-1

```
003.000                       00001              ORG 003000A
003.000   076 001             00002   START      MVI A,001Q
003.002   323 000             00003              OUT 000Q
003.004   315 061 003         00004              CALL DEL10
003.007   076 000             00005              MVI A,000Q
003.011   323 000             00006              OUT 000Q
003.013   036 013             00007              MVI E,013Q
003.015   315 061 003         00008   N1         CALL DEL10
003.020   035                 00009              DCR E
003.21    302 015 003         00010              JNZ N1
003.024   076 002             00011              MVI A,002Q
003.026   323 000             00012              OUT 000Q
003.030   315 061 003         00013              CALL DEL10
003.033   076 000             00014              MVI A,000Q
003.035   323 000             00015              OUT 000Q
003.037   076 002             00016              MVI A,002Q
003.041   036 272             00017   S          MVI E,300Q
003.043   315 061 003         00018   N2         CALL DEL10
003.046   035                 00019              DCR E
003.047   302 043 003         00020              JNZ N2
003.052   075                 00021              DCR A
003.053   302 041 003         00022              JNZ S
003.056   303 000 003         00023              JMP START
003.061   006 207             00024   DEL10      MVI B,207Q
003.063   315 073 003         00025   TIME       CALL TIMEOUT
003.066   005                 00026              DCR B
003.067   302 063 003         00027              JNZ TIME
003.072   311                 00028              RET
003.073   016 035             00029   TIMEOUT    MVI C,035Q
003.075   026 177             00030   TIME1      MVI D,177Q
003.077   025                 00031   TIME2      DCR D
003.100   302 077 003         00032              JNZ TIME2
003.103   015                 00033              DCR C
003.104   302 075 003         00034              JNZ TIME1
003.107   311                 00035              RET
003.110   000                 00036              NOP
003.111   000                 00037              END START
```

TABLE 18

MMD-1 Entries For Sampling Interval

Sample Interval	Address 003.040	Address 003.042
30 min.	001	264
45 Min.	001	377
60 Min.	002	300
90 Min.	004	204

C.2 OPERATING CONDITIONS

Gas Chromatograph

	C_4 Column	C_3 Column
Temperature	95°C	45 on Variac
Injector Temp. °C	150	150
Detector Temp. °C	175	175
Flow Rate N_2	15 ml/min. (STP)	≈45 ml/min. (STP)
	(6.5 turns)	(3.5 on rotameter)

FID

	C_4 Column	C_3 Column
Polarity	minus	minus
Attenuation	x1	x1
Amplification	x10	x100
H_2 pressure (psig)	30	30
Air pressure (psig)	40	40

Integrator

	C_4 Column	C_3 Column
Noise Adjust	1-2	1-2
Slope Sensitivity	64	32
Filtering	6	4
Baseline Correction Rate	Fast	Fast

C.3   GC RETENTION TIMES

The retention times for various compounds are shown in Tables 19 and 20 .

C.4   AIR DRYING SYSTEM

The IR/32 optics bench required a dry gas source for use as a sample chamber purge and for pressure on the air bearing.   The house air was cleaned and dried by the system shown in Figure 48 It consisted of 2 chambers operated in parallel so that one is always clean.   Each chamber (3'x3" pipes) contains roughly 1 pound 5A molecular sieve and 4 pounds of silica gel.   The arrows indicate the direction of flow.   The process chamber air is dried and sent to the IR bench.   The system of check valves and valve distributes a small portion of the dry air back through the chamber.

A 1 psi difference across the check valve prevents flow. For chamber A operation, valves V3 and V1 do not allow flow. Flow proceeds through V4 to the IR.   Globe valve V5 allows slow flow through valve V2 and chamber B.   The key to the operation is valve V5 allowing a slow flow at a low pressure (the regenerating chamber is essentially at atmosphere pressure).

The molecular sieve and silica gel are regenerated by heating the chambers to roughly $150^{\circ}C$.   Typically, two days

TABLE 19

Retention Times On Spherosil Column

Propylene and propane	8:00
iso-butyraldehyde	18:00
n-butyraldehyde	22:00
4-heptanone	120:00
2-methyl-3-hexanone	95:00
butanol (broad)	60:00

TABLE 20

Retention Times On Capillary Column

40°C for 8 min., 12°C/min. to 150°C,

150°C for 5 min.

Compound	Time
Ethanol	
Acetone	2.98
Propionaldehyde	3.00
Pentane	3.07
2-propanol	3.17
Iso-butyraldehyde	4.20
1-propanol	4.48
1-hexene	4.86
Hexane	5.11
N-butyraldehyde	5.10
t-3 hexene	5.18
c-3 hexene	5.25
Methyl Ethyl Ketone	5.25
t-2 hexene	5.35
c-2 hexene	5.69
Iso-butanol	6.30
Cyclohexane	7.95
N-butanol	8.10
2-methyl butyraldehyde	8.42
Cyclohexene	9.01
Valernaldehyde	9.92
Toluene	12.70
2-hexanone	13.30
Di-isopropyl ketone	13.40
Hexanal	13.84
Iso-propyl-n-propyl ketone	14.70
2-ethyl pentanal	15.10
2-methyl hexanal	15.29
4-heptanone	15.52
1-heptanal	16.19

under heat will be sufficient to dry the dessicant. One chamber will produce dry air for roughly one week.
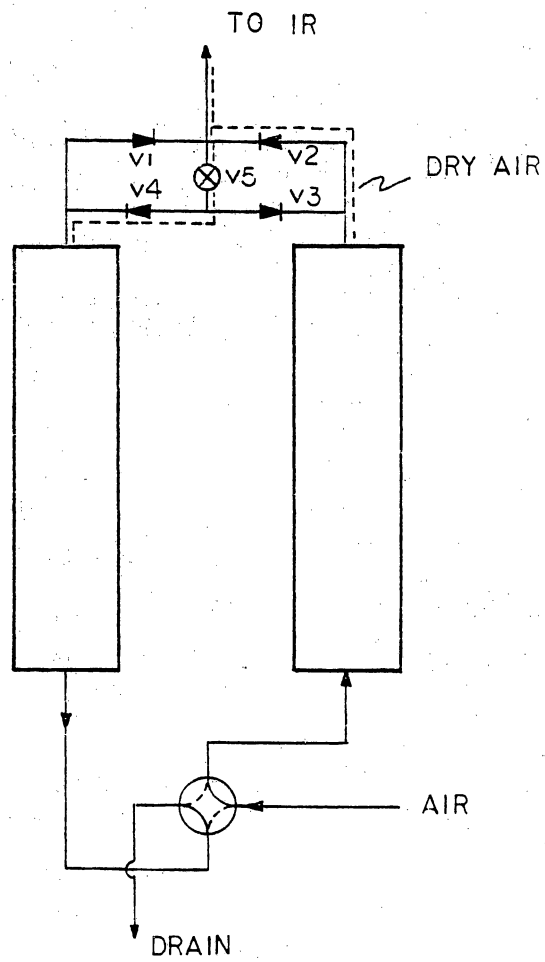
Figure 48:   Flow Diagram For Air Drying System

Appendix D

MASS SPECTRA

The following spectra were taken from the product stream for catalyst AY. The catalyst was precarbonylated prior to reaction conditions. Included are some unassigned spectra. Others have been confirmed by obtaining retention times of the pure materials.
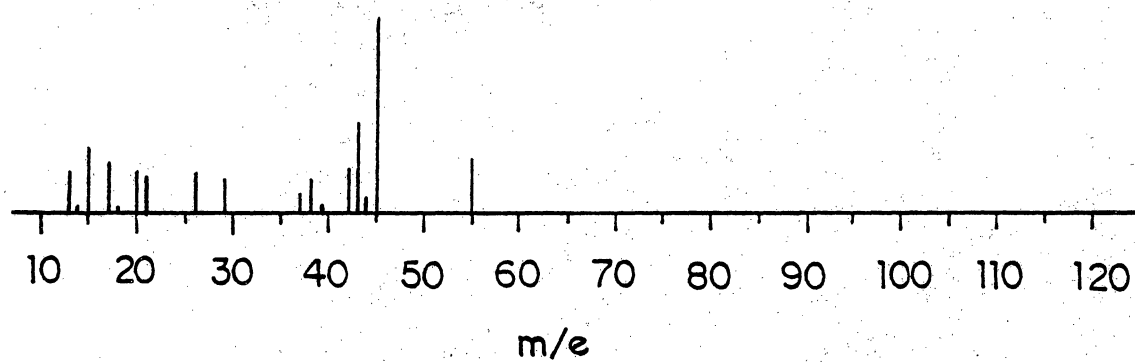
MASS	ABUND.	MASS	ABUND.	MASS	ABUND.
13	19.7	21	18.4	42	22.4
14	2.6	26	19.7	43	44.7
15	31.6	29	17.1	44	7.9
17	25.0	37	10.5	45	100.0
18	2.6	38	17.1	55	28.9
20	22.4	39	3.9		

Figure 49:   Mass Spectrum for 2-Propanol
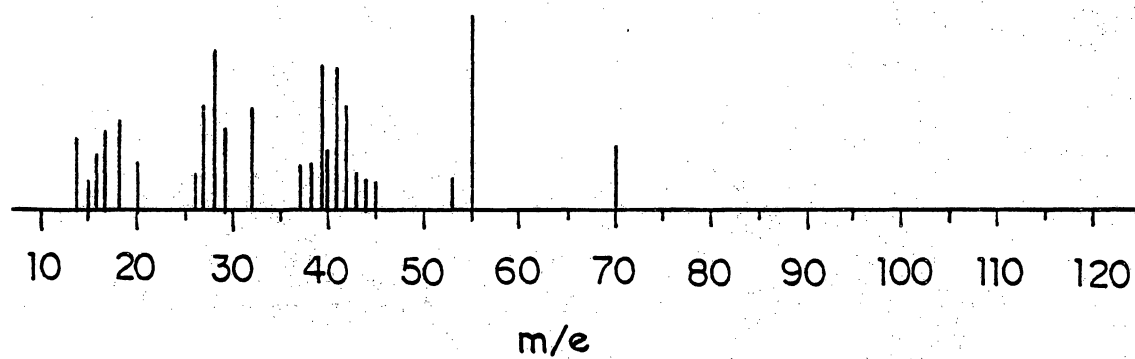
MASS	ABUND.	MASS	ABUND.	MASS	ABUND.
14	36.9	28	82.9	42	53.2
15	13.5	29	39.6	43	18.0
16	30.6	32	52.3	44	14.4
17	41.4	37	14.4	45	13.5
18	45.9	38	19.8	53	16.2
20	14.4	39	73.9	55	100.0
26	13.5	40	30.6	70	34.2
27	51.4	41	72.1		

Figure 50:   Mass Spectrum for 2-Pentene
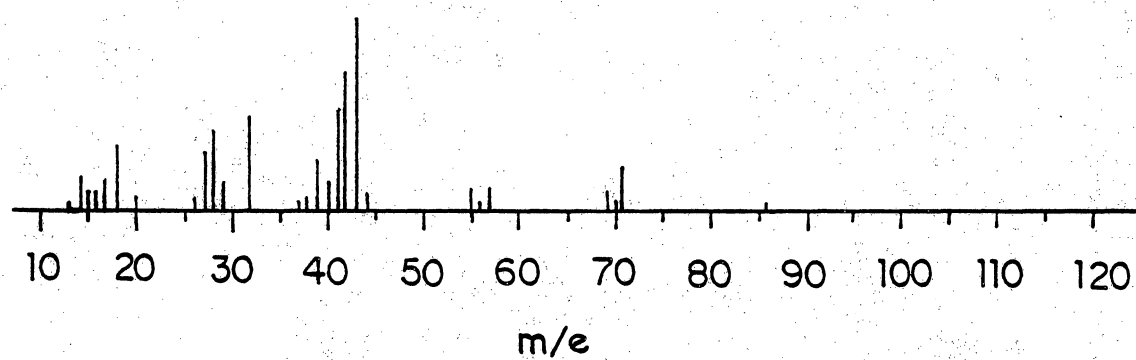
MASS	ABUND.	MASS	ABUND.	MASS	ABUND.
13	4.4	28	40.9	43	100.0
14	16.8	29	15.0	44	9.5
15	10.2	32	48.5	55	10.9
16	11.7	37	5.1	56	6.2
17	13.1	38	6.6	57	12.0
18	34.7	39	25.9	69	9.9
20	6.9	40	13.9	70	6.6
26	6.2	41	53.6	71	21.9
27	30.7	42	70.8	86	4.7

Figure 51: Mass Spectrum for Unknown - Retention time =
            4.42
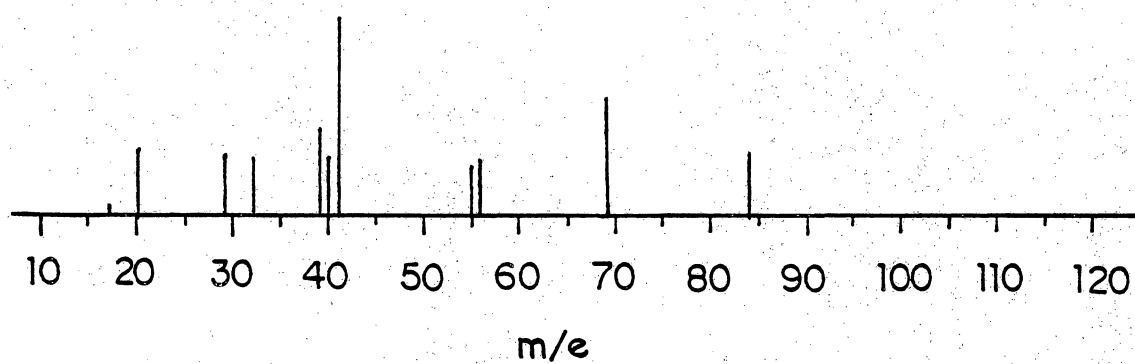
MASS	ABUND.	MASS	ABUND.	MASS	ABUND.
17	3.8	32	28.8	55	23.1
20	30.8	39	42.3	56	25.0
28	21.2	40	26.9	69	57.7
29	28.8	41	100.0	84	32.7

Figure 52:   Mass Spectrum for Unknown - Retention Time = 6.08
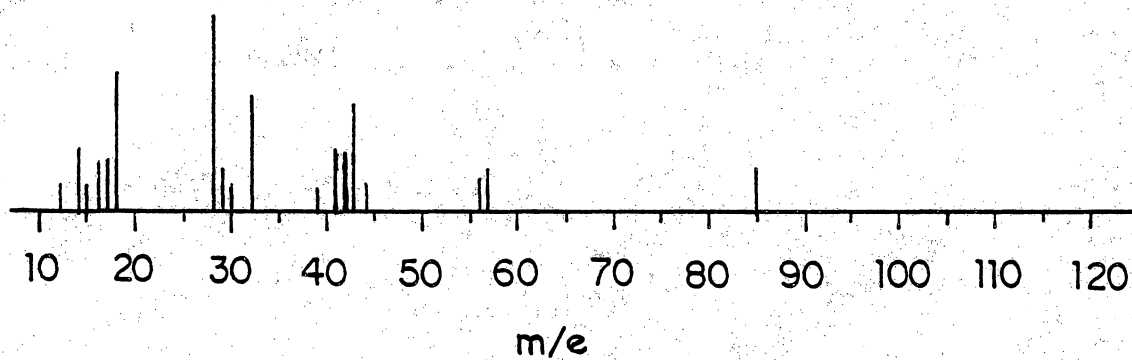
MASS	ABUND.	MASS	ABUND.	MASS	ABUND.
12	13.0	28	100.0	42	31.5
14	33.3	29	20.4	43	54.6
15	12.0	30	13.0	44	13.0
16	24.1	32	59.3	56	14.8
17	25.0	39	11.1	57	19.4
18	69.4	41	33.3	85	19.4

Figure 53:   Mass Spectrum for Unknown - Retention Time = 8.22
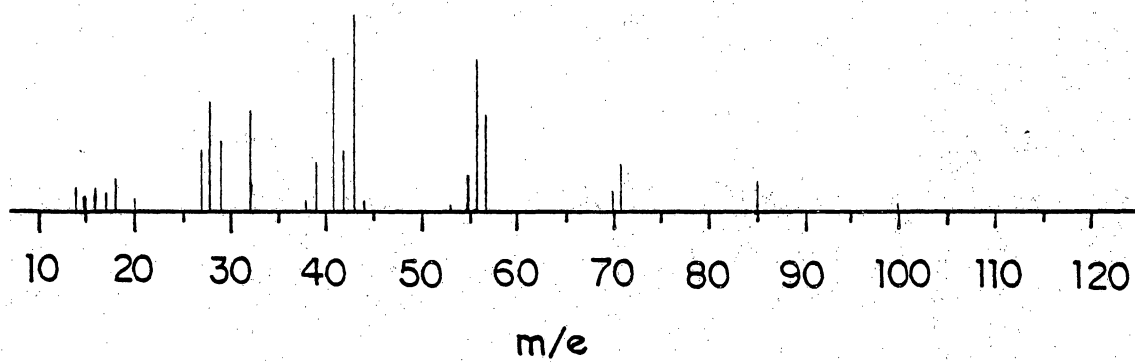
MASS	ABUND.	MASS	ABUND.	MASS	ABUND.
14	11.5	29	34.1	53	3.0
15	7.8	32	49.6	55	14.5
16	10.5	38	4.5	56	77.7
17	8.0	39	22.3	57	48.1
18	13.8	41	76.7	70	9.5
20	5.5	42	29.8	71	23.1
27	30.6	43	100.0	85	14.8
28	55.6	44	7.0	100	3.3

Figure 54:   Mass Spectrum for Unknown - Retention Time = 8.42

MASS	ABUND.	MASS	ABUND.	MASS	ABUND.
11	3.6	32	3.3	55	3.3
14	3.8	39	11.2	57	3.8
15	4.5	41	26.2	70	11.2
20	4.3	43	100.0	71	26.2
28	21.0	44	3.6	114	5.5
29	5.0				
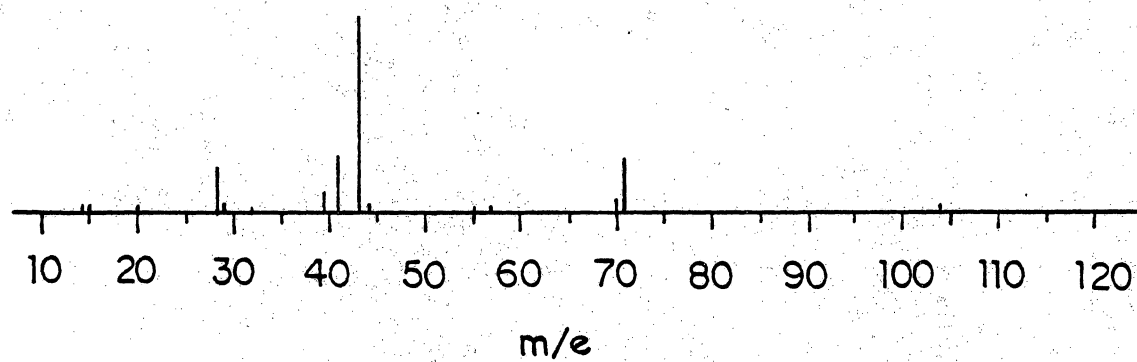
Figure 55: Mass Spectrum for 2,4-Dimethyl pentanone
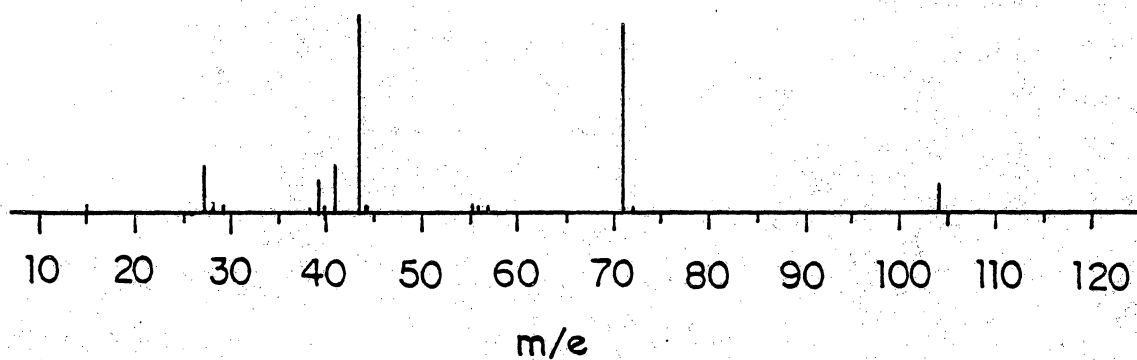
MASS	ABUND.	MASS	ABUND.	MASS	ABUND.
15	2.5	40	2.5	56	1.0
27	21.3	41	23.9	57	1.4
28	3.5	43	100.0	71	47.9
29	2.7	44	3.7	72	2.4
38	1.4	55	2.6	114	13.6
39	12.3				

Figure 56: Mass Spectrum for 2-methyl-3-hexanone
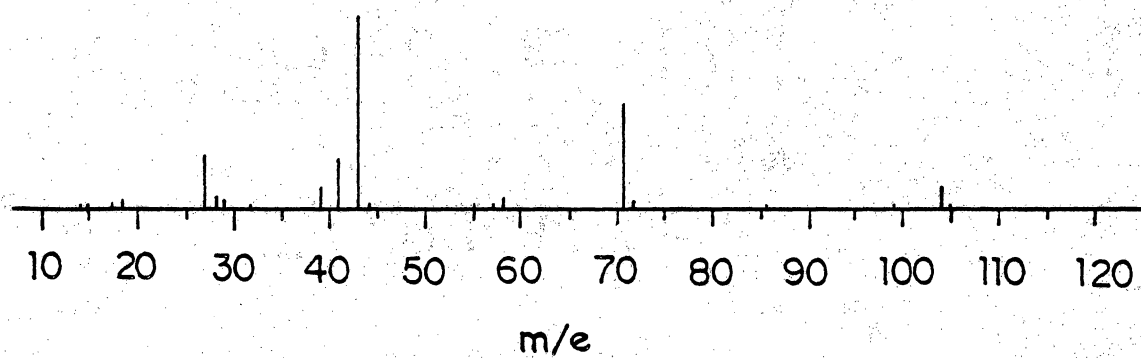
MASS	ABUND.	MASS	ABUND.	MASS	ABUND.
14	2.1	32	1.7	58	6.0
15	2.9	39	12.2	71	64.4
17	1.2	41	26.0	72	3.4
18	3.0	43	100.0	86	1.6
27	24.2	44	3.8	99	1.7
28	7.6	55	2.8	114	12.8
29	5.1	57	2.3	115	1.1

Figure 57:   Mass Spectrum for 4-heptanone

Appendix E

RATE CALCULATIONS

E.1   RESPONSE FACTORS

Flame ionization detectors yield a different relative response for compounds with different functional groups (i.e. alcohols, aldehydes, ketones, etc.). Therefore, the FID was calibrated to give a response factor for iso-butyraldehyde.

Known weight percent solutions of iso-butyraldehyde in cyclohexane were injected into the GC. Simple alphatic hydrocarbons have response factors of unity. Therefore, the aldehyde response factor (R_I) was given by

$$W_I = A_I R_I / (A_c R_c + A_I R_I) \qquad (9)$$

or

$$W_I / (1 - W_I) = (A_I / A_c) R_I \qquad (10)$$

where W_I is the mole fraction aldehyde. By plotting $W_I / 1 - W_I$ versus A_I / A_c, R_I can be obtained by the slope. Figure 58 shows the results. Mole fractions varied from 0.012 to 0.044. The slope was 1.62. This agrees well with the literature values (81).
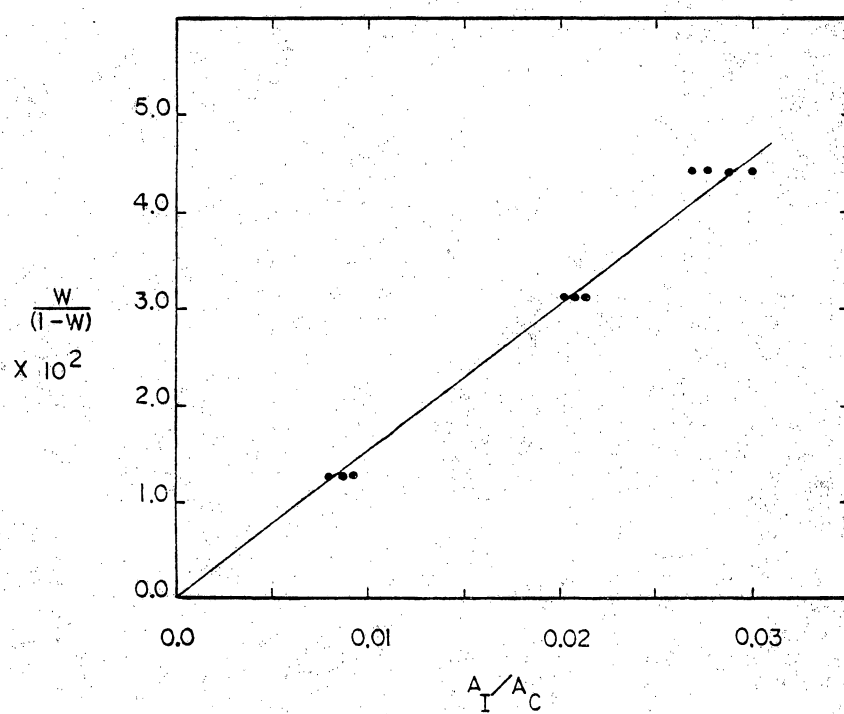
Figure 58:   Response Factor for Iso-butyraldehyde

E.2 ROTAMETER CALIBRATIONS

Each rotameter was calibrated with the reactant gas used. Flow measurements were taken over the full scale. A bubble flow meter and stopwatch were used to measure volumn displaced per unit time. A constant head pressure of 20 psig was maintained. The following equation was used to standardize the flow rates to standard temperature and pressure (25°C and 760 mm Hg).

$$Q_{SC} = Q_{ACT} \times 298K/(T_{ACT}+273) \times P_{ACT}/760 \quad (11)$$

where T_{ACT} and P_{ACT} are ambient temperature and pressure. The calibration curves for propylene, hydrogen, carbon monoxide, and nitrogen are shown in Figures 59-62 .
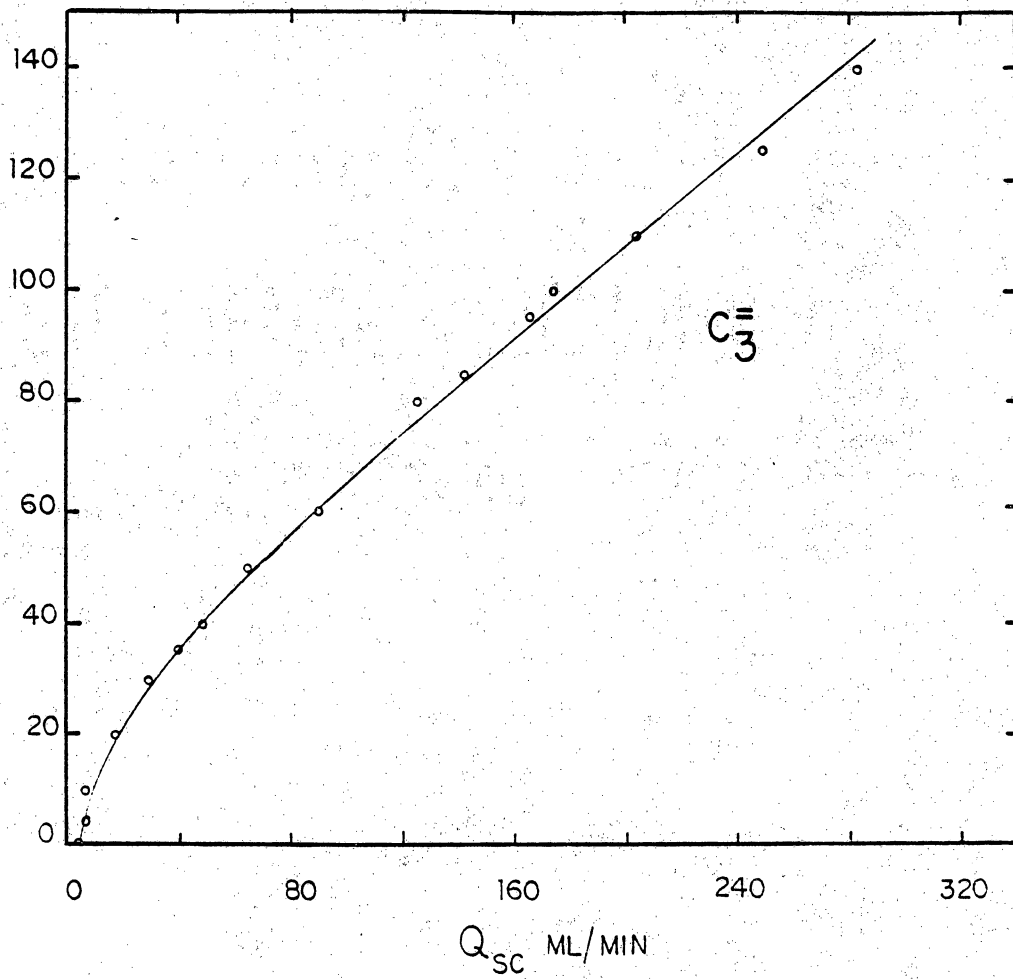
Figure 59: Calibration Curve for Propylene Rotameter
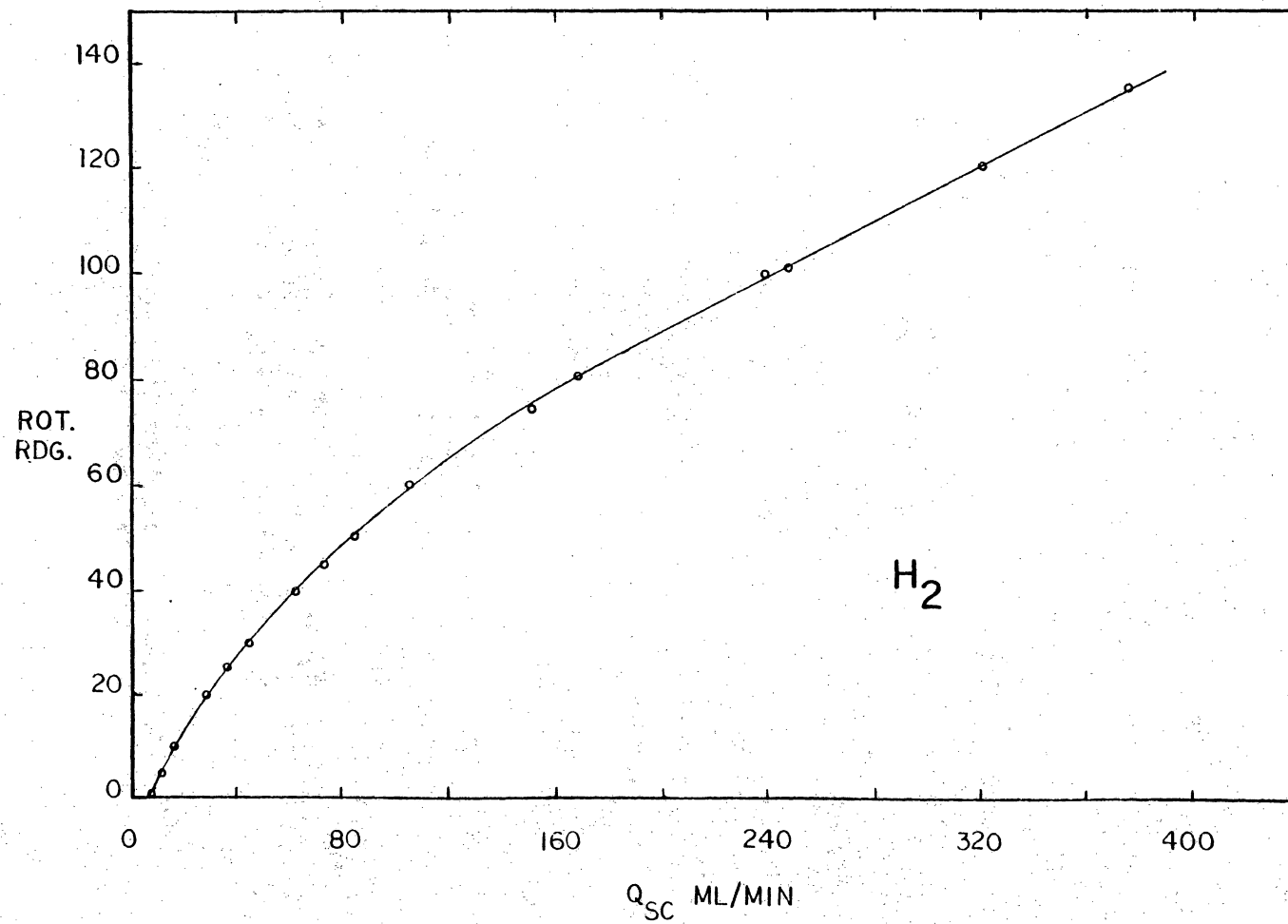
Figure 60: Calibration Curve for Hydrogen Rotameter
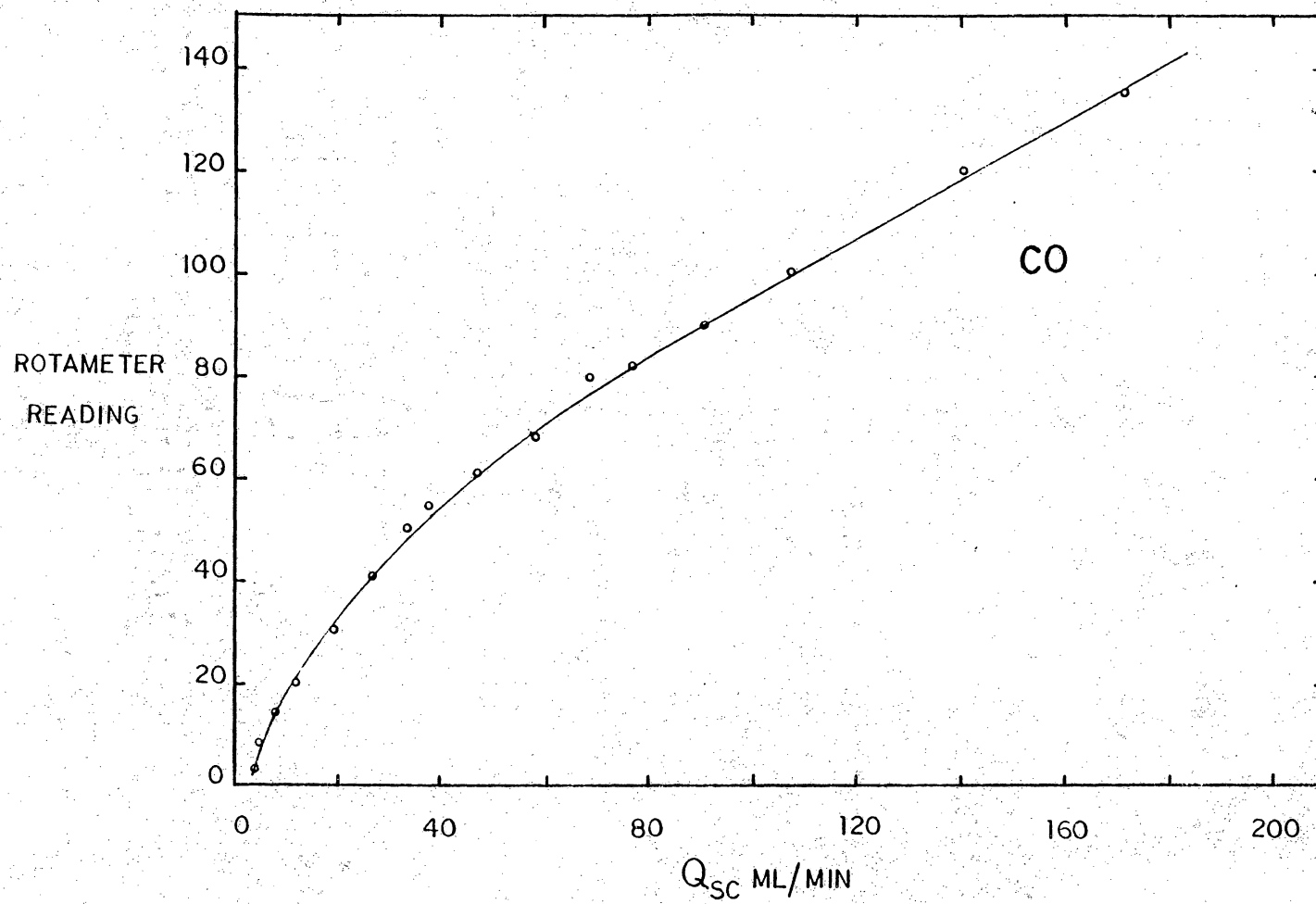
Figure 61: Calibration Curve for Carbon Monoxide Rotameter
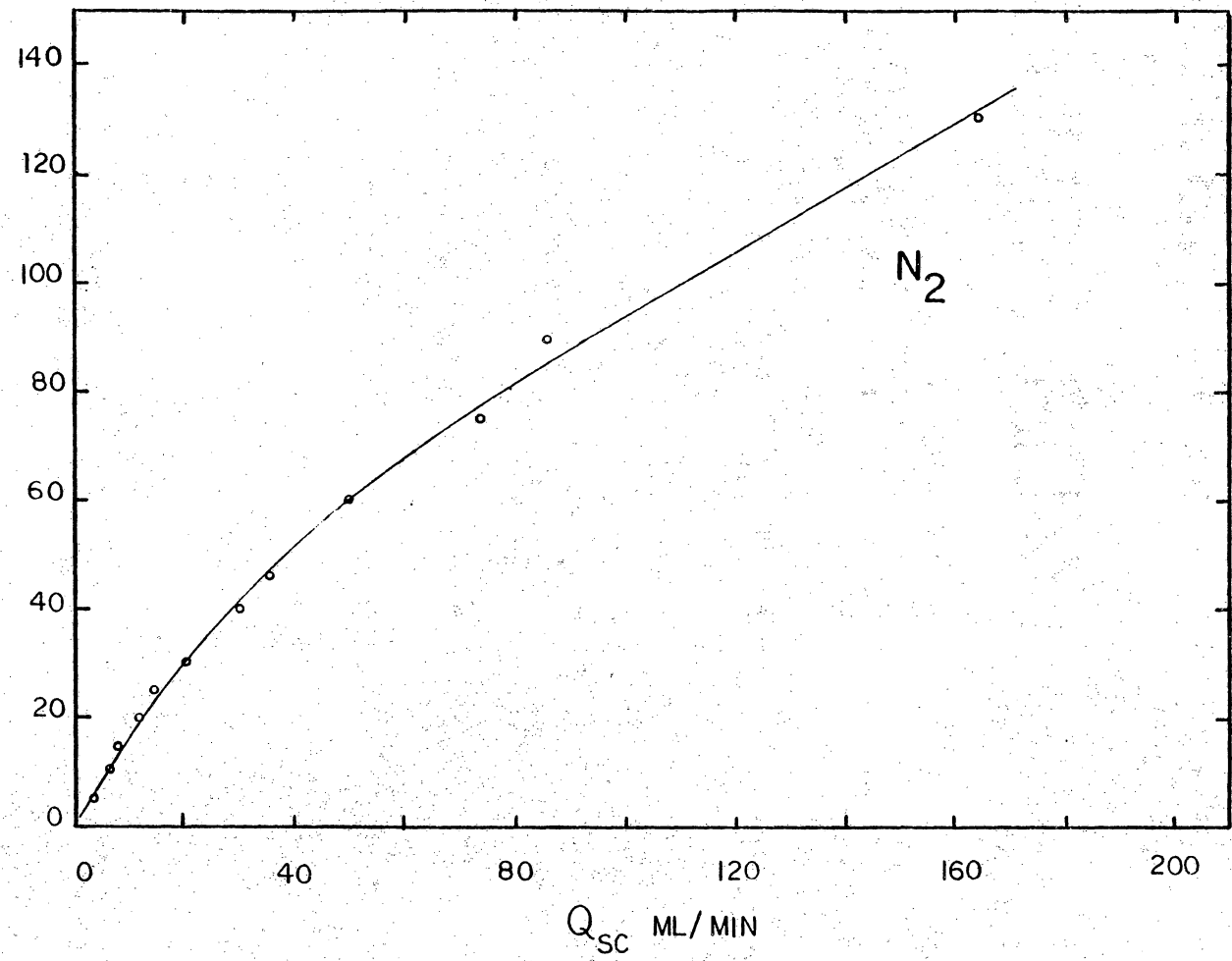
Figure 62: Calibration Curve for Nitrogen Rotameter

E.3   RATE CALCULATION

The differential reactor rate equation is:

$$r_A = \xi_A/(W/F) \tag{12}$$

Where r is the rate of production of A, ξ_A is the conversion to A, W is the weight of catalyst, and F is the flow rate of A. The conversion was calculated from GC peak areas measured by the integrator. For propylene hydroformylation, rates were based on propylene conversion. It was found that some propane was present in the feed. Therefore, it had to be taken into account. A derivation for calculation of propane and iso-butyraldehyde rates follows. Since different size samples were measured for each column, the areas from the integrator counts were normalized to the 500 µl sample. The loop volumes were experimentally measured to be 514 µl (V_A) and 20 µl (V_B) each.

Let the areas for each component be represented by A_s=propane, A_u=propene, A_I=iso-butyraldehyde, A_n=n-butyraldehyde, A_o=other products. Also R=response factors for aldehydes, C=fraction of propane in the feed, and $F=V_A/V_B$.

Propane:

The conversion of propene to propane, ξ_H, is

$$\xi_H = A_S/A_T - C \tag{13}$$

where

$$A_T = A_S + A_U + A_I' + A_N' + A_O \tag{14}$$

and

$$A_I' = A_I R, \quad A_N' = A_N R \tag{15,16}$$

For the aldehydes, the conversions are:

$$\xi_I = A_I'/(A_T(1-C)) \tag{17}$$

$$\xi_N = A_N'/(A_T(1-C)) \tag{18}$$

The (1-C) factor bases the rates on only the propylene entering (excluding propane).

The rates were simply calculated by substituting ξ_H, ξ_I, and ξ_N into equation (12).

A FORTRAN computer program shown below was written to perform the rate calculations.

E.4 RATE DATA MANIPULATION

Figure 63 contains a flow chart for the programs used to obtain plots, activation energies, and mean rate values. The programs were run through interactive WATFIV. EXEC files were used to call programs and data files and to write out the results to other files. Flag values denoted the data to be manipulated. Each program contains documentation which describes the relevant features, i.e., flag values, EXEC programs to be used.
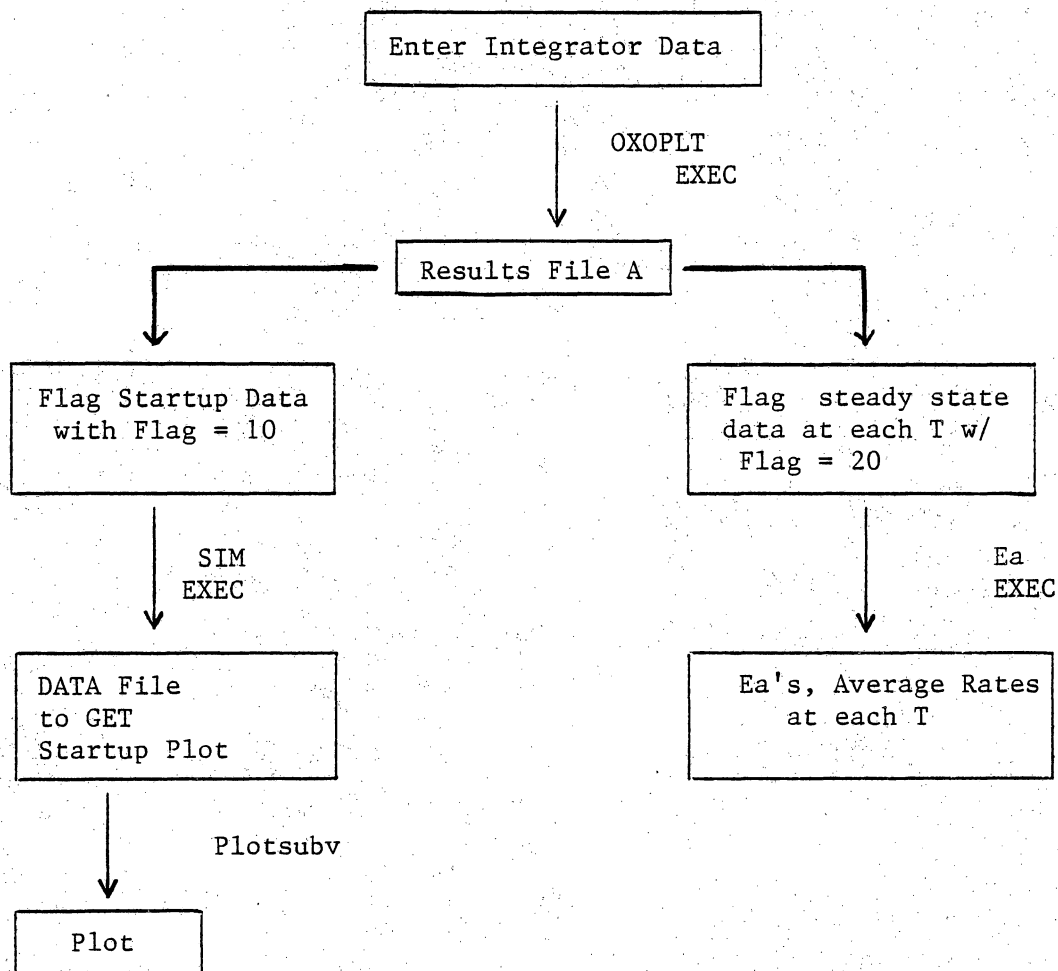
Figure 63: Algorithm for Data Manipulation

OXOPLT EXEC A

```
 TRACE ALL
GLOBAL TXTLIB PREVIEW TCSLIB FORTXLIB VPIUTIL
FILEDEF 8 TERM
FILEDEF 9 DISK  1 DATA A (LRECL 80 RECFM F BLKSIZE 80 PERM
FILEDEF 12 DISK  1 TEST A (LRECL 80 RECFM F BLKSIZE 80 PERM
FORTGI OXO
LOAD OXO (START
 EXIT
```

```
C
C
C
C                          OXO FORTRAN
C                          ----------
C
C     THIS PROGRAM IS USED TO CALCULATE THE RATES FOR THE
C     PROPYLENE HYDROFORMYLATION REACTOR SYSTEM.  IT IS SET UP TO
C     RUN FROM 'OXOPLT EXEC', WHICH IS RUN THRU INTERACTIVE
C     WATFIV.  RAW DATA AND OUTPUT SRE EXTERNAL TO THIS FILE.
C
C
C                          NOMENCLATURE
C
C     AH,AC= AREA OF PROPANE, AND PROPYLENE
C     AI,AN = AREA OF ISO- AND N- BUTYRALDEHYDE
C     ATOTAL = TOTAL AREA
C     FLAG = DENOTATION WHETHER A STEADY STATE VALUE
C            = 1, DENOTES STEADY STATE, OTHER .NE. STEADY STATE
C     TIME = TIME AT WHICH SAMPLE WAS TAKEN
C     TEMP = TEMPERATURE AT TIME OF SAMPLE
C     RH,RI,RN = RATES OF HYDROGENATION AND  HYDROFORMYLATION
C     RO =  RATES FOR ALL OTHER AREAS OF UNKNOWNS
C     LOOPF = FACTOR TO CORRECT FOR DIFFERENT LOOPS:
C             FOR 500 LOOP, LOOPFAC = 25.7
C             FOR 250 LOOP,    "    = 12.5
C     FLOWC3 = FLOW RATE OF PROPYLENE
C     START = STARTING TIME OF CATALYTIC RUN
C     WTCAT = WT. OF CATALYST LOADED IN REACTOR
C     WTRH = WT. FRACTION OF RHODIUM IN ZEOLITE
C     SPTIME = SPACE TIME OF REACTANTS
C
C
      DIMENSION SH(200),SI(200),SN(200), T2(200)
      DIMENSION AH(200),AC(200),AN(200),AI(200),ATOTAL(200),FLAG(200),
     *    TIME(200), TEMP(200), RH(200), RI(200), RN(200), T(200),
     *    AO(200), RO(200)
      REAL LOOPF
      INTEGER FLOWC3, FLAG
C
C     ENTER GENERAL DATA FOR CATALYST RUN
C
      READ(9,10) START, WTCAT, WTRH, FLOWC3, LOOPF
      N = 1
C
C     ENTER SAMPLE DATA
C
    5 READ(9,20,END=30) FLAG(N),TIME(N),TEMP(N),AH(N),AC(N),AI(N),AN(N),
     *    AO(N)
      N = N + 1
```

```
         GO TO 5
30       CONTINUE
C
C            CALCULATE SPACE TIME
C
         SPTIME = WTCAT*WTRH/(FLOAT(FLOWC3)*6.E1/2.24E4)
         N = N - 1
C
C            LOOP CALCULATES RATES FOR I-TH SAMPLE
C
C
         START = INT(START)+(START-INT(START))/6.E-1
C
         C3 = 3.5E-4
         J = 1
            FACTOR = 1.
            DO 40 I = 1,N
               IF(FLAG(I) .EQ. 2) LOOPF= 25.7
               IF(FLAG(I) .EQ. 3) LOOPF= 12.5
               IF(FLAG(I) .EQ. 1) FACTOR = 2.
C
C
               AH(I)=AH(I)*LOOPF
               AC(I) = AC(I) * LOOPF
               AI(I) = 1.62*AI(I)
               AN(I) = 1.62*AN(I)
               ATOTAL(I) = AH(I)+AC(I)+AI(I)+AN(I)+ AO(I)
               RH(I) =(AH(I)/ATOTAL(I) - C3)/SPTIME*FACTOR
               IF(RH(I) .LT. 0.0) RH(I) = 0.0
               RI(I) =(AI(I)/ATOTAL(I)/(1.-C3))/SPTIME*FACTOR
               RN(I)= (AN(I)/ATOTAL(I)/(1.-C3))/SPTIME*FACTOR
               RO(I)= (AO(I)/ATOTAL(I)/(1.-C3))/SPTIME*FACTOR
C
C                TIME IS CONVERTED TO DELTA TIME FROM TIME
C                OF REACTANTS INITIATION -- IN TENTHS OF HOURS
C
               TIME(I) =INT(TIME(I)) +(TIME(I)-INT(TIME(I)))/6.E-1
               IF(TIME(1) .LE. START) TIME(1) = TIME (1) + 12.0
               IF(I-1 .EQ. 0 ) GO TO 23
               IF(TIME(I) .LE. TIME(I-1)) TIME(I) = TIME (I) + 12.0*J
               IF(TIME(I) .LE. TIME(I-1)) J = J + 1
23             T(I) =  TIME(I)-START
               IF(I-1 .EQ. 0 ) GO TO 40
               IF(T(I) .LE. T(I-1)) T(I) = T(I) + 12.0
40          CONTINUE
         DO 21 I=1,N
21       WRITE(12,50) FLAG(I),T(I),TEMP(I),RH(I),RI(I),RN(I)
50       FORMAT(I2,2X,5(E10.4,4X))
10       FORMAT(F5.2,F7.4,F7.4,I3,F5.1)
20       FORMAT(I1,F6.2,F6.1,5F11.0)
51       FORMAT(1X,I2)
```

```
888   STOP
      END
```

```
   9.20 0.7909 0.035  15 25.7
0   9.30 150.0     87110.   2634390.          0.          0.   36462.
0  10.00 150.      70840.   2499730.       2692.       7145.   89716.
0  10.35 150.      81530.   2131100.      11957.      14984.  105901.
0  11.00 150.      67840.   2279080.      28281.      23504.   88148.
0  11.30 150.      57130.   2265400.      83246.      46325.   61941.
0  12.15 150.      53440.   2284300.      92318.      44974.   32902.
0  12.45 150.      49300.   2258600.      95301.      53110.   37216.
0   1.30 150.      62270.   2873160.     100646.      76616.   26114.
0   2.45 150.      85560.   2959880.      98601.      92439.   19904.
0   4.55 150.      70000.   2849840.      87827.     116669.   14810.
0   6.00 150.      65000.   2850000.      84741.     125692.   14985.
0   7.05 150.      56860.   2816250.      83298.     130376.   13280.
0   8.10 150.0     59180.   2803930.      82102.     133662.    8243.
0   9.10 150.      60870.   2797330.      84125.     139074.   16452.
0  10.15 150.      59000.   2809100.      88432.     150984.   15388.
0  11.20 150.      60330.   2805240.      90190.     156432.   14782.
0  12.25 150.      60690.   2803930.      88800.     156930.    6867.
0   1.30 150.      61250.   2783430.      89470.     157984.    3745.
1   2.35 150.      60250.   2783190.      89994.     160308.    7556.
1   3.40 150.      59930.   2781250.      88827.     159682.    4097.
1   4.45 150.      60580.   2770950.      89540.     159065.    4390.
1   5.50 150.      58380.   2763960.      89793.     159875.    4158.
1   8.00 150.      58560.   2758610.      91239.     161822.    5541.
0  10.10 135.      26800.   2751300.      55663.     102401.    1598.
0  11.15 135.0     28390.   2756560.      58925.     103645.    2447.
0  12.20 135.      29920.   2758480.      58323.     102872.       0.
0   1.25 135.      30340.   2758740.      55823.     101483.       0.
0   2.30 120.      14440.   2770280.      27122.      49449.       0.
0   3.35 120.      13900.   2764790.      32777.      58968.       0.
0   4.40 120.      14560.   2763680.      32823.      59066.       0.
0   5.45 120.      14590.   2768110.      30584.      56352.       0.
0   6.50 120.      15630.   2770920.      30543.      56274.       0.
0   7.55 120.      14670.   2749900.      30082.      56110.       0.
0   9.00 150.      60070.   2715930.      96671.     165807.   11899.
0  10.05 149.      56740.   2723260.      84624.     147436.   17756.
0  11.10 149.      55290.   2718370.      83287.     145512.   15830.
0  12.15 149.      56440.   2723110.      85979.     147772.   18340.
0   1.20 149.      60800.   2871540.      86931.     152277.   16140.
0   2.25 149.      59570.   2857830.      88387.     156560.   14899.
0   3.30 149.      59250.   2848590.      87086.     155652.   16544.
0   4.35 149.      58610.   2853790.      86431.     154012.    3266.
0   5.40 149.      58450.   2842920.      88329.     155968.    4877.
0   6.45 149.      57300.   2841110.      86656.     155865.    4007.
0   7.50 149.      49040.   2912370.      74521.     134496.   12444.
0   8.55 149.      52730.   2811550.      74509.     131719.   14239.
0  10.00 149.      52430.   2771010.      73684.     130430.   10174.
0  11.05 149.      67720.   2814830.      72488.     128389.   14612.
0  12.10 149.      53570.   2763580.      72132.     127292.   11693.
0   2.20 149.      40550.   1912610.      61985.     113999.       0.
0   3.25 149.      40000.   2157940.      62223.     113722.    6247.
0   4.30 149.      41430.   1923060.      62126.     112960.    1570.
0   5.35 149.      45630.   1929400.      61652.     113230.    2841.
0   6.40 149.      38090.   1924110.      61670.     112612.     890.
0   7.45 149.      38500.   1919790.      61668.     111507.    1105.
```

10	0.1667E+00	0.1500E+03	0.4593E-01	0.0	0.0
10	0.6667E+00	0.1500E+03	0.3943E-01	0.9570E-04	0.2540E-
10	0.1250E+01	0.1500E+03	0.5283E-01	0.4933E-03	0.6182E-
10	0.1667E+01	0.1500E+03	0.4133E-01	0.1100E-02	0.9140E-
10	0.2167E+01	0.1500E+03	0.3503E-01	0.3266E-02	0.1817E-
10	0.2917E+01	0.1500E+03	0.3253E-01	0.3599E-02	0.1753E-
10	0.3417E+01	0.1500E+03	0.3035E-01	0.3762E-02	0.2096E-
10	0.4167E+01	0.1500E+03	0.3015E-01	0.3125E-02	0.2379E-
10	0.5417E+01	0.1500E+03	0.4010E-01	0.2951E-02	0.2766E-
10	0.7583E+01	0.1500E+03	0.3413E-01	0.2740E-02	0.3640E-
10	0.8667E+01	0.1500E+03	0.3170E-01	0.2648E-02	0.3928E-
10	0.9750E+01	0.1500E+03	0.2808E-01	0.2641E-02	0.4133E-
10	0.1083E+02	0.1500E+03	0.2935E-01	0.2612E-02	0.4252E-
10	0.1183E+02	0.1500E+03	0.3024E-01	0.2680E-02	0.4431E-
10	0.1292E+02	0.1500E+03	0.2919E-01	0.2807E-02	0.4792E-
10	0.1400E+02	0.1500E+03	0.2988E-01	0.2865E-02	0.4968E-
10	0.1508E+02	0.1500E+03	0.3007E-01	0.2822E-02	0.4986E-
10	0.1617E+02	0.1500E+03	0.3057E-01	0.2863E-02	0.5055E-
21	0.1725E+02	0.1500E+03	0.3007E-01	0.2880E-02	0.5131E-
21	0.1833E+02	0.1500E+03	0.2994E-01	0.2846E-02	0.5115E-
21	0.1942E+02	0.1500E+03	0.3037E-01	0.2878E-02	0.5113E-
21	0.2050E+02	0.1500E+03	0.2935E-01	0.2896E-02	0.5155E-
21	0.2267E+02	0.1500E+03	0.2949E-01	0.2947E-02	0.5227E-
0	0.2483E+02	0.1350E+03	0.1344E-01	0.1827E-02	0.3361E-
20	0.2592E+02	0.1350E+03	0.1423E-01	0.1929E-02	0.3394E-
20	0.2700E+02	0.1350E+03	0.1501E-01	0.1907E-02	0.3364E-
20	0.2808E+02	0.1350E+03	0.1523E-01	0.1825E-02	0.3318E-
0	0.2917E+02	0.1200E+03	0.7005E-02	0.8899E-03	0.1622E-
20	0.3025E+02	0.1200E+03	0.6738E-02	0.1077E-02	0.1938E-
20	0.3133E+02	0.1200E+03	0.7083E-02	0.1079E-02	0.1942E-
20	0.3242E+02	0.1200E+03	0.7087E-02	0.1004E-02	0.1850E-
20	0.3350E+02	0.1200E+03	0.7617E-02	0.1001E-02	0.1845E-
20	0.3458E+02	0.1200E+03	0.7179E-02	0.9940E-03	0.1854E-
0	0.3567E+02	0.1500E+03	0.3071E-01	0.3168E-02	0.5433E-
0	0.3675E+02	0.1490E+03	0.2895E-01	0.2771E-02	0.4827E-
0	0.3783E+02	0.1490E+03	0.2827E-01	0.2733E-02	0.4776E-
0	0.3892E+02	0.1490E+03	0.2880E-01	0.2815E-02	0.4839E-
0	0.4000E+02	0.1490E+03	0.2943E-01	0.2699E-02	0.4728E-
0	0.4108E+02	0.1490E+03	0.2411E-01	0.2303E-02	0.4079E-
0	0.4217E+02	0.1490E+03	0.2891E-01	0.2726E-02	0.4872E-
0	0.4325E+02	0.1490E+03	0.2855E-01	0.2702E-02	0.4815E-
0	0.4433E+02	0.1490E+03	0.2858E-01	0.2771E-02	0.4894E-
0	0.4542E+02	0.1490E+03	0.2803E-01	0.2722E-02	0.4896E-
0	0.4650E+02	0.1490E+03	0.2342E-01	0.2293E-02	0.4138E-
0	0.4758E+02	0.1490E+03	0.2609E-01	0.2370E-02	0.4189E-
0	0.4867E+02	0.1490E+03	0.2632E-01	0.2377E-02	0.4208E-
0	0.4975E+02	0.1490E+03	0.3344E-01	0.2291E-02	0.4058E-
0	0.5083E+02	0.1490E+03	0.2697E-01	0.2333E-02	0.4116E-
0	0.5300E+02	0.1490E+03	0.2946E-01	0.2888E-02	0.5312E-
0	0.5408E+02	0.1490E+03	0.2577E-01	0.2578E-02	0.4711E-
0	0.5517E+02	0.1490E+03	0.2993E-01	0.2878E-02	0.5233E-
0	0.5625E+02	0.1490E+03	0.3284E-01	0.2841E-02	0.5218E-
0	0.5733E+02	0.1490E+03	0.2751E-01	0.2860E-02	0.5223E-
0	0.5842E+02	0.1490E+03	0.2787E-01	0.2866E-02	0.5183E-
0	0.5917E+02	0.1490E+03	0.2806E-01	0.2868E-02	0.5225E-

EA EXEC A


```
                         TRACE ALL
GLOBAL TXTLIB FORTXLIB VPIUTIL
FILEDEF 8 TERM
FILEDEF 9 DISK   1 TEST A (LRECL 80 RECFM F BLKSIZE 80 PERM
FILEDEF 12 DISK   1 EA A (LRECL 80 RECFM F BLKSIZE 80 PERM
FORTGI MEAN
LOAD MEAN (START
 EXIT
```

```
C
C
C                         MEAN FORTRAN
C
C         THIS PROGRAM TAKES THE RATE DATA GENERATED FROM 'OXO',
C         SORTS FLAGGED DATA SO THAT AN ACTIVATION ENERGY CAN BE
C         BE CALCULATED AND A MEAN RATE VALUE DETERMINED AT EACH
C         TEMPERATURE.  IT IS RUN OUT OF THE ' EA EXEC ',
C         (INTERACTIVE WATFIV). A FILE IS GENERATED WITH FILETYPE
C         ' EA ' WHICH CONTAINS THE MEAN RATES, A LIST OF THE STEADY
C         STATE VALUES AT EACH TEMP., NATURAL LOG OF THE SS RATES,
C         AND AN ACTIVATION ENERGY TABLE, WITH AN COEFFICIENT OF
C         FIT (R-SQUARE). RATES ARE FLAGGED WITH VALUES GREATER THAN
C         OR EQUAL TO 20.
C
C
C
      DIMENSION T(200),TEMP(200),RH(200),RI(200),RN(200)
      DIMENSION IND(200),ISS(100),RHM(90),RIM(90),RNM(90),TMEAN(90)
      DIMENSION TEMPI(100),RHH(100),RII(100),RNN(100)
      REAL MI,MH,MN,MERRI,MERRH,MERRN
      EXTERNAL LINREG,RMEAN
      N = 1
   5  READ(9,60,END=20) IND(N),T(N),TEMP(N),RH(N),RI(N),RN(N)
  60  FORMAT(I2,2X,5(E10.4,4X))
      N = N + 1
      GO TO 5
  20  N = N-1
C
C         COLLECT ALL STEADY STATE VALUES AND STORE THEIR INDEX IN ISS
C
      K = 0
      NTEMP = 0
      IFLAG =1
C
C         LOOP SORTS DATA BY IND(I) VALUES AND KEEPS TRACK OF HOW
C         MANY POINTS ARE AT EACH TEMP.
C
      DO 30 I = 1,N
      IF(IND(I) .GE. 20)K = K + 1
      IF (IND(I).GE.20 ) ISS(K) = I
  30  CONTINUE
C
C         THE DATA IS SEPARATED INTO INDIVIDUAL RATES SO THAT
C         ACTIVATION ENERGIES CAN BE CALCULATED.
C
      DO 40 J = 1,K
      TEMP(J)=TEMP(ISS(J))
      RH(J) = RH(ISS(J))
```

```
              RI(J) = RI(ISS(J))
              RN(J) = RN(ISS(J))
              TEMPI(J)=1.0/(TEMP(ISS(J))+ 273.)
              IF(RH(J) . EQ. 0.0) GO TO 32
              RHH(J) = ALOG(RH(ISS(J)))
32            RII(J) = ALOG(RI(ISS(J)))
              RNN(J) = ALOG(RN(ISS(J)))
40            CONTINUE
C         IF(J.EQ. 1) GOTO 40
C         A = TEMP(J-1) -3.
C         B = TEMP(J-1) +3.
C         IF((TEMP(J).LT.A) .AND.( TEMP(J).GT.B)) NTEMP = NTEMP+1
C
C             SUBROUTINE RMEAN IS CALLED TO CALCULATE AVERAGE RATES
C
          CALL RMEAN(TEMP,RH,RI,RN,K,NTEMP,RHM,RIM,RNM,TMEAN)
          WRITE(12,70)(TEMP(I),RH(I),RI(I),RN(I),I=1,K)
          WRITE(12,70)(TMEAN(I),RHM(I),RIM(I),RNM(I),I=1,NTEMP)
          WRITE(8,70) (TEMP(I),RH(I),RI(I),RN(I),I=1,K)
          WRITE(8,70)(TMEAN(I),RHM(I),RIM(I),RNM(I),I=1,NTEMP)
          WRITE(12,70)(TEMPI(I),RHH(I),RII(I),RNN(I),I=1,K)
          IF(NTEMP .EQ. 1) GO TO 100
C
C          SUBROUTINE LINREG IS CALLED TO CALCULATE ACTIVATION ENERGIES
C          FOR EACH RATE.
C
C
          CALL LINREG(TEMPI,RHH,K,MH,BH,MERRH,BERRH,R2H)
          CALL LINREG(TEMPI,RII,K,MI,BI,MERRI,BERRI,R2I)
          CALL LINREG(TEMPI,RNN,K,MN,BN,MERRN,BERRN,R2N)
C
C          SLOPES ARE CONVERTED TO KCAL/MOLE.
C
          EAH=1.987E-3* MH
          EAHERR =1.987E-3*MERRH
          EAI =1.987E-3* MI
          EAIERR =1.987E-3*MERRI
          EAN =1.987E-3*MN
          EANERR =1.987E-3*MERRN
          WRITE(8,50)
          WRITE(8,51) EAH,EAHERR,R2H
          WRITE(8,52) EAI,EAIERR,R2I
          WRITE(8,53) EAN,EANERR,R2N
          WRITE(12,50)
          WRITE(12,51) EAH,EAHERR,R2H
          WRITE(12,52) EAI,EAIERR,R2I
          WRITE(12,53) EAN,EANERR,R2N
50    FORMAT(///,17X,'ACTIVATION ENERGY',10X,'ERROR',7X,'RSQUARE')
51    FORMAT(// ,8X,'C3H8',8X,F10.2,10X,F10.2,4X,F10.4)
52    FORMAT(/ ,6X,'I-C4H8O',7X,F10.2,10X,F10.2,4X,F10.4)
```

```
  53   FORMAT(/ ,6X,'N-C4H8O',7X,F10.2,10X,F10.2,4X,F10.4)
C
  70   FORMAT(////4(E10.4,3X))
 100   STOP
       END
```

```
C
C
C       ROUTINE PERFORMS A LINEAR REGRESSION ON THE RATE DATA.
C


        SUBROUTINE LINREG(X,Y,N,M,B,MERROR,BERROR,R)
C
        DIMENSION X(100),Y(100)
        REAL M,MERROR
        SUMX = 0.
        SUMY = 0.
        SUMXSQ = 0.
        SUMXY = 0.
        SUMYSQ = 0.0
            DO 10 I = 1,N
            SUMX = X(I) + SUMX
            SUMXSQ = X(I) * X(I) + SUMXSQ
            SUMXY = SUMXY + X(I) * Y(I)
            SUMYSQ = SUMYSQ + Y(I) *Y(I)
   10       SUMY = Y(I) + SUMY
        DELTA = N * SUMXSQ - SUMX*SUMX
        M = (N* SUMXY - SUMX * SUMY)/DELTA
        B = (SUMXSQ* SUMY - SUMX*SUMXY)/DELTA
        SUMDIF = 0.0
            DO 20 I = 1, N
   20       SUMDIF = SUMDIF + (Y(I) -B-M*X(I))*(Y(I) - B - M*X(I))
        A = SUMDIF/(N-2)
C
C
C       ERRORS ARE CALCULATED FOR SLOPE (MERROR) AND INTERCEPT (BERROR)
C

        MERROR = SQRT(N*A/DELTA)
        BERROR = SQRT(A*SUMXSQ/DELTA)
        R = (N*SUMXY - SUMX*SUMY)/SQRT(DELTA*(N*SUMYSQ-SUMY*SUMY))
        RETURN
        END
C
C
C       ROUTINE CALCULATES AVERAGE RATES FOR ALL THREE REACTIONS
C

        SUBROUTINE RMEAN(X,R1,R2,R3,N,L,R1M,R2M,R3M,XM)
        DIMENSION X(N),R1(N),R2(N),R3(N),R1M(20),R2M(20),R3M(20),XM(20)
        DIMENSION  NUM(10)
        L = 1
        R1M(1) = 0.
        R2M(1) = 0.
        R3M(1) = 0.
        XM(1) = 0.
        NUM(L)= 0
            DO 20 M = 2,N
```

```
      IF(X(M) .GT. (X(M-1)-3.) .AND. X(M).LT.(X(M)+3.))  GO TO 10
      L = L+1
      R1M(L) = R1(1)
      R2M(L) = R2(1)
      R3M(L) = R3(1)
      XM(L) = 1.
      NUM(L)= 1
10    R1M(L) = R1M(L) + R1(M)
      R2M(L) = R2M(L) + R2(M)
      R3M(L) = R3M(L) + R3(M)
      NUM(L) = NUM(L) + 1
      XM(L) = XM(L) + X(M)
20    CONTINUE
      DO 30 J= 1,L
      R1M(J) = R1M(J)/FLOAT(NUM(J))
      R2M(J) = R2M(J)/FLOAT(NUM(J))
      R3M(J) = R3M(J)/FLOAT(NUM(J))
30    XM(J) = XM(J)/FLOAT(NUM(J))
      RETURN
      END
```

```
0.1500E+03    0.3007E-01    0.2880E-02    0.5131E-02
0.1500E+03    0.2994E-01    0.2846E-02    0.5115E-02
0.1500E+03    0.3037E-01    0.2878E-02    0.5113E-02
0.1500E+03    0.2935E-01    0.2896E-02    0.5155E-02
0.1500E+03    0.2949E-01    0.2947E-02    0.5227E-02
0.1350E+03    0.1423E-01    0.1929E-02    0.3394E-02
0.1350E+03    0.1501E-01    0.1907E-02    0.3364E-02
0.1350E+03    0.1523E-01    0.1825E-02    0.3318E-02
0.1200E+03    0.6738E-02    0.1077E-02    0.1938E-02
0.1200E+03    0.7083E-02    0.1079E-02    0.1942E-02
0.1200E+03    0.7087E-02    0.1004E-02    0.1850E-02
0.1200E+03    0.7617E-02    0.1001E-02    0.1845E-02
0.1200E+03    0.7179E-02    0.9940E-03    0.1854E-02
```

```
0.1500E+03    0.2979E-01    0.2892E-02    0.5152E-02
0.1350E+03    0.1482E-01    0.1887E-02    0.3359E-02
0.1200E+03    0.7141E-02    0.1031E-02    0.1886E-02
```

```
0.2364E-02    -.3504E+01    -.5850E+01    -.5272E+01
0.2364E-02    -.3509E+01    -.5862E+01    -.5276E+01
0.2364E-02    -.3494E+01    -.5851E+01    -.5276E+01
0.2364E-02    -.3528E+01    -.5844E+01    -.5268E+01
0.2364E-02    -.3524E+01    -.5827E+01    -.5254E+01
0.2451E-02    -.4252E+01    -.6251E+01    -.5686E+01
0.2451E-02    -.4199E+01    -.6262E+01    -.5695E+01
0.2451E-02    -.4184E+01    -.6306E+01    -.5708E+01
0.2545E-02    -.5000E+01    -.6834E+01    -.6246E+01
0.2545E-02    -.4950E+01    -.6832E+01    -.6244E+01
0.2545E-02    -.4949E+01    -.6904E+01    -.6293E+01
0.2545E-02    -.4877E+01    -.6907E+01    -.6295E+01
0.2545E-02    -.4937E+01    -.6914E+01    -.6290E+01
```

	ACTIVATION ENERGY	ERROR	RSQUARE
C3H8	-15.75	0.22	-0.9989
I-C4H8O	-11.36	0.30	-0.9960
N-C4H8O	-11.07	0.22	-0.9980

SIM EXEC A

```
                    TRACE ALL
GLOBAL TXTLIB PREVIEW TCSLIB FORTXLIB VPIUTIL
FILEDEF 12 DISK   1 TEST A (LRECL 80 RECFM F BLKSIZE 80 PERM
FILEDEF 10 DISK   2 DATA A (LRECL 80 RECFM F BLKSIZE 80 PERM
FORTGI SIMPLT
LOAD SIMPLT (START
 EXIT
```

```
C
C         THIS PROGRAM IS DESIGNED TO PRODUCE A FILE
C         SO THAT A PLOT WITH TWO Y-AXES CAN BE SENT TO THE
          VERSATEC OR CALCOMP PLOTTER. THE RATE DATA CALCULATED
C         IN OXO IS READ AND SORTED TO OBTAIN THE VALUES TO BE
C         PLOTTED.   IT IS RUN THRU THE ' SIM EXEC ' FILE,
C         (WATFIV INTERACTIVE).
C
C         DATA IS FLAGGED BY HAVING 'FLAG VALUES GREATER THAN
C         OR EQUAL TO 10.
C
C
C
C
          DIMENSION SH(200),SI(200),SN(200), T2(200)
          DIMENSION L(200),AC(200),AN(200),AI(200),ATOTAL(200),FLAG(200),
               TIME(200), TEMP(200), RH(200), RI(200), RN(200), T(200)
          REAL LOOPF
          INTEGER FLOWC3,FLAG
          EXTERNAL YTWICE
C
C         ENTER GENERAL DATA FOR CATALYST RUN
C
          N = 1
C
C         ENTER SAMPLE DATA
C
 5        READ(12,50,END=30) FLAG(N),T(N),TEMP(N),RH(N),RI(N),RN(N)
          WRITE(10,51) FLAG(N),T(N),TEMP(N),RH(N),RI(N),RN(N)
C
 50       FORMAT(I2,1X,5(E11.4,3X))
 51       FORMAT(' ',I2,2X,5(E11.4,3X))
          N = N + 1
          GO TO 5
 30       CONTINUE
          N = N-1
          K = 0
C
C              LOOP SORTS OUT THE RATE DATA BY FLAG VALUE AND
C              KEEPS TRACK OF HOW MANY POINTS OUR TO BE PLOTTED.
C              EACH RATE IS KEPT SEPARATE BY RH, RI, RN VECTORS.
C
          DO 88 I = 1,N
          IF(FLAG(I) .GE. 10) K = K + 1
 88       IF(FLAG(I) .GE. 10) L(K) = I
            DO 89 J = 1,K
            T(J) = T(L(J))
            RH(J) = RH(L(J))
            RI(J) = RI(L(J))
 89         RN(J) = RN(L(J))
```

```
C89          WRITE(8,31) T(J),RH(J),RI(J),RN(J)
C31          FORMAT(4(E10.4,4X))
        CALL YTWICE(T,RN,RI,K,RH)
  10    FORMAT(F5.2,F7.4,F7.4,I3,F5.1)
  20    FORMAT(I1,F6.2,F6.1,4F11.0)
 888    STOP
        END
C
C               SUBROUTINE YTWICE IS CALLED TO CREATE PLOT FILE
C
        SUBROUTINE YTWICE(X,YL1,YL2,N,YR)
        DIMENSION YL1(200),YL2(200),X(200),Z(400),YR(200)
           CALL PLOTS(0,0,50)
           CALL PLOT(1.0,1.0,-3)
           CALL SCALE(X,7.0,N,1)
C
C              THE TWO HYDROFORMYLATION RATES ARE PUT INTO ONE VECTOR.
C              THIS ALLOWS BOTH RATES TO BE PUT ON ONE AXIS. THE SCALE
C              ROUTINE THEN TAKES THE WHOLE RANGE OF THE TWO RATES
C              INTO ACCOUNT.
C
               DO 222 I = 1,N
               Z(I) = YL1(I)
               J = N + I
 222           Z(J) = YL2(I)
        N2 = 2*N
           CALL SCALE(Z,5.,N2,1)
C
C          SET UP LEFT HAND Y AXIS
C
        IN1= N2 + 1
        IN2 =N2 + 2
C       WRITE(8,11) Z(IN1), Z(IN2)
  11    FORMAT(1X,2(E14.8, 3X))
        CALL AXIS(0.,0.,21HHYDROFORMYLATION RATE,21,5.0,90.,
              Z(IN1),Z(IN2))
           J1 = N + 1
           J2 = N + 2
C
C          THE X AXIS IS DRAWN BY AXIS
C
        CALL AXIS(0.,0.,9HTIME (HR),-9,7.,0.,X(J1),X(J2))
C
C          THE SCALING FOACTORS FOR THE LEFT AXIS IS PUT INTO THE
C          LAST 2 LOCATIONS OF THE RATE VECTORS. THEN THE TWO LINES
C          ARE DRAWN SEPARTELY WITH DIFFERENT SYMBOLS.
C
           YL1(J1) =Z(IN1)
           YL1(J2) =Z(IN2)
           YL2(J1) =Z(IN1)
```

```
      YL2(J2) =Z(IN2)
   CALL LINE (X,YL1,N,1,-1,1)
   CALL LINE (X,YL2,N,1,-1,6)
C
C
C     THE RIGHT AXIS IS SIMPLY DONE W/O EXTRA VECTORS.
C
      CALL SCALE(YR,5.,N,1)
   CALL AXIS(7.0,0.,18HHYDROGENATION RATE,-18,5.0,90.,YR(J1),YR(J2))
   CALL LINE (X,YR,N,1,-1,9)
   CALL PLOT(12.,0.,999)
   RETURN
   END
```

Appendix F

PARTIAL PRESSURE ANALYSIS

A nonlinear regression was performed on the rate data taken as a function of partial pressures and temperatures. The program NLIN in SAS was used to estimate the parameters of the power law model. The residual sum of squares was minimized for each estimate. The solution was sensitive to the initial guess for all three rates. Therefore, the problem was divided into two parts. In one program, the estimates for activation energy was determined. These values were then used to determine the power law estimates. A grid search was performed on each variable so that good initial guesses could be used. The program and the results are shown below.

```
//B0707EJR JOB 211D5,RODE
/*LONGKEY YRAM
//STEP1 EXEC SAS
//SYSIN  DD  *
TITLE ARAI Y PARTIAL PRESSURE STUDY
          R =YK * C3**B * CO**C * H2**D;
   DATA ;
   INPUT T C3 H2 CO RH RI RN;
   CARDS;
     149.  3.  3.  1.  0.2895E-01    0.2771E-02    0.4827E-02
     149.  3.  3.  1.  0.2891E-01    0.2726E-02    0.4872E-02
     149.  3.  3.  1.  0.2855E-01    0.2702E-02    0.4815E-02
     149.  3.  3.  1.  0.2858E-01    0.2771E-02    0.4894E-02
     149.  3.  3.  1.  0.2803E-01    0.2722E-02    0.4896E-02
     149.  3.  2.  1.  0.2342E-01    0.2293E-02    0.4138E-02
     149.  3.  2.  1.  0.2609E-01    0.2370E-02    0.4189E-02
     149.  3.  2.  1.  0.2632E-01    0.2377E-02    0.4208E-02
     149.  3.  2.  1.  0.2697E-01    0.2333E-02    0.4116E-02
     149.  1.  3.  1.  0.1081E-01    0.1058E-02    0.1877E-02
     149.  1.  3.  1.  0.1150E-01    0.1031E-02    0.1795E-02
     149.  1.  3.  1.  0.1127E-01    0.1028E-02    0.1805E-02
     149.  1.  3.  1.  0.1137E-01    0.1027E-02    0.1800E-02
     149.  1.  3.  1.  0.1152E-01    0.1021E-02    0.1815E-02
     149.  1.  3.  1.  0.1173E-01    0.1019E-02    0.1813E-02
     149.  1.  3.  1.  0.1169E-01    0.1019E-02    0.1831E-02
     149.  1.  3.  1.  0.1204E-01    0.1037E-02    0.1879E-02
     149.  2.  3.  1.  0.2162E-01    0.2117E-02    0.3754E-02
     149.  2.  3.  1.  0.2299E-01    0.2061E-02    0.3589E-02
     149.  2.  3.  1.  0.2254E-01    0.2057E-02    0.3610E-02
     149.  2.  3.  1.  0.2274E-01    0.2054E-02    0.3601E-02
     149.  2.  3.  1.  0.2304E-01    0.2042E-02    0.3630E-02
     149.  2.  3.  1.  0.2347E-01    0.2037E-02    0.3625E-02
     149.  2.  3.  1.  0.2337E-01    0.2037E-02    0.3662E-02
     149.  2.  3.  1.  0.2408E-01    0.2074E-02    0.3759E-02
     149.  3.  3.  2.  0.1713E-01    0.1677E-02    0.3162E-02
     149.  3.  3.  2.  0.1762E-01    0.1686E-02    0.3292E-02
     149.  3.  3.  2.  0.1700E-01    0.1689E-02    0.3233E-02
     149.  3.  3.  2.  0.1662E-01    0.1667E-02    0.3192E-02
     149.  3.  3.  2.  0.1622E-01    0.1685E-02    0.3274E-02
     149.  3.  3.  3.  0.1170E-01    0.1362E-02    0.2719E-02
     149.  3.  3.  3.  0.1101E-01    0.1261E-02    0.2508E-02
     149.  3.  3.  3.  0.1173E-01    0.1265E-02    0.2522E-02
     149.  3.  3.  3.  0.1136E-01    0.1246E-02    0.2557E-02
     149.  3.  3.  3.  0.1129E-01    0.1237E-02    0.2440E-02
   ;
   PROC NLIN METHOD = GAUSS EFORMAT CONVERGENCE= 1.E-10 ITER=100;
   PARMS B= 0.900
         C = -0.60
         D = 0.30;
   A = 4123567.4;
   EA = 15755.0;
   YK = A * EXP(-EA/(1.987*(273. + T)));
   MODEL RH = YK   * (C3/9.)**B *(CO/9.)**C * (H2/9.)**D;
   DER.B= YK *B*(C3/9.)**(B-1.)*(CO/9.)**C*(H2/9.)**D;
   DER.C= YK *(C3/9.)**B*C*(CO/9.)**(C-1.)*(H2/9.)**D;

   DER.D= YK *(C3/9.)**B*(CO/9.)**C*D*(H2/9.)**(D-1.);
   OUTPUT PARMS= B C D  PREDICTED=PY RESIDUAL=RY;
   PROC PRINT;
/*
```

NON-LINEAR LEAST SQUARES ITERATIVE PHASE

DEPENDENT VARIABLE: RN   METHOD: MARQUARDT

ITERATION	B	C	D	RESIDUAL SS
0	1.000000E+00	-6.000000E-01	4.000000E-01	1.78135504E-05
1	1.000000E+00	-6.000000E-01	4.000000E-01	1.78135504E-05

NOTE: CONVERGENCE CRITERION MET.
ARAI Y PARTIAL PRESSURE STUDY

R =YK * C3**B * CO**C * H2**D
17:19 SATURDAY, FEBRUARY 23, 1985

NON-LINEAR LEAST SQUARES SUMMARY STATISTICS   DEPENDENT VARIABLE RN

SOURCE	DF	SUM OF SQUARES	MEAN SQUARE
REGRESSION	3	3.87917733E-04	1.29305923E-04
RESIDUAL	32	1.78135504E-05	5.56673451E-07
UNCORRECTED TOTAL	35	4.05731333E-04	
(CORRECTED TOTAL)	34	3.63757587E-05	

PARAMETER	ESTIMATE	ASYMPTOTIC STD. ERROR	ASYMPTOTIC 95 % CONFIDENCE INTERVAL LOWER	UPPER
B	1.000000000E+00	3.08341400E-02	9.37193334E-01	1.06280667E+00
C	-6.000000000E-01	3.90108373E-02	-6.79461941E-01	-5.20538059E-01
D	4.000000000E-01	1.29160926E-01	1.36989570E-01	6.63090630E-01

X1   X   A1 02/23/85 17:20 CHERXN   F 132   215 RECS   VA TECH   PRINTED 02/23/85 17:21   PAGE 004

ASYMPTOTIC CORRELATION MATRIX OF THE PARAMETERS

	B	C	D
B	1.000000	0.457625	-0.149924
C	0.457625	1.000000	0.776873
D	-0.149924	0.776873	1.000000

ARAI Y PARTIAL PRESSURE STUDY

R =YK * C3**B * CO**C * H2**D   3
17:19 SATURDAY, FEBRUARY 23, 1985

OBS	T	C3	H2	CO	RH	RI	RN	B	C	D	PY	RY
1	149	3	3	1	0.02895	0.002771	0.004827	1	-0.6	0.4	0.00402929	0.00079771
2	149	3	3	1	0.02891	0.002726	0.004872	1	-0.6	0.4	0.00402929	0.00063671
3	149	3	3	1	0.02855	0.002702	0.004815	1	-0.6	0.4	0.00402929	0.00069657
4	149	3	3	1	0.02858	0.002771	0.004894	1	-0.6	0.4	0.00402929	0.00068671
5	149	3	3	1	0.02803	0.002722	0.004896	1	-0.6	0.4	0.00402929	0.00066671
6	149	3	2	1	0.02342	0.002293	0.004153	1	-0.6	0.4	0.00342603	0.00071197
7	149	3	2	1	0.02609	0.002370	0.004189	1	-0.6	0.4	0.00342603	0.00076297
8	149	3	2	1	0.02632	0.002377	0.004208	1	-0.6	0.4	0.00342603	0.00073197
9	149	3	2	1	0.02697	0.002333	0.004116	1	-0.6	0.4	0.00342603	0.00063997
10	149	1	3	1	0.01031	0.001058	0.001377	1	-0.6	0.4	0.00134310	0.00053390
11	149	1	3	1	0.01150	0.001031	0.001795	1	-0.6	0.4	0.00134310	0.00045190
12	149	1	3	1	0.01127	0.001023	0.001605	1	-0.6	0.4	0.00134310	0.00046190
13	149	1	3	1	0.01137	0.001027	0.001300	1	-0.6	0.4	0.00134310	0.00045690
14	149	1	3	1	0.01152	0.001021	0.001815	1	-0.6	0.4	0.00134310	0.00047170
15	149	1	3	1	0.01173	0.001019	0.001313	1	-0.6	0.4	0.00134310	0.00046690
16	149	1	3	1	0.01169	0.001019	0.001831	1	-0.6	0.4	0.00134310	0.00048790
17	149	1	3	1	0.01204	0.001037	0.001879	1	-0.6	0.4	0.00134310	0.00053590
18	149	2	3	1	0.02162	0.002117	0.003754	1	-0.6	0.4	0.00268619	0.00106781
19	149	2	3	1	0.02299	0.002061	0.003559	1	-0.6	0.4	0.00268619	0.00090281
20	149	2	3	1	0.02254	0.002057	0.003610	1	-0.6	0.4	0.00268619	0.00092381
21	149	2	3	1	0.02274	0.002054	0.003601	1	-0.6	0.4	0.00268619	0.00091481
22	149	2	3	1	0.02304	0.002042	0.003630	1	-0.6	0.4	0.00268619	0.00094381
23	149	2	3	1	0.02347	0.002037	0.003625	1	-0.6	0.4	0.00268619	0.00093881
24	149	2	3	1	0.02337	0.002037	0.003662	1	-0.6	0.4	0.00268619	0.00097581
25	149	2	3	1	0.02408	0.002074	0.003759	1	-0.6	0.4	0.00268619	0.00107281
26	149	3	3	2	0.01713	0.001677	0.003162	1	-0.6	0.4	0.00265834	0.00050366
27	149	3	3	2	0.01762	0.001686	0.003292	1	-0.6	0.4	0.00265834	0.00063366
28	149	3	3	2	0.01700	0.001689	0.003233	1	-0.6	0.4	0.00265834	0.00057466
29	149	3	3	2	0.01662	0.001667	0.003192	1	-0.6	0.4	0.00265834	0.00053366
30	149	3	3	2	0.01622	0.001685	0.003274	1	-0.6	0.4	0.00265834	0.00061566
31	149	3	3	3	0.01170	0.001362	0.002719	1	-0.6	0.4	0.00208428	0.00063472
32	149	3	3	3	0.01101	0.001261	0.002503	1	-0.6	0.4	0.00208428	0.00042272
33	149	3	3	3	0.01173	0.001265	0.002522	1	-0.6	0.4	0.00208428	0.00043772
34	149	3	3	3	0.01136	0.001246	0.002557	1	-0.6	0.4	0.00208428	0.00047272
35	149	3	3	3	0.01129	0.001237	0.002440	1	-0.6	0.4	0.00208428	0.00035572

The vita has been removed from
the scanned document